

10. PREDICTION OF HF FORMATION DURING SUPPRESSION

Gregory T. Linteris
Building and Fire Research Laboratory

Grzegorz W. Gmurczyk
Science Applications International Corporation

Contents

	Page
10. PREDICTION OF HF FORMATION DURING SUPPRESSION	201
10.1 Introduction	203
10.2 Background	203
10.3 Technical Approach	205
10.4 Equilibrium Calculations with Halogenated Inhibitors	206
10.4.1 Results	206
10.4.2 Conclusions	210
10.5 Premixed Flame Structure Calculations and Burning Velocity Measurements	210
10.5.1 Introduction	210
10.5.2 Background	214
10.5.3 Experiment - Nozzle Burner	215
10.5.4 Experiment - Bomb	215
10.5.5 Model	216
10.5.6 Results	216
10.5.7 Conclusions	239
10.6 Physical/Chemical Model	241
10.6.1 Steady-state - Premixed Flames	241
10.6.2 Steady-state - Diffusion Flames	241
10.6.3 Transient State	247
10.7 Experiments	249
10.7.1 Propane Diffusion Flame Tests for HF	249
10.7.2 Liquid Heptane Diffusion Tests for HF	249
10.7.3 Premixed Flame Tests for HF	251
10.7.4 HF Sampling Technique	251
10.7.5 Transient State Measurements	251
10.8 Results	253
10.8.1 Steady-state - Premixed Flames	253
10.8.2 Steady-state - Gaseous Diffusion Flames	257
10.8.3 Steady-state - Liquid Diffusion Flames	272
10.8.4 Transient-state - Gaseous Diffusion Flames	274

10.9	HF Production in Larger Scale Tests	274
10.9.1	Comparison with Predictions	283
10.10	Parametric Analysis	285
10.10.1	Results	285
10.10.2	Conclusions	288
10.11	Predicting HF in Dry-Bay and Engine Nacelle Fires	292
10.11.1	Engine Nacelle Fires	292
10.11.2	Dry-Bay Fires	294
10.12	Summary	295
10.13	Acknowledgments	298
10.14	References	298
Appendix A.	The Computer Program Predicting Formation of HF	302

10.1 Introduction

The acid gases hydrogen fluoride, hydrogen chloride, and hydrogen bromide (HX, where X denotes a halogen), are thought to be the most damaging and dangerous of the potential decomposition products, and much study has been devoted to determining the amounts of these chemicals formed during fire suppression by CF_3Br and halon alternatives. While CF_3Br is known to readily decompose to form HF, HBr, and COF_2 in laboratory premixed and diffusion flames and in larger scale fires, the amounts were not considered to be a major threat compared to that of the fire itself. The alternative agents have been found to produce significantly more acid gas than CF_3Br , and consequently, there exists a need to understand and predict the mechanisms of formation of acid gases in laboratory flames, and ultimately, suppressed fires.

The goal of this project is to develop an ability to predict the quantity of HF formed during suppression of aircraft fires. In order to understand the formation rates of acid gases in dry bay and engine nacelle fires it is necessary to examine the thermodynamics and chemical kinetics relevant to the formation of the acid gases as well as the effects of the flow field and mixing on the chemistry. An engine nacelle fire may be similar to a steady turbulent spray diffusion flame, whereas a dry bay fire may resemble a rapidly advancing turbulent premixed flame. Because suppression of the dry bay fires occurs in a time of about 100 ms, it is also necessary to consider transient effects on the acid gas formation. The formation of toxic and corrosive by-products in flames/fires inhibited by halogenated hydrocarbons is controlled by transport rates of the agent into the flame, chemical kinetic rates, or equilibrium thermodynamics. These factors are affected by the fuel type, local mixture composition, inhibitor type and concentration, and the characteristics of the flow field such as mixing rate, strain rate, and stabilization mechanism in the case of laboratory burner flames.

The approach taken in the present work is to examine the HF production in the fire, for a range of conditions. Specifically, the effects of fuel type, fire type and size, agent chemical composition and application rate, and room humidity are considered with respect to their effect on the HF formation, both for steady-state and transient conditions. The quantity of agent required to suppress various types of fires has been used as a measure of an agent's utility. In addition, the amount of any unwanted decomposition by-products formed during fire suppression has been identified as a potentially important parameter. The rates of HF generation can then be used as a source term in more detailed models which include the effects of variable mixing rates of the inhibitor, mixing rates of post-fire gases, ventilation rates of the space, and HF condensation to surfaces.

The influence of the key parameters through systematic experiments on laboratory-scale flames has been studied. Agents were added to the air stream of co-flow diffusion flames under steady-state and transient conditions. The apparatus used to obtain these data, the results and their interpretation are presented below.

10.2 Background

The halogen acid or hydrogen halide HX (where X represents the halogen) is a thermodynamically stable product in mixtures containing hydrogen and halogen atoms. Formation of acid gases in inhibited hydrocarbon flames has been studied for many years. Nonetheless, there have been no attempts to predict the amounts of HF formed in suppressed fires which are applicable to a broad range of fire types and conditions and which are based on first principles. Since formation of HF could be an important parameter in selecting an agent to replace CF_3Br , it is essential to develop a method to estimate the amount of HF formed in suppressed fires as compared to the amount formed

with CF_3Br . Once the magnitude of the HF source (the suppressed fire) is determined, the relative importance of that amount of HF, and its deposition and dilution rates can be determined for the particular application.

The previous research can be categorized as either global measurements of HF produced in suppressed fires, or detailed flame structure measurements. Burdon *et al.*, (1995) ignited mixtures of fuel, air, and CH_3Br in flasks, analyzed the products and found copious amounts of HBr. Numerous premixed low pressure flame studies (Wilson, 1965; Biordi *et al.*, 1973; Safieh *et al.*, 1982; VanDoooren *et al.*, 1988) used mass spectroscopy to measure the profiles of hydrogen halides and other products in hydrogen, carbon monoxide, and hydrocarbon flames inhibited by CH_3Br , CF_3Br , and CF_3H . These studies indicated conversion efficiencies of the halogens in the inhibitor into halogen acids on the order of unity.

Acid gas formation in hydrocarbon-air pool fires suppressed by CF_3Br has been studied by Sheinson *et al.*, (1981); Sheinson and Alexander, (1982). His studies, in test volumes of 1.7 and 650 m^3 , stressed the difficulties in probe sampling for acid gases. The latter study described an in situ IR absorption method for measuring HBr and HF. To overcome these limitations and also provide time-resolved acid gas concentration data (Smith *et al.*, 1993) developed a new HX sampling technique and obtained HX and inhibitor concentrations as functions of time for discharge of CF_3Br into a 56 m^3 space. In a series of experiments with a variety of fuels and halogenated inhibitors (Yamashika, 1973) showed that the extinction time for a compartment fire sprayed with inhibitor is dependent upon the discharge rate and room volume. He then showed (1974) that the amounts of hydrogen halides and carbonyl halides are also dependent upon the discharge rate. Using a simple model of acid gas formation based on the steady-state rates, he developed a model of transient acid gas formation to explain his results. In more recent studies (Ferreira, 1992a, 1992b) CF_3Br , C_3HF_7 , and C_4F_{10} were injected into an enclosure fire and measured the HF produced using ion-selective electrodes.

Di Nenzo *et al.*, (1992) introduced halon alternatives into compartment fires and measured the HF, HCl, and COF_2 produced using Fourier transform infrared spectroscopy. These studies again confirmed the importance of injection rate and fuel consumption rate on the amount of acid gas produced. Filipczak, 1993 introduced CF_2ClBr and CF_3Br into a methane flame and measured the O_2 , CO_2 , H_2O , HF, HCl, HBr, and unreacted inhibitor using a mass spectrometer. Hoke and Herud, (1993) are currently developing a fast-response ion-selective electrode for measuring HF and HCl produced in extinguished fires in crew compartments of combat vehicles. Previous research related to understanding acid gas formation in inhibited flames can be seen to include both detailed flame structure measurements and global measurements of HF produced in suppressed fires. The former provide the basis for obtaining a good understanding of the underlying chemical kinetics of the formation of acid gases.

The global measurements provide important information on the magnitude of the acid gases produced and allow a comparison of the relative amount of acid gases formed by new halon alternatives. There has remained a need to develop a fundamental basis for interpreting the data on acid gas formation in fires suppressed by halon alternatives and to understand the chemical kinetic rates of acid gas formation in diffusion flames inhibited by these alternative agents. In particular, there has existed a need to understand the relationship between fuel and inhibitor type, flame characteristics, agent transport rates, and the concentrations of by-products formed.

10.3 Technical Approach

The technical approach in the present project has included theoretical, numerical, and experimental components. The theoretical components have included thermodynamic calculations, numerical calculations of the flame structure of premixed flames inhibited by fluorocarbons, and development of a global model for HF formation in premixed and diffusion flames. Experiments have included premixed and diffusion flames of liquid or gaseous fuels with steady-state or transient addition of the agent. The need for and contribution of each of these components of the project are outlined below.

Equilibrium calculations are an essential first step for understanding the agent decomposition and HF formation in flames inhibited by fluorinated hydrocarbons. Although kinetic limitations are important to the formation of many products of combustion, the thermodynamics provide the driving force for reaction, and hence must be examined prior to investigating the kinetics. In order to obtain a broad understanding of the inhibited flames, numerous equilibrium calculations have been performed for a variety of fuels and agents. Presented in Section 10.4 are some representative results which illustrate the dominant features of the halogenated agents in hydrocarbon flames.

Although chemical equilibrium calculations are an essential first step towards understanding HF formation, combustion systems often display chemical kinetic limitations to the formation of final products. Consequently, it was important to consider next an inhibited flame in which chemical kinetic limitations could be considered. Premixed flames were selected for study since the complete flame structure is readily calculated using available techniques, and the computational time is not prohibitive. Once solutions are obtained, a wealth of information is available concerning the species reaction and transport in the flame, so that detailed information is available concerning byproduct formation. In order to provide a first level of validation of the kinetic mechanisms, burning velocity measurements were made and compared with the predicted burning velocities from the numerical calculations. Section 10.5 describes the modeling results for inhibited premixed flames along with comparison with experimental burning rates for initial model validation. The important implications for HF formation predicted by the modeling results are discussed for both normal and high-pressure flames.

After obtaining the necessary theoretical background from the chemical equilibrium and premixed flame structure calculations, it was possible to develop a simple model of HF production in both premixed and diffusion steady-state flames. This model was subsequently extended to transient conditions. Section 10.6 describes the physical and chemical basis of the model, presents the equations which describe the amount of HF formation, and describes phenomenologically the fate of the agent as the inhibitor concentration in the air stream increases.

In order to provide an experimental basis for the model and then test its performance, extensive measurements of HF formation in laboratory flames have been performed. In these tests, fuel flow rate, fuel type, agent type and concentration and air flow have been varied. Experiments were performed for premixed and diffusion flames, and for liquid and gaseous fuels, in both steady-state and transient conditions. The model for HF formation has been validated using these experiments. In addition, the HF formation in a large number of intermediate scale tests at the Naval Research Laboratory has been predicted by the model and compared to the actual HF measurements. The experimental configurations for all of the apparatuses are described in Section 10.7. The experimental results along with interpretation of the results are presented in Section 10.8. In Section 10.9, the model is used to predict the HF formation in intermediate-scale tests performed at the Naval Research Laboratory.

The model for predicting HF formation appears to work well. As a result, it is a useful tool for understanding the effects of various parameters on HF formation that would otherwise require much

money and time to exhaustively explore. As described in Section 10.10, we have performed extensive parametric analyses to illustrate the effects of fuel type, fire size, inhibitor type and concentration, inhibitor concentration necessary for extinction, fire-out time, and the presence of water vapor in the air. In the final section (10.11), we describe the parameters likely to be important in dry-bay and engine nacelle fires, and present the straightforward application of the model for predicting HF formation for a wide range of fire types.

10.4 Equilibrium Calculations with Halogenated Inhibitors

In order to first understand the basic driving force for reaction of the halogenated inhibitors, extensive thermodynamic equilibrium calculations were performed. These provided information on the likely product species for a variety of fuel-air mixture ratios, fuel and agent type, and agent concentration.

10.4.1 Results. Calculations have been performed for methane-air flames at various stoichiometries and concentrations of C_2HF_5 . Although methane and C_2HF_5 were selected for these figures, this is arbitrary; the features of the analyses are qualitatively the same for any hydrocarbon fuel and fluorinated hydrocarbon (or perfluorocarbon) inhibitor. The results are shown in Figures 1 through 6. Detailed examination of figures such as these has illustrated the thermodynamic driving forces in hydrocarbon flames inhibited by fluorinated agents, and allowed development of an appropriate model for HF formation. Some of the pertinent characteristics of these inhibited flames are described below.

Figures 1 through 3 show the effects of increasing C_2HF_5 mole fraction on the equilibrium temperature and species mole fractions at nominal fuel-air equivalence ratios ϕ of 0.6, 0.8 and 1.0. Note that in these calculations, the equivalence ratio is calculated based on the oxygen demand of the fuel only, and does not include the oxygen demand of the inhibitor. In Figure 1, the flame is fuel lean ($\phi = 0.6$). At an inhibitor concentration of zero, the major products are H_2O and CO_2 ; however, the flame has an excess of oxygen, and the flame temperature is low, about 1700 K. Adding inhibitor has the effect of increasing the flame temperature since the HFC's behave, thermodynamically, much as a fuel species. As C_2HF_5 is added, the temperature increases, and the fluorine in the inhibitor forms HF, diverting some of the hydrogen away from water, so that the water concentration in the flame decreases. The additional carbon in C_2HF_5 is converted to CO_2 . At an inhibitor concentration of about 5 to 6 %, the hydrogen to fluorine ratio in the flame is near unity. At this C_2HF_5 mole fraction, the temperature and $[CO_2]$ reach peak values, and water is absent as a product. Addition of more C_2HF_5 leads to COF_2 and CO formation because hydrogen and oxygen concentrations, respectively, are insufficient: The temperature decreases above 6 % C_2HF_5 because of the shortage of both hydrogen and oxygen, although HF concentration increases, at a slower rate, due to the hydrogen in the inhibitor molecule itself. For the conditions of this figure, the point of unity fluorine to hydrogen ratio, temperature peak and CO_2 peak occur at the same C_2HF_5 volume fraction (about 6 %); this is not always the case. For comparison purposes, it should be noted that a premixed stoichiometric flame in the nozzle burner described in later sections blows off at a C_2HF_5 mole fraction of about 0.09 for methane flames, and 0.05 for propane. Diffusion flames of propane blow off at a C_2HF_5 mole fraction of 0.105 in the air stream.

Figures 2 and 3, for values of ϕ of 0.8 and 1.0, show the same trends. Water disappears at the point of unity hydrogen to fluorine ratio; and CF_2O forms when water is gone. Carbon monoxide forms when there is insufficient oxygen, and the peak temperature occurs at the C_2HF_5 mole fraction where the CO production increases. This last effect implies that CO to CO_2 conversion has the largest effect on heat release, or, conversely, that the oxygen demand has more effect on peak temperature

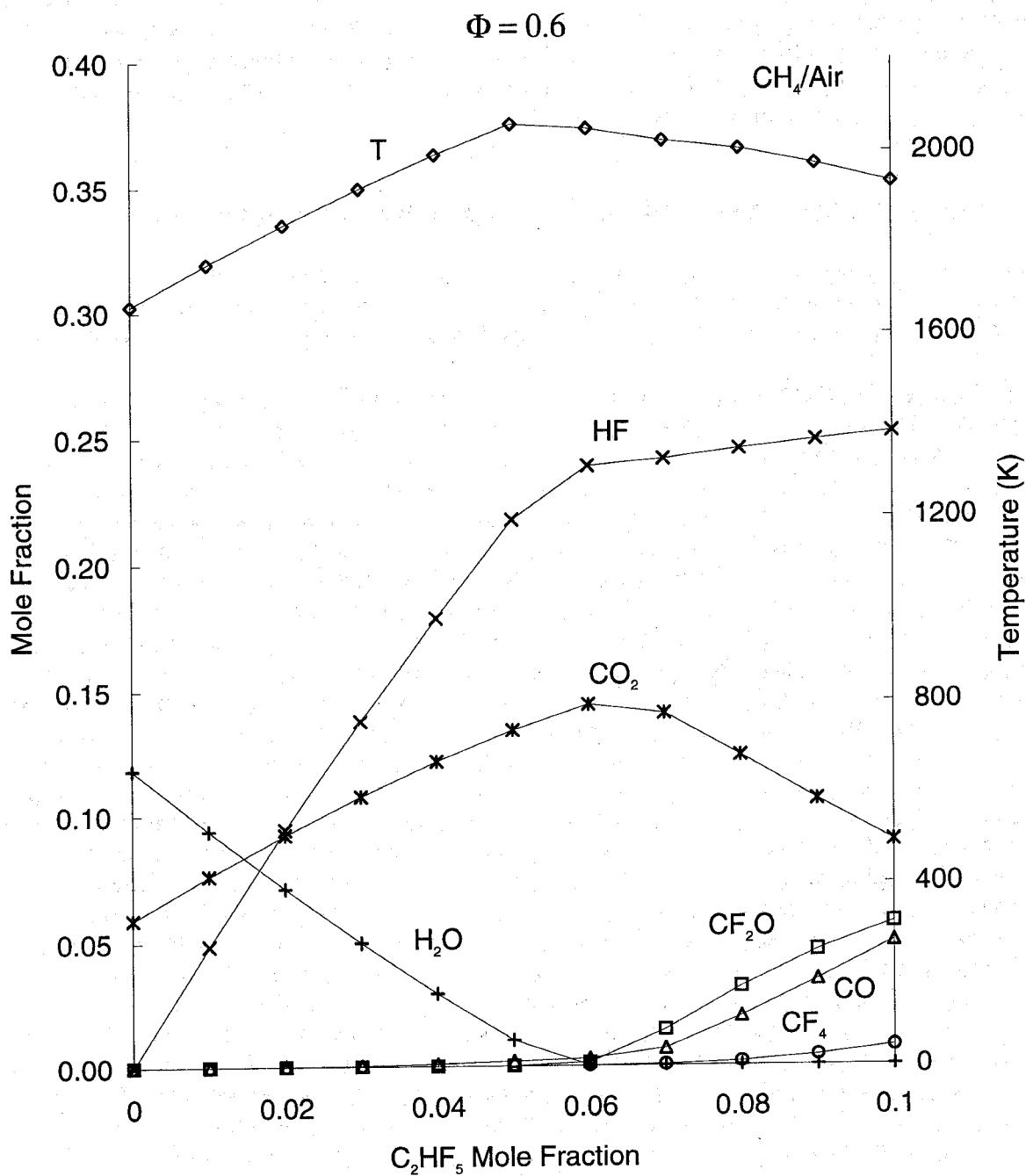


Figure 1. Equilibrium temperature and composition of combustion/inhibition products in the lean $\phi = 0.6$ CH₄/Air mixture versus C₂HF₅ mole fraction.

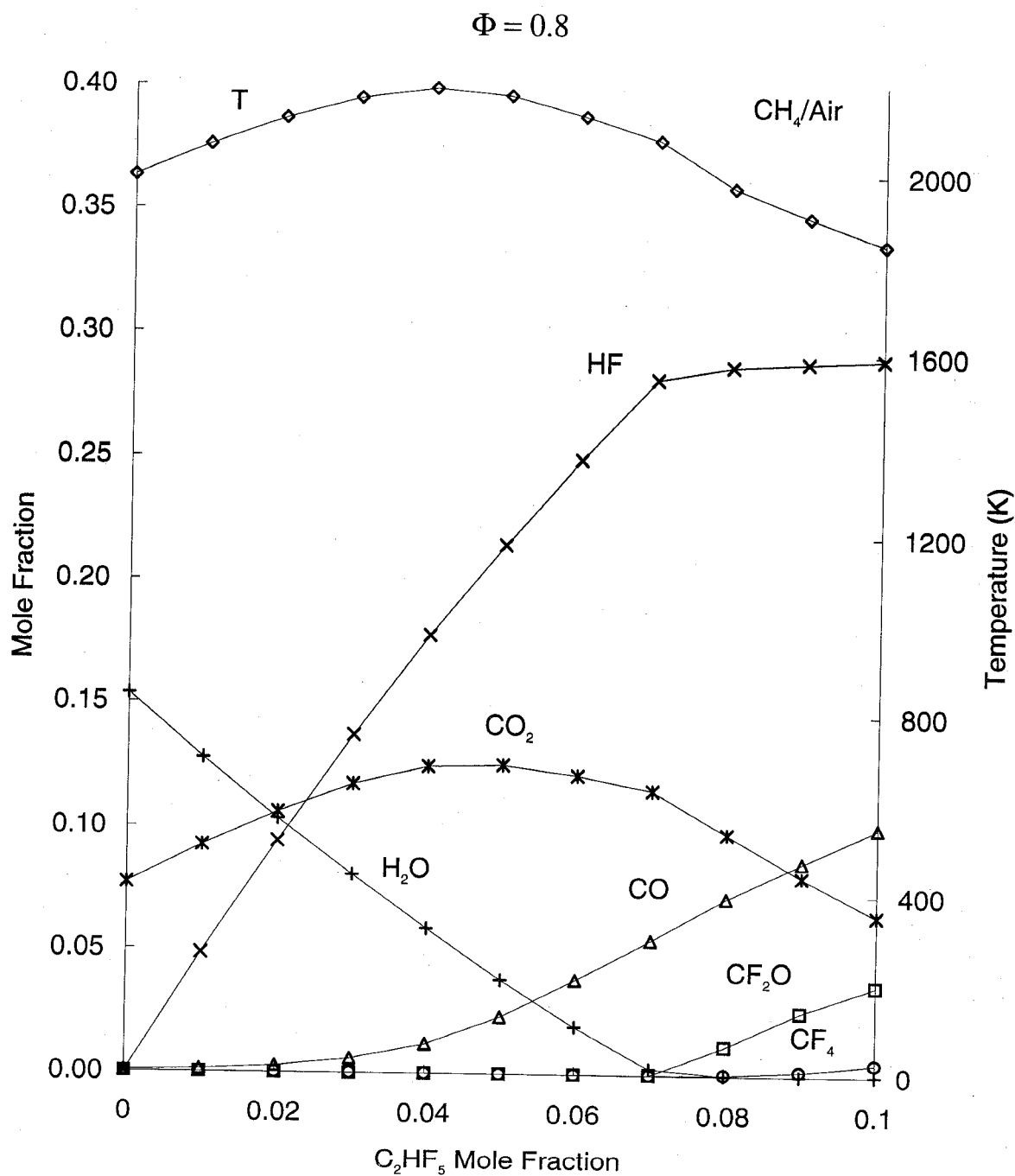


Figure 2. Equilibrium temperature and composition of combustion/inhibition products in the lean $\phi = 0.8$ CH_4/Air mixture versus C_2HF_5 mole fraction.

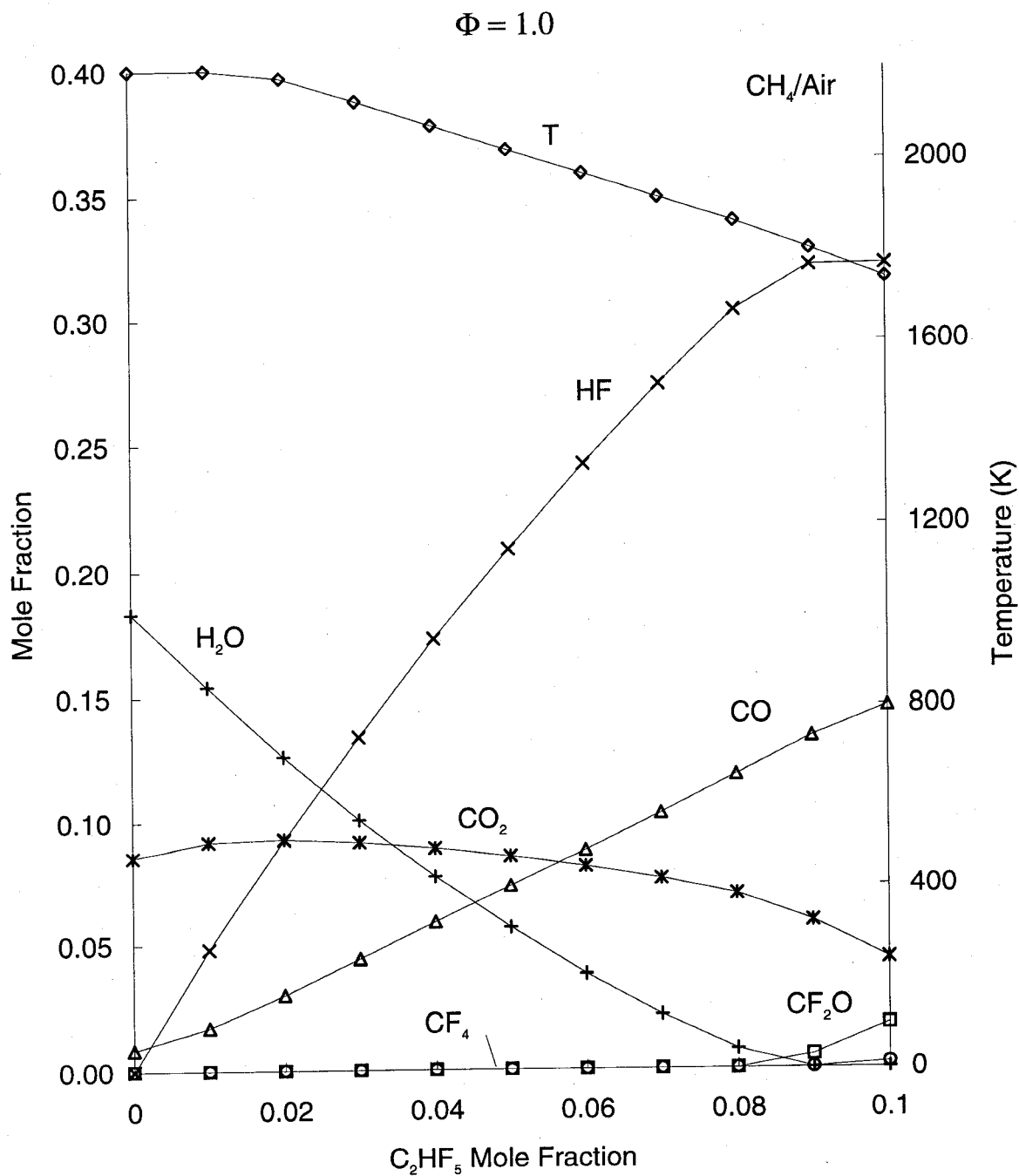


Figure 3. Equilibrium temperature and composition of combustion/inhibition products in the stoichiometric $\phi = 1.0$ CH₄/Air mixture versus C₂HF₅ mole fraction.

than the hydrogen demand. Carbonyl fluoride COF_2 forms when there is insufficient hydrogen for formation of HF. The species CF_4 appears when there is insufficient water, and either insufficient oxygen or carbon for formation of COF_2 . The CF_4 concentration is typically about 20 % of the COF_2 concentration.

Figures 4, 5, 6 show the influence of a varying equivalence ratio on the equilibrium product mole fractions and temperature at a constant inhibitor mole fraction of 0.025, 0.05, and 0.10, respectively. As in ordinary hydrocarbon-air flames, the temperature is decreased for rich flames due to incomplete conversion of CO to CO_2 , and for lean flames due to dilution by excess air. As described above, the peak value of the temperature occurs at lower nominal equivalence ratios as the amount of inhibitor increases (*e.g.*, Figures 1, 2, 3), due to the oxygen requirement of the inhibitor.

As for hydrogen, the primary source is the fuel, so that for richer flames, the formation of water increases, while for leaner flames, the formation of COF_2 increases. For this agent and fuel, limits to HF formation only occur at high C_2HF_5 mole fractions and leaner flames (*e.g.*, Figure 4). The greatly reduced peak temperature occurs for the lean conditions in Figure 4 due to the hydrogen limits; insufficient hydrogen forces formation of CF_2O and CF_4 rather than HF and CO_2 , limiting the peak temperature.

10.4.2 Conclusions. From examination of the results of equilibrium calculations, the following characteristics have been observed for inhibited hydrocarbon-air flames:

1. Peak temperature occurs near the onset of CO formation.
2. Addition of inhibitor shifts the peak temperature to leaner nominal stoichiometries, since the agent acts as an additional fuel species.
3. For conditions typical of flames, the major product species which contain fluorine are HF and COF_2 .
4. Hydrogen fluoride is formed preferentially over water as an endpoint for hydrogen.
5. Carbonyl fluoride and water do not exist at the same conditions, water exists only when $[\text{H}]/[\text{F}] < 1$, COF_2 when $[\text{H}]/[\text{F}] > 1$.
6. Fuel serves as the primary source of hydrogen, which is necessary for the formation of HF.

10.5 Premixed Flame Structure Calculations and Burning Velocity Measurements

10.5.1 Introduction. It is important to recall that the above section describes thermodynamic considerations only. Generally, reactant mixtures in diffusion flames like to combine at conditions which produce the maximum temperature; however, there can be both transport and kinetic limitations. That prevents attainment of chemical equilibrium. For flames with halogens, presence of the halogen may influence the kinetic rates for consumption of the fuel and inhibitor. Consequently, there may be a competition between the tendency to move to conditions which produce high temperatures, and conditions which produce fast rates of consumption of the reactant species. For diffusion flames, the

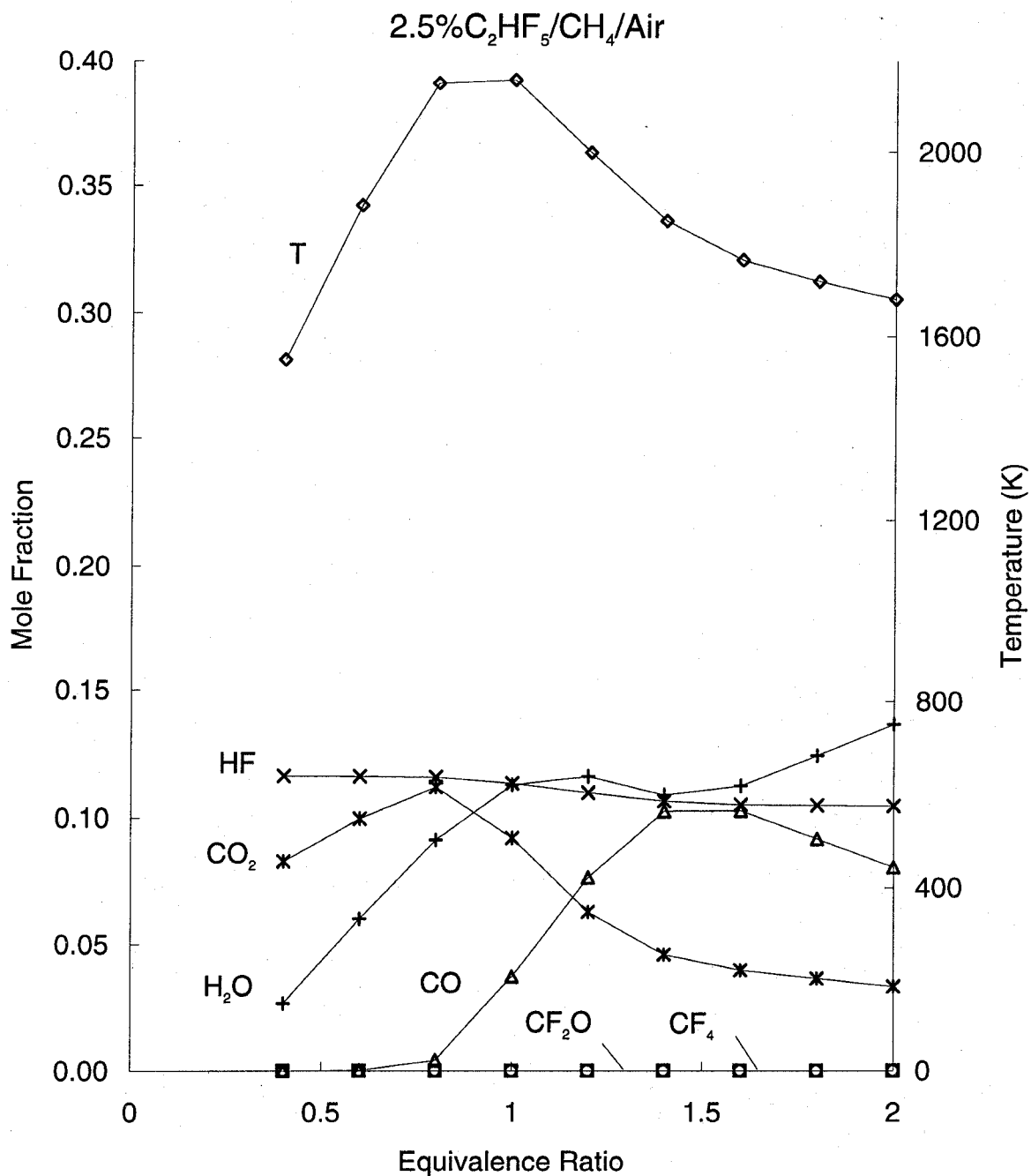


Figure 4. Equilibrium temperature and composition of combustion/inhibition products in the 2.5 % C₂HF₅/CH₄/Air mixture versus mixture equivalence ratio.

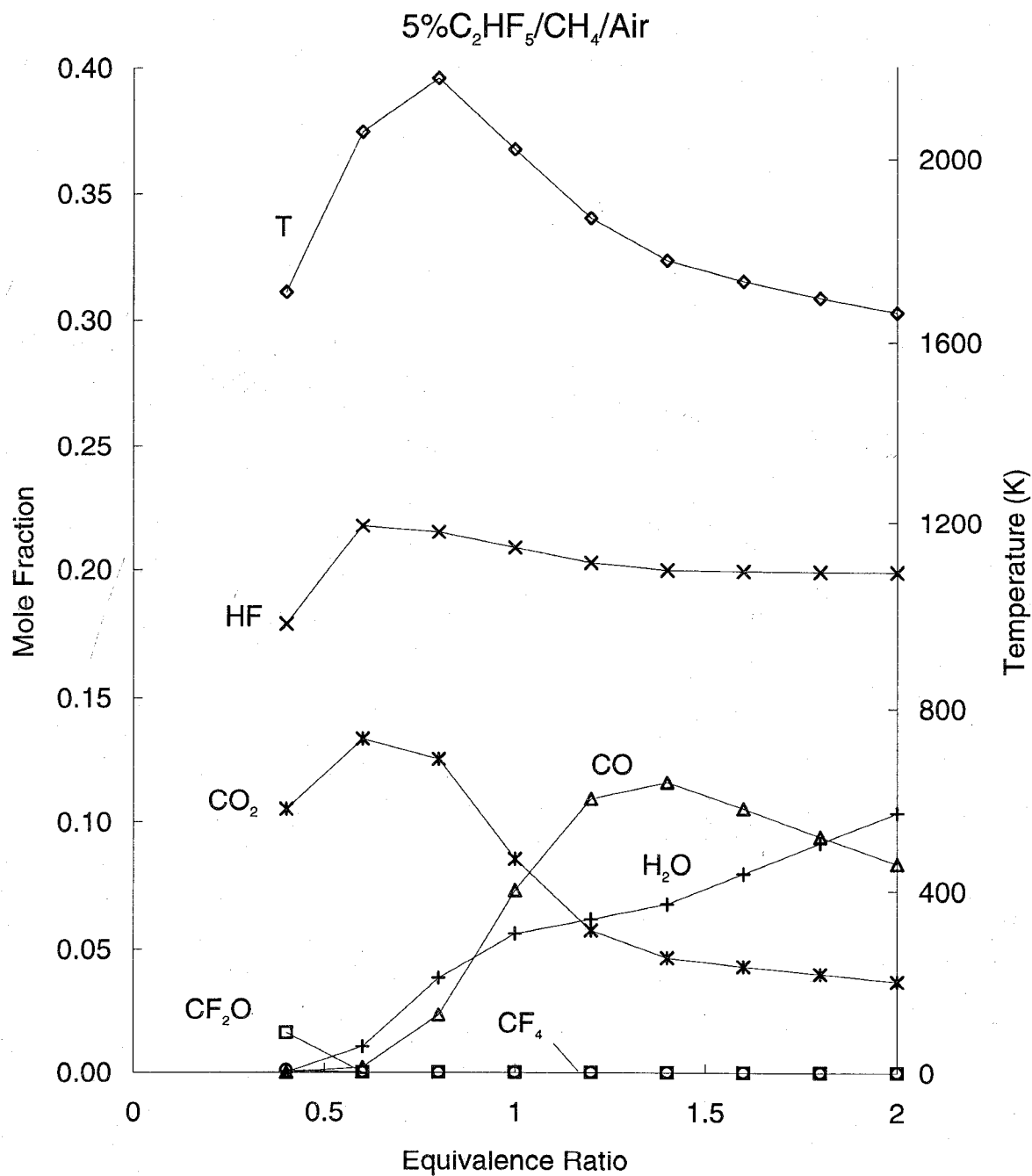


Figure 5. Equilibrium temperature and composition of combustion/inhibition products in the 5% $C_2HF_5/CH_4/Air$ mixture versus mixture equivalence ratio.

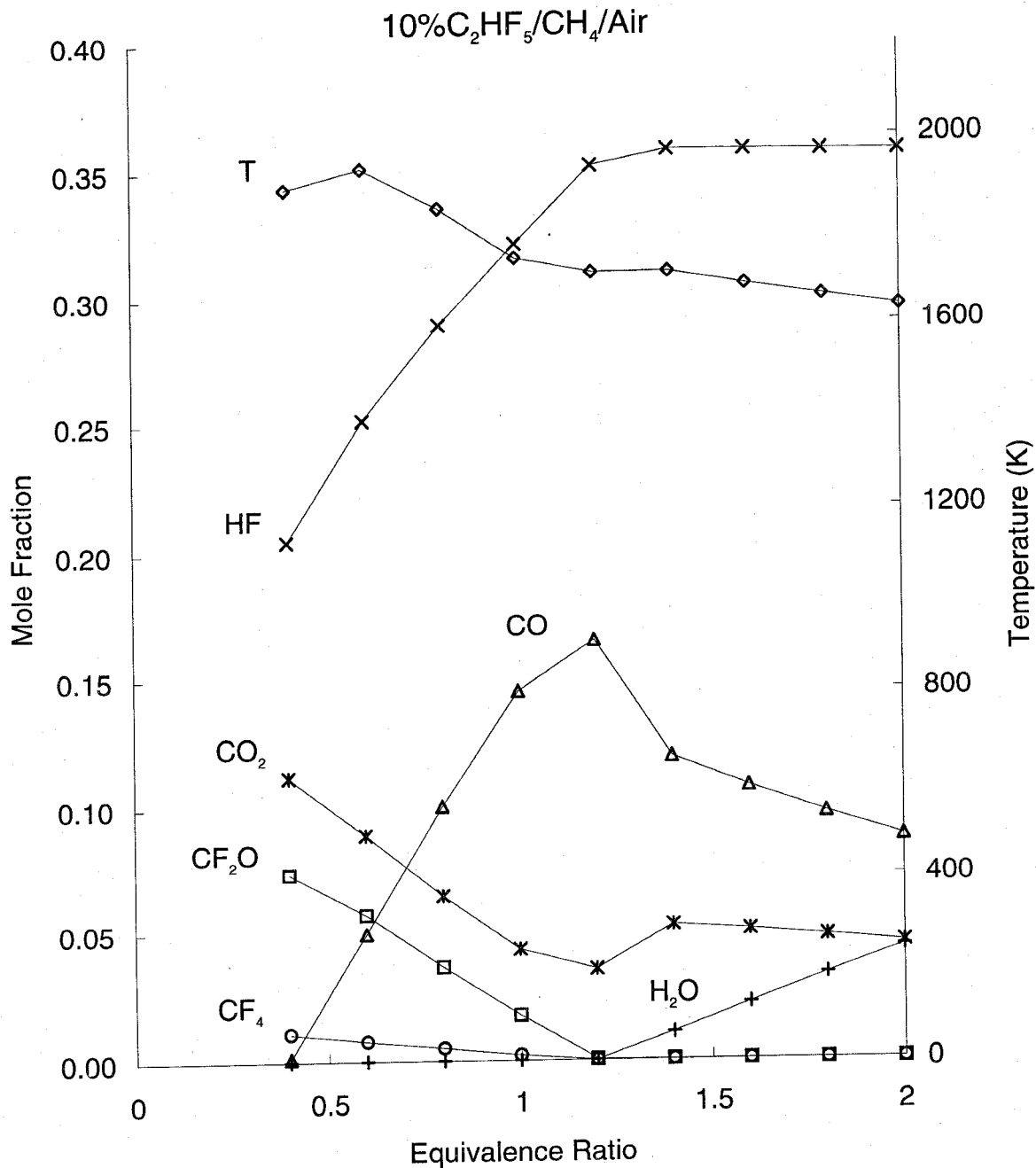


Figure 6. Equilibrium temperature and composition of combustion/inhibition products in the 10 % $C_2HF_5/CH_4/Air$ mixture versus mixture equivalence ratio.

transport rates of species into the reaction zone depend upon the rate at which they are consumed there. Thus, species which are consumed slowly will build in concentration, which reduces the transport rate to the reaction zone. That prevents attainment of chemical equilibrium. In order to consider simultaneously the interplay of thermodynamics and kinetics in a flame (while still avoiding the added complexity of non-premixed conditions), this section describes numerical calculations of the structure of premixed flames. These calculations allow consideration of the effect of the inhibitor on the overall reaction rate (which is affected by both temperature and species concentrations). In addition, the premixed flame calculations permit examination of the exact chemical routes of formation of HF, so that additional factors which may increase or decrease HF formation rates may be considered.

In order to begin to understand the chemical kinetic limitations to HF formation, numerical modeling studies have been performed for premixed flames inhibited by the fluorinated inhibitors. The flame structure (temperature and species concentration profiles through the flame) have been calculated for premixed methane-air flames in the presence of fluorinated hydrocarbon inhibitors. From these solutions, the chemical reaction rates and the convective and diffusion transport rates of every species can be determined at each point in the flame, allowing a comprehensive understanding of HF formation for these laboratory flames. The knowledge obtained is then used to provide guidance in interpreting large-scale tests of HF formation under other flame conditions.

As a first test of the performance of the chemical kinetic mechanism, the burning velocities of methane-air flames in the presence of the inhibitors have been measured. As will be demonstrated below, the agreement is good, providing increased confidence in the capabilities of the model. Two separate experiments and the accompanying numerical analyses are presented in this section. The first set of experiments involves a nozzle burner, used to produce nearly adiabatic atmospheric pressure flames. In the second set of experiments (conducted at the Massachusetts Institute of Technology), the measurements of burning velocity are extended to higher initial pressure and temperature through the use of a constant volume combustion device (bomb) - (Hochgreb *et al.*, 1994; VanDerWege *et al.*, 1995). The predicted burning velocity reductions for each device are compared with the results of numerical calculations. The calculated flame structure is then used to understand the HF formation under both atmospheric pressure and at elevated pressures and temperatures (which may be representative of suppressed dry-bay fires).

10.5.2 Background. Early studies of the inhibitory effects of halogenated hydrocarbons on flames were conducted in premixed systems (Burgoyne *et al.*, 1948; Coleman, 1951; Belles *et al.*, 1957; Simmons *et al.*, 1956; Garner *et al.*, 1957; Rosser *et al.* 1959; Lask and Wagner, 1962). The premixed laminar burning velocity is a fundamental parameter describing the overall reaction velocity, heat release, and heat and mass transport in a flame. In addition, the reduction in the premixed flame burning velocity is useful for understanding the mechanism of chemical inhibition of fires since diffusion flames often have a stabilization region which is premixed, and good correlation has been found between the reduction in burning velocity and the concentration of inhibitors found to extinguish diffusion flames (Hastie, 1975). Premixed flame burners have flow fields which are relatively easily characterized, making interpretation of the inhibitor's effect on the overall reaction rate straightforward.

The present research extends the investigations of burning velocity reduction to fluorinated inhibitors in hydrocarbon flames and applies a newly-developed kinetic mechanism to model the experiments. The burning velocity measurements are examined as a first step in the validation of the mechanism, and the numerical results are used to study the mode of inhibition of the fluorinated agents and the mechanisms of HF formation.

10.5.3 Experiment - Nozzle Burner. Numerous techniques exist for measuring burning velocities of flames, and there are good reviews in the literature (Linnett, 1953; Andrews and Bradley, 1972). All of the flame and burner geometries employed, however, cause deviations from the desired one-dimensional, planar, adiabatic flame. In the present research, a premixed conical Bunsen-type nozzle burner is used for the atmospheric pressure experiments. This method was selected for the flame speed measurements because its simplicity allows rapid assessment of the behavior of a number of halon alternatives. The low rate of heat loss to the burner, the low strain rate, and the low curvature facilitate comparisons of the experimental burning velocity with the predictions of a one-dimensional numerical calculation of the flame structure. Although measurement of a true one-dimensional, planar, adiabatic burning velocity is difficult, the relative change in the burning velocity can be measured with more confidence. Consequently, the burning velocity reduction in the present work is normalized by the uninhibited burning velocity. For comparison with the results of other researchers, the absolute burning velocities of the uninhibited flames are also presented.

The burner consisted of a Mache-Hebra nozzle burner (Mache and Hebra, 1954; Van Wouterghem and Van Tiggelen, 1954) 27 cm long, with an inner diameter of 22 mm and wall thickness of 1.5 mm. A contraction at the top to a nozzle diameter of 1.02 (+/- 0.005 cm) occurs over a length of 3 cm. The nozzle contour is designed to produce straight-sided schlieren and visible images which are very closely parallel. The burner is placed in a square acrylic chimney 10 cm wide and 86 cm tall with provision for co-flowing air or nitrogen gas (for the present data, the co-flow velocity is zero). Gas flows are measured with digitally-controlled mass flow controllers (Sierra Model 860¹) with a claimed repeatability of 0.2 % and accuracy of 1 %, which have been calibrated with bubble and dry (American Meter Co. DTM-200A) flow meters so that their accuracy is 1 %. The fuel gas is methane (Matheson UHP). House compressed air (filtered and dried) is used after it has been additionally cleaned by passing it through an 0.01 mm filter, a carbon filter, and a desiccant bed to remove small aerosols, organic vapors, and water vapor. The product gas temperature of the uninhibited flames is measured with Pt/Pt 6 % Rh - Pt/Pt 30 % Rh thermocouples which are coated with Yttrium oxide to reduce catalytic reaction on the thermocouple surface. Measurements with two bead diameters (344 and 139 μm) allow correction for radiation losses.

For the present data, the visible flame height is maintained at a constant value of 1.3 cm to provide similar velocities of heat loss to the burner, while the desired equivalence ratio and inhibitor concentration are preserved. An optical system provides simultaneously the visible and schlieren images of the flame. A 512 by 512 pixel CCD array captures the image which is then digitized by a frame-grabber board in an Intel 486-based computer. The flame area is determined (assuming axial symmetry) from the digitized schlieren image using custom-written image processing software. The average mass burning velocity for the flame is determined using the total area method.

10.5.4 Experiment - Bomb. For the elevated pressure experiments, a constant volume combustion device is used which is amenable to flame speed measurements at elevated and reduced pressures. The experimental apparatus consists of a spherical container 15.24 cm in diameter with one inlet port through which the combustible mixture is introduced. Ignition is provided by two extended electrodes at the center of the bomb. A pressure transducer monitors the pressure of the device as the fuel is consumed. The surface of the bomb was coated with vacuum grease to avoid corrosion by the

¹Certain trade names and company products are mentioned in the text or identified in an illustration in order to specify adequately the experimental procedure and equipment used. In no case does such identification imply recommendation or endorsement by the National Institute of Standards and Technology, nor does it imply that the products are necessarily the best available for the purpose.

products of combustion. The bomb was initially evacuated, and precalculated partial pressures of inhibitor, fuel and air were added. Care was taken to remove the acid combustion products before evacuating the bomb for the next experiment. A more detailed description of the apparatus is given by Metghalchi and Keck (1980).

After introduction of the combustible mixture in the bomb, the flame is ignited at the center and a calibrated pressure trace is obtained. Given the initial conditions, it is possible to relate the pressure signal to the extent of reaction. By solving the energy and mass conservation equations, the flame speed is determined as a function of the temperature and pressure of the adiabatically compressed, unburned mixture ahead of the flame. Allowances are made for property variation in the burned and unburned gases due to temperature change and heat transfer to the wall.

10.5.5 Model. The structure of the inhibited premixed methane-air flame is calculated using currently available techniques (Kee *et al.*, 1980; Kee *et al.*, 1983; Kee *et al.*, 1988). The equations of mass, species, and energy conservation are solved numerically for the initial gas compositions of the experiments. The solution assumes isobaric, adiabatic, steady, planar, one-dimensional, laminar flow and neglects radiation and the Dufour effect (concentration gradient-induced heat transfer) but includes thermal diffusion. The calculations employ a chemical kinetic mechanism recently developed at NIST (Burgess *et al.*, 1994; Burgess *et al.*, 1995) for fluorine inhibition of hydrocarbon flames, which is based on earlier work (Burgess *et al.*, 1993; Westmoreland *et al.*, 1994; Nyden *et al.*, 1994). The 83-species mechanism uses a hydrocarbon sub-mechanism and adds C_1 (200 reactions) and C_2 (400 reactions) fluorochemistry. The hydrocarbon sub-mechanism has been updated to use GRI-Mech (31 species, 177 reactions (Frenklach *et al.*, 1994) which more closely predicts our experimental uninhibited burning velocities. The fluorinated-species thermochemistry in the references (Burgess *et al.*, 1994; Burgess *et al.*, 1995) is from the literature when available and is otherwise estimated using empirical methods (such as group additivity) and through application of ab initio molecular orbital calculations. Fluorinated species reaction rates from the literature were used when available and these were extended to wider temperature and pressure ranges using standard methods based on classic statistical mechanics and quantum mechanics. Where no rate data were available, rate constants were estimated by analogy with hydrocarbon reactions. Although all of the reactions are not necessary to describe the present flames adequately, the comprehensive full mechanism is used for these initial calculations. Reduction of the mechanism will be performed later after more experimental validation. It should be emphasized that the mechanism adopted for the present calculations should be considered only as a starting point. Numerous changes to both the rates and the reactions incorporated may be made once a variety of experimental and theoretical data are available for testing the mechanism.

10.5.6 Results. In the nozzle burner flames, the radiation-corrected temperature of the uninhibited flames is measured at 4 mm above the flame tip to be 2054, 2075, and 2050 (+/- 70 K) for $\phi = 0.95$, 1.0, and 1.05 respectively, while the adiabatic flame temperature is calculated to be 2191, 2229, and 2234 K. In these experiments, the measured final temperatures at a point slightly downstream from the reaction zone are about 150 K lower than the calculated adiabatic flame temperatures. Heat losses to the burner, although important near the rim, are not expected to be large compared to the heat release integrated over the entire flame. The quartz tube of the burner was not observed to increase appreciably in temperature during the experiments. The observed heat loss may be due to non-one-dimensional effects, radiation, or chemical non-equilibrium in the post-combustion gases. Nonetheless, since the temperature difference is not too great, it seemed most appropriate to model the flame as freely-propagating rather than burner-stabilized (where heat losses, for example in a flat flame burner, are greater).

The average burning velocity is determined using the total area method described above, in which the flow rate of reactants is divided by the measured schlieren image area. Figure 7 presents the measured mass burning velocity (expressed as the equivalent flame velocity for flame propagation into reactants at 298 K) as a function of equivalence ratio for the uninhibited methane-air flame, together with the results of Rosser *et al.*, (1959) and Vagelopoulos *et al.*, (1994). The present data are about 7 % higher than the results of Rosser *et al.* (1959) for $\phi < 1.0$ and up to 30 % higher for $\phi > 1.0$. In the recent experiments of Vagelopoulos *et al.*, 1994, the measured burning velocities of premixed planar counterflow flames are extrapolated to zero stretch. For values of ϕ from 0.8 to 1.2 the present data are 3 to 7 % higher than their results. This discrepancy may result from curvature and stretch in the present flame which occurs in the conical Bunsen type flame. Figure 7 also shows the burning velocity as a function of stoichiometry calculated using the present mechanism. The agreement between the experiment and model is very good for the number of grid points used in the calculation; however, using three hundred or more grid points gives burning velocities slightly lower, so that the experimental results would be about 7 % too high for values of ϕ from 0.8 to 1.2. Nonetheless, this agreement is considered to be good, and is expected since GRI-Mech is being developed using existing experimental methane-air burning velocities and the present experimental results are close to those of other researchers.

The results for the flames inhibited by N_2 , CF_4 , CH_2F_2 , and CF_3H are presented in Figures 8 - 11 respectively. The figures show the burning velocity of the inhibited flame (normalized by the burning velocity of the uninhibited flame) for values of ϕ of 0.9, 1.0, and 1.1 (here, the equivalence ratio is calculated based on the oxygen demand of the fuel only). The mole fraction of the inhibitor in Figure 8, as well as in all other figures, refers to the entire reactant mixture: fuel + oxidizer + inhibitor. As a baseline case, Figure 8 shows the results for a flame inhibited by N_2 . The excellent agreement in Figure 8 is again a consequence of the performance of GRI-Mech. Most of the scatter in the plots of the experimental burning velocity results from flame fluctuations: the camera framing rate is 30 Hz and flame area is obtained from a single image; signal averaging would reduce this scatter.

In Figures 9 - 11, the numerical results are presented in two ways: the solid lines present solutions which allow full chemistry, while the dotted lines present solutions in which the inhibitor is constrained to be inert so that only the thermal and transport properties of the flame are modified by the inhibitor. Experimental and numerical results are presented for inhibitor mole fractions up to 0.08 when possible. Although measurements of the burning velocity reduction of even higher inhibitor mole fractions is desirable, flames could not be stabilized much beyond 8 % for most of the inhibitors. For the lean stoichiometry and the inhibitors CF_4 and CF_3H , flames could not be stabilized for inhibitor mole fractions above about 4 %. Figure 9 shows the results for CF_4 . The lines are nearly coincident for the inert calculations at $\phi = 1.0$ and 1.1, and the reacting calculation at $\phi = 0.9$ and 1.0. The experiments show slightly more inhibition for richer flames; whereas the model shows more inhibition for the leaner flame. The calculation which assumes CF_4 to be inert shows slightly less inhibition than the solution which allows decomposition, but again, the difference is small. The calculated burning velocity is in excellent agreement with the numerical solution which allows reaction of CF_4 . Clearly, decomposition of CF_4 in the flame is kinetically limited. Tetrafluoromethane influences the burning velocity mainly through its role as an inert species which lowers the flame temperature.

Figure 10 presents the results for CH_2F_2 . Again, rich flames show more inhibition than the lean flames but the effect is large for CH_2F_2 . The fuel effect of adding CH_2F_2 to lean flames increases the adiabatic flame temperature above the uninhibited case for low CH_2F_2 mole fractions, promoting a higher burning velocity. In competition with this effect is the slower kinetics caused by presence of the fluorine compounds as discussed below. Note that although the adiabatic flame temperature is higher for lean flames with up to 5 % CH_2F_2 , the burning velocity is still reduced relative to the

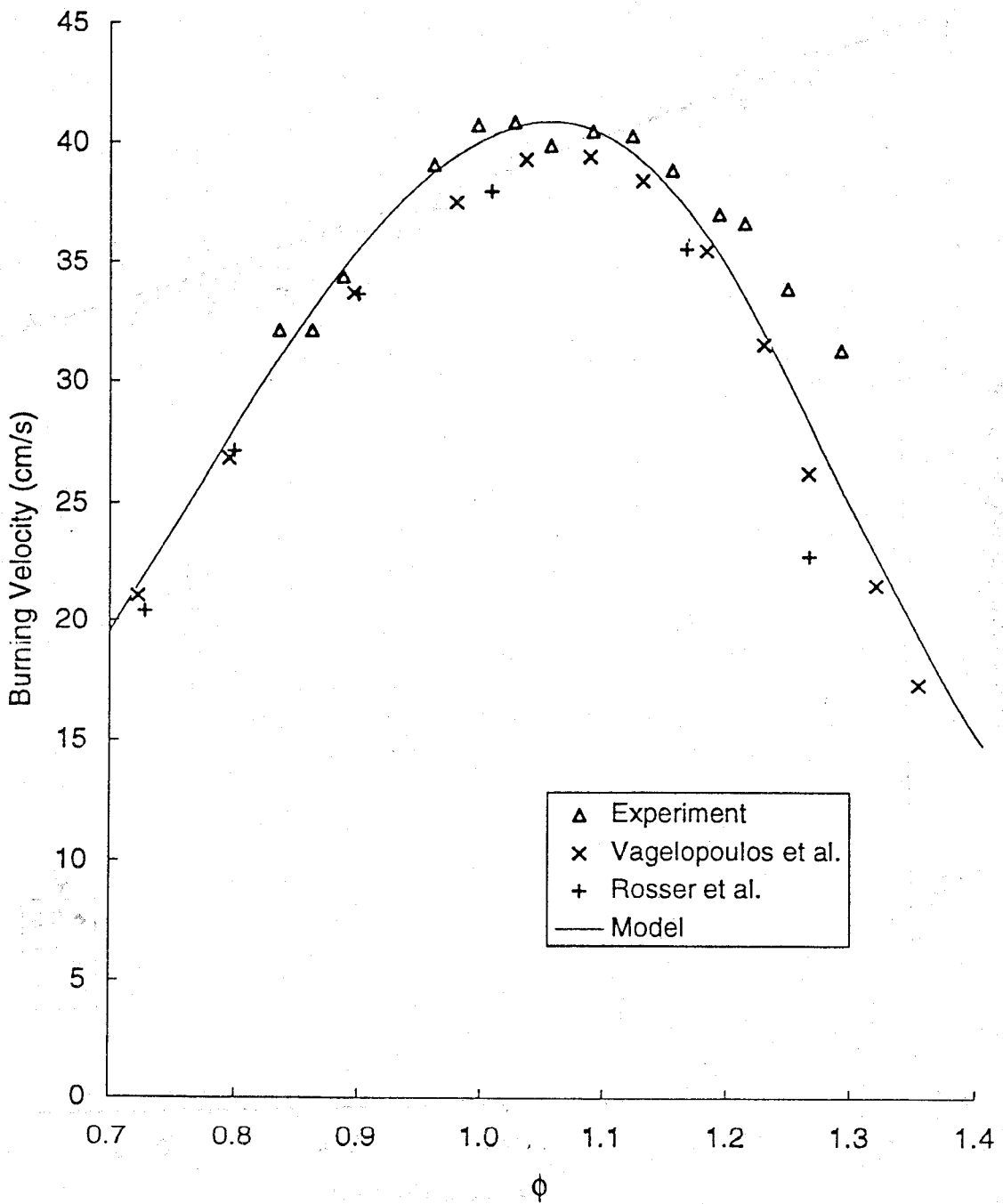


Figure 7. Burning velocity determined using the total area method from the schlieren image of the premixed methane-air flame in the nozzle burner as a function of fuel-air equivalence ratio.

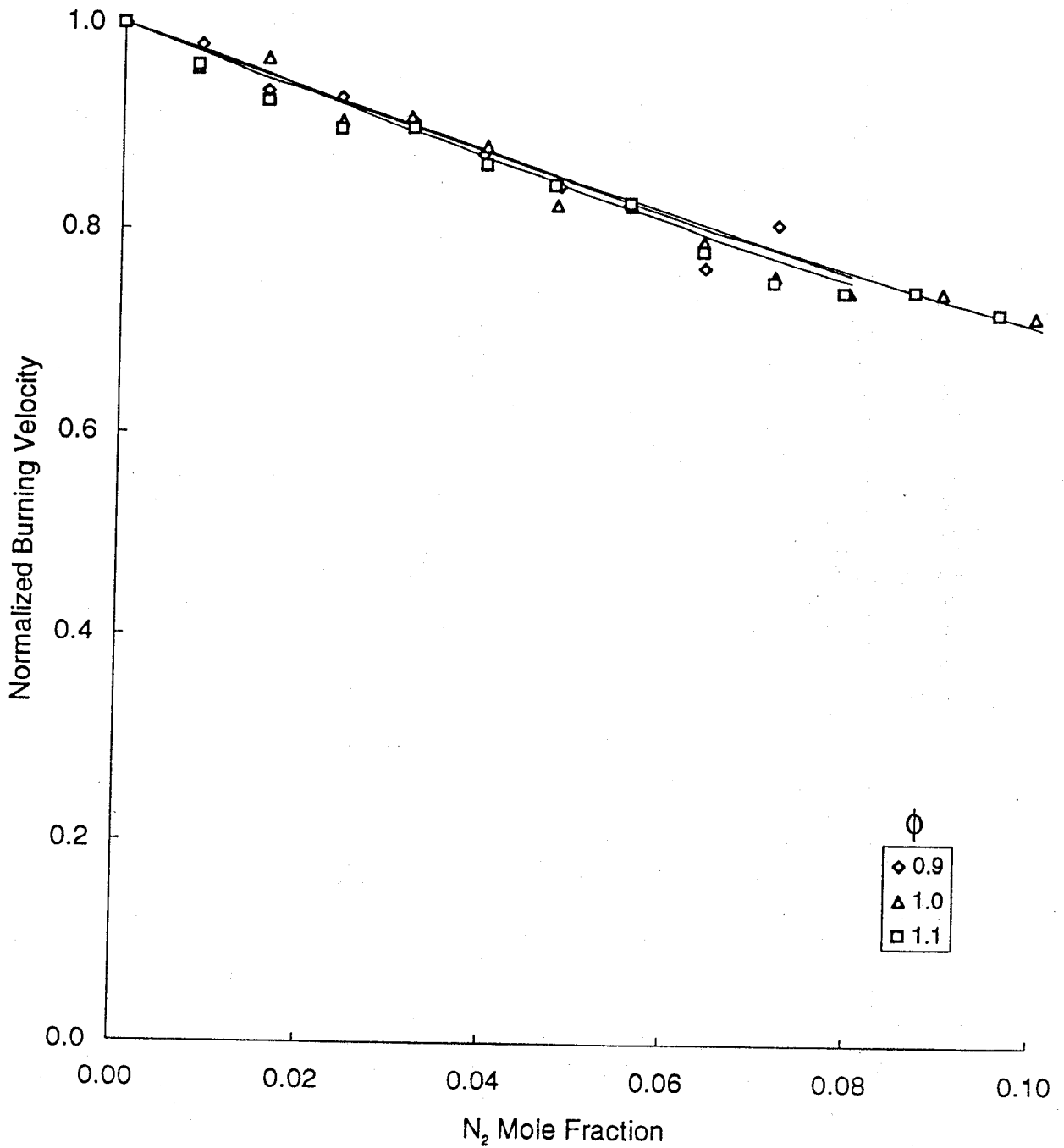


Figure 8. Normalized burning velocity of premixed methane-air flame normalized by the uninhibited burning velocity at the same stoichiometry as a function of the N₂ mole fraction of the total reactant stream.

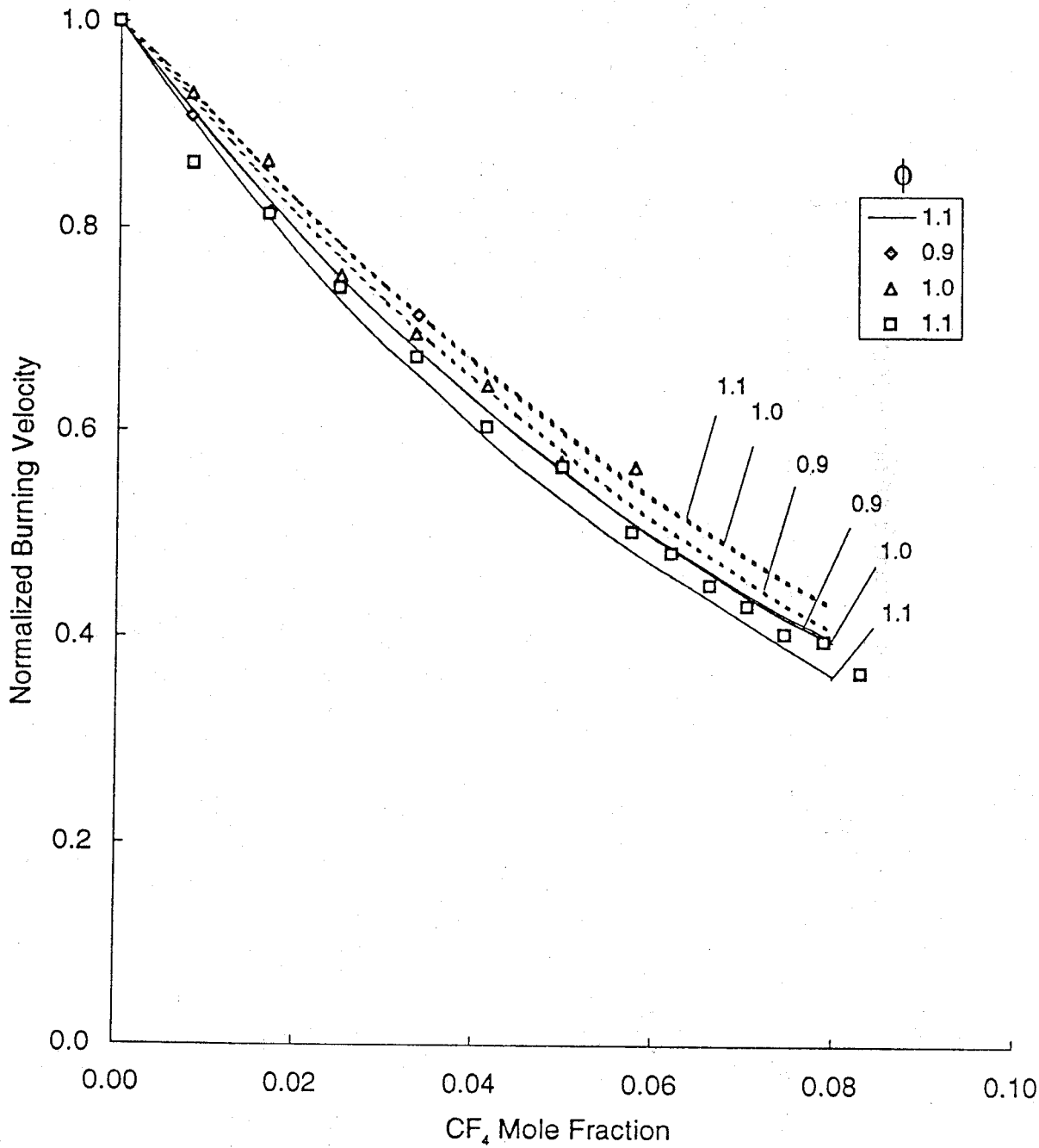


Figure 9. Normalized burning velocity of premixed methane-air flame as a function of the CF_4 mole fraction for $\phi = 0.9, 1.0,$ and 1.1 . Symbols: experimental data; solid lines: reacting inhibitor; dotted lines: inert inhibitor.

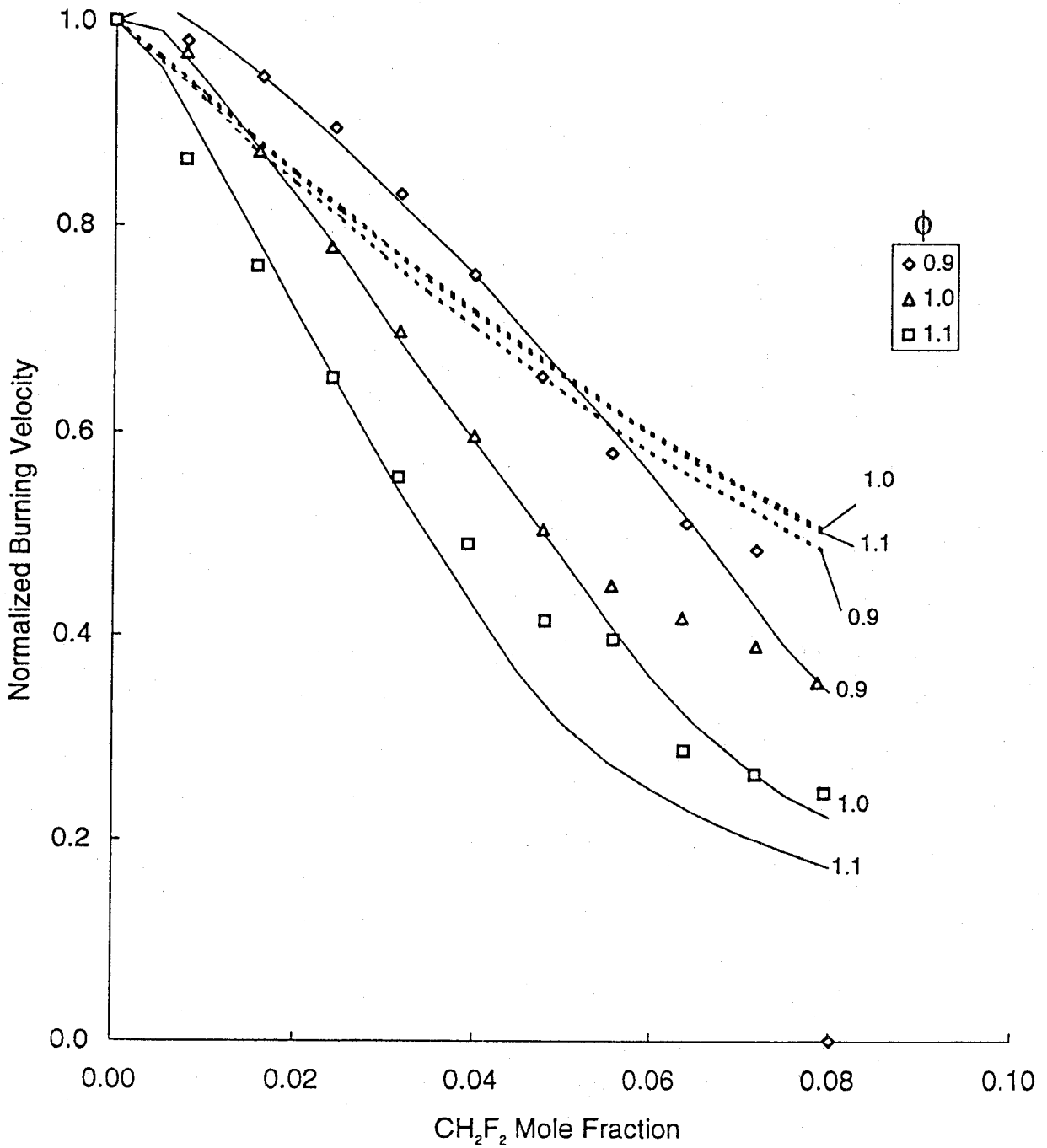


Figure 10. Normalized burning velocity of premixed methane-air flame as a function of the CH_2F_2 mole fraction for $\phi = 0.9, 1.0,$ and 1.1 . Symbols: exp. data; solid lines: reacting inhibitor; dotted: inert inhibitor.

uninhibited flame. The calculated burning velocities are very close to the measured values for CH_2F_2 mole fractions up to 5 %; as the inhibitor mole fractions reach 8 %, the calculations over-predict the burning velocity reductions by up to 17 %.

The results for CF_3H are shown in Figure 11. The mechanism is showing the proper qualitative features of the inhibition including the dependence on stoichiometry and the reduced inhibitory effect at higher inhibitor mole fractions; however, the calculation is showing up to 20 % more reduction in burning velocity than is observed in the experiments. Figure 12 summarizes the calculated burning velocity for inhibition by CH_4 and CF_4 , CH_2F_2 , and CF_3H at $\phi = 0.9$ and 1.1; a fit to experimental results for CF_3Br (Rosser *et al.*, 1994) are included for comparison. All calculations predict that the rate of reduction in the burning velocity with addition of inhibitor becomes less at higher inhibitor concentrations, and predict a strong effect of ϕ on the inhibition effect. The fluoromethanes are much less effective than CF_3Br at reducing the burning velocity of methane-air flames at these equivalence ratios. Interestingly, all of the fluoromethanes are less efficient at reducing the burning velocity of the rich methane-air flames than methane itself. For the slightly fuel lean flames, the fuel effect (increasing burning velocity of lean flames with addition of the inhibitor) is larger for methane than for the fluoromethanes, yet upon entering the fuel rich regime, the effect of methane as an inhibitor again is greater than the fluoromethanes.

Figures 13 - 15 present the burning velocity reduction caused by addition of the inhibitors C_2F_6 , C_2HF_5 , and $\text{C}_2\text{H}_2\text{F}_4$. As the figures show, the greatest reduction in burning velocity was obtained with the perfluorinated agent C_2F_6 , followed by C_2HF_5 and $\text{C}_2\text{H}_2\text{F}_4$. For the agent C_2F_6 , the burning rate calculated by assuming the agent to be inert under-predicts the burning velocity reduction by about 25 %, while the calculation which allows full reaction over-predicts by about 14 %. As shown in Figures 14 and 15, the results for C_2HF_5 and $\text{C}_2\text{H}_2\text{F}_4$ are similar. An important feature of the inhibition is its dependence on the equivalence ratio, with larger burning velocity reductions occurring in the richer flames. This dependence on the equivalence ratio becomes greater as the hydrogen content of the inhibitor increases. This feature is not captured by the inert calculations; in fact, they predict the opposite: a small decrease in inhibitor effectiveness as ϕ increases from 0.9 to 1.1. An additional observation, clearly illustrated in Figures 14 and 15, is that all of the inhibitors show reduced effectiveness as the inhibitor concentration increases. This has been observed for one-carbon fluorinated agents, where the mechanism for inhibitor consumption shifts from radical attack at low concentration, to thermal decomposition at high inhibitor concentration (Linteris, 1994). The results for the three-carbon fluorinated agents are presented in Figures 16 and 17. These agents, C_3F_8 and C_3HF_7 , are about as effective, on a volume basis, as the two-carbon inhibitors, and show the same large dependence on the equivalence ratio and on the inhibitor mole fraction. However, in the case of C_3HF_7 , the inhibition effect is strongest in the lean flame, whereas in all other cases the rich flames are inhibited most. The reasons for this are presently unclear but are of great interest.

As described above, the combustion bomb allows burning velocity measurements to be conducted for higher initial temperature and pressure. For the present experiments, the range of unburned gas pressures is 203 to 709 kPa (2 - 7 bar), and the temperatures, 330 to 500 K. Figure 18 shows a curve fit to the burning rate data collected in the bomb as a function of temperature and pressure. To allow comparison, the bomb results were extrapolated to the conditions of the nozzle burner described above. In the presence of the inhibitor CF_3H , the reduction in burning velocity as a function of CF_3H mole fraction is shown in Figure 19. As the figure indicates, the two experiments yield approximately the same burning rate reduction.

The measured burning rate as a function of unburned gas temperature (which is related to the unburned gas pressure) is shown in Figure 20. Experimental curves are shown for 0, 1, 2, and 5 % inhibitor at equivalence ratios near unity. The figure also shows the results of the numerical calculations of the burning rate using the kinetic mechanism described above. Although the burning

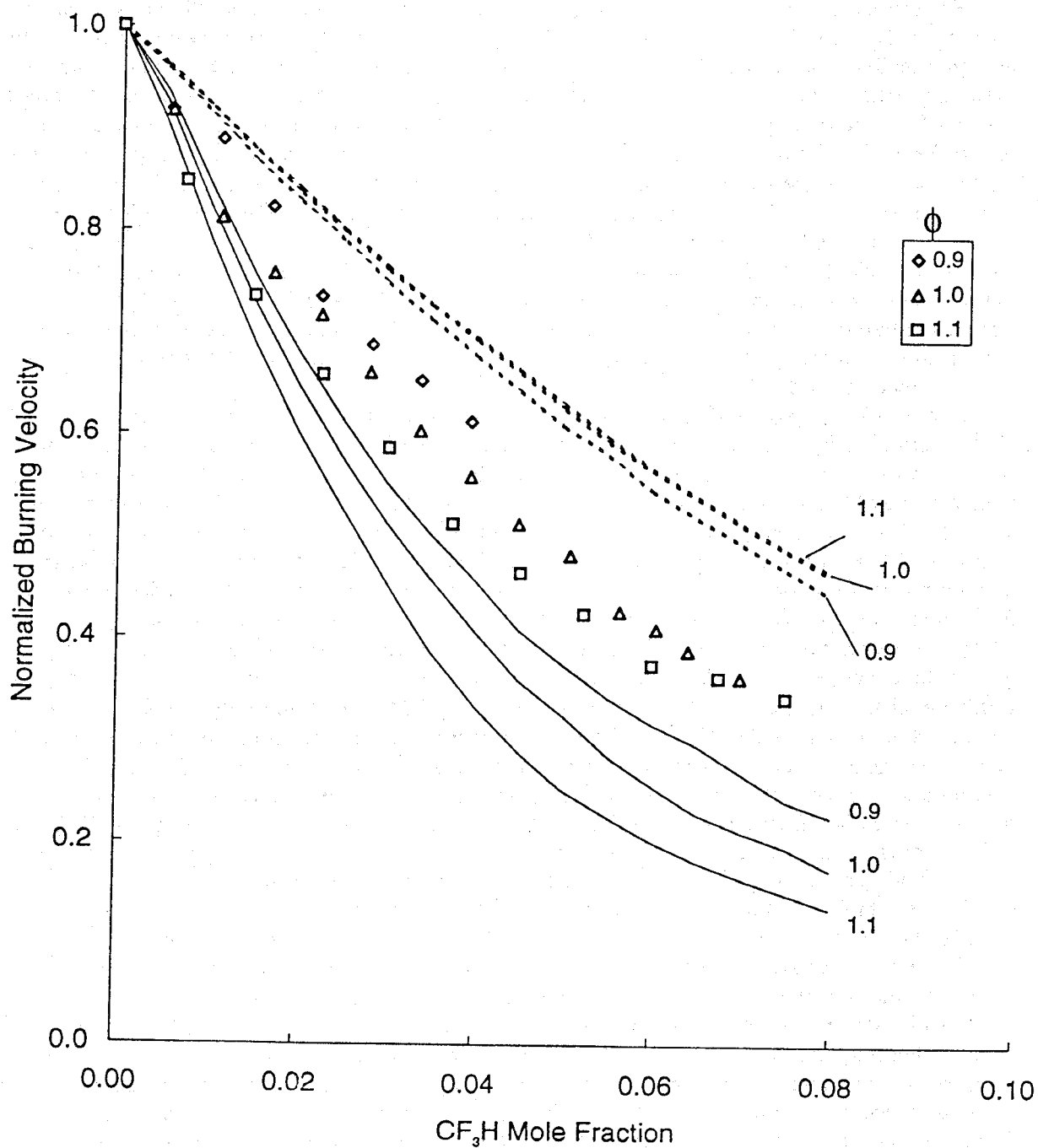


Figure 11. Normalized burning velocity of premixed methane-air flame as a function of the CF_3H mole fraction for $\phi = 0.9, 1.0,$ and 1.1 . Symbols: exp. data; solid lines: reacting inhibitor; dotted lines: inert inhibitor.

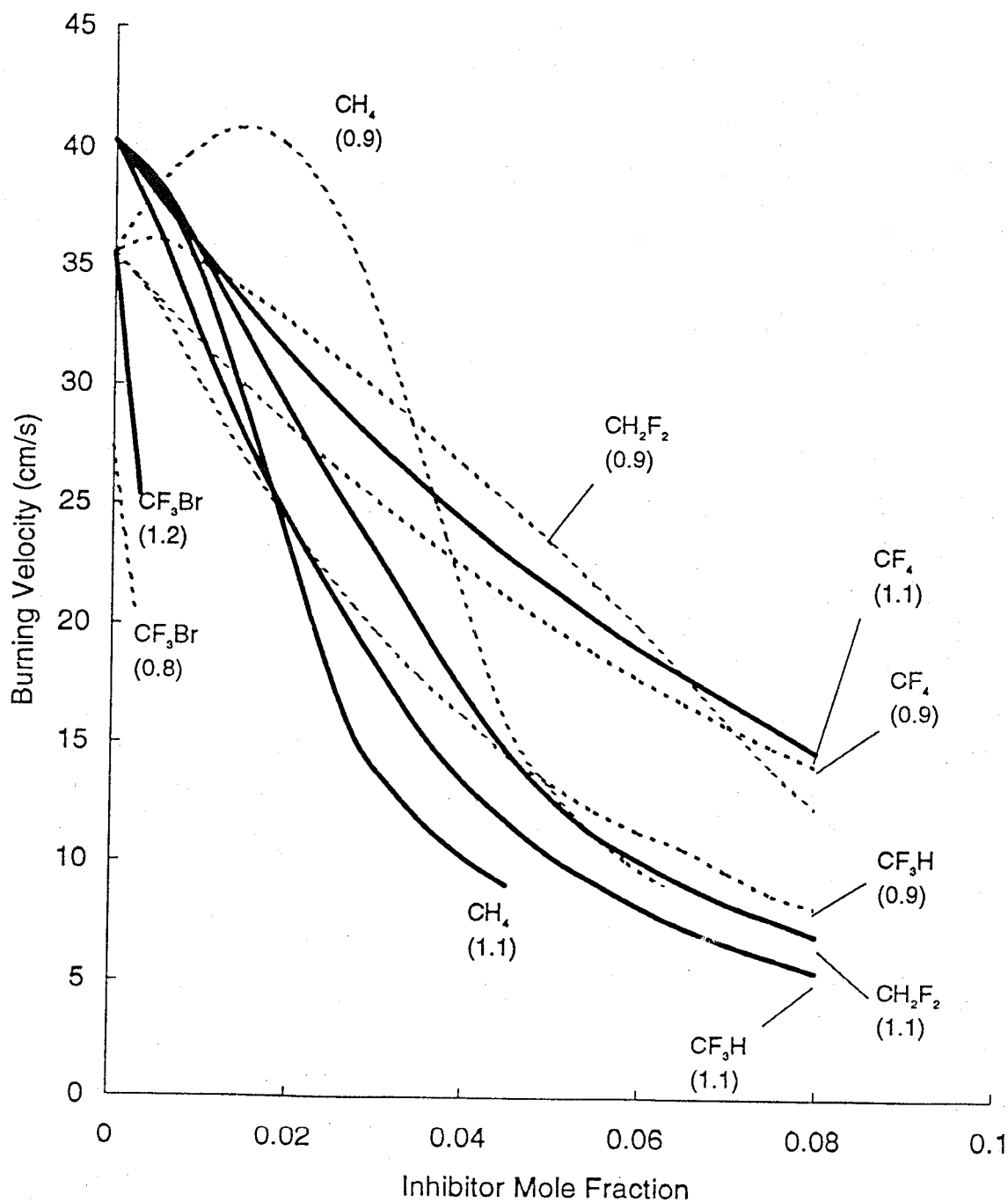


Figure 12. Calculated burning velocity of lean (dotted lines) and rich (solid lines) methane-air flames with addition of the agents CH₄, CH₂F₂, CF₃H, CF₄, and CF₃Br as flame inhibitors.

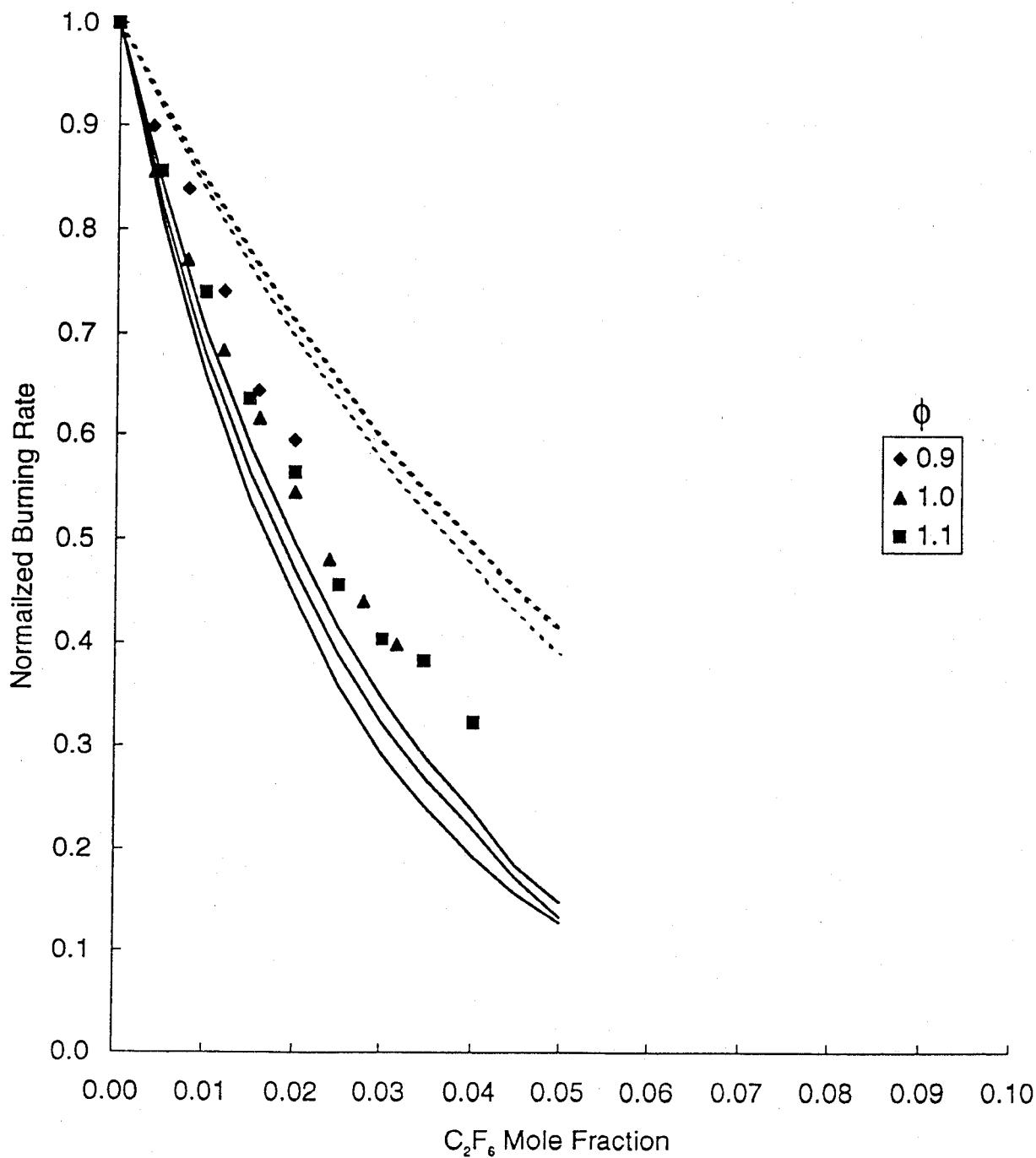


Figure 13. Normalized burning rate of premixed methane-air flame versus C_2F_6 mole fraction at $\phi = 0.9, 1.0,$ and 1.1 . Symbols: exp. data; solid lines: numerical - full chemistry; dotted: inhibitor not reacting.

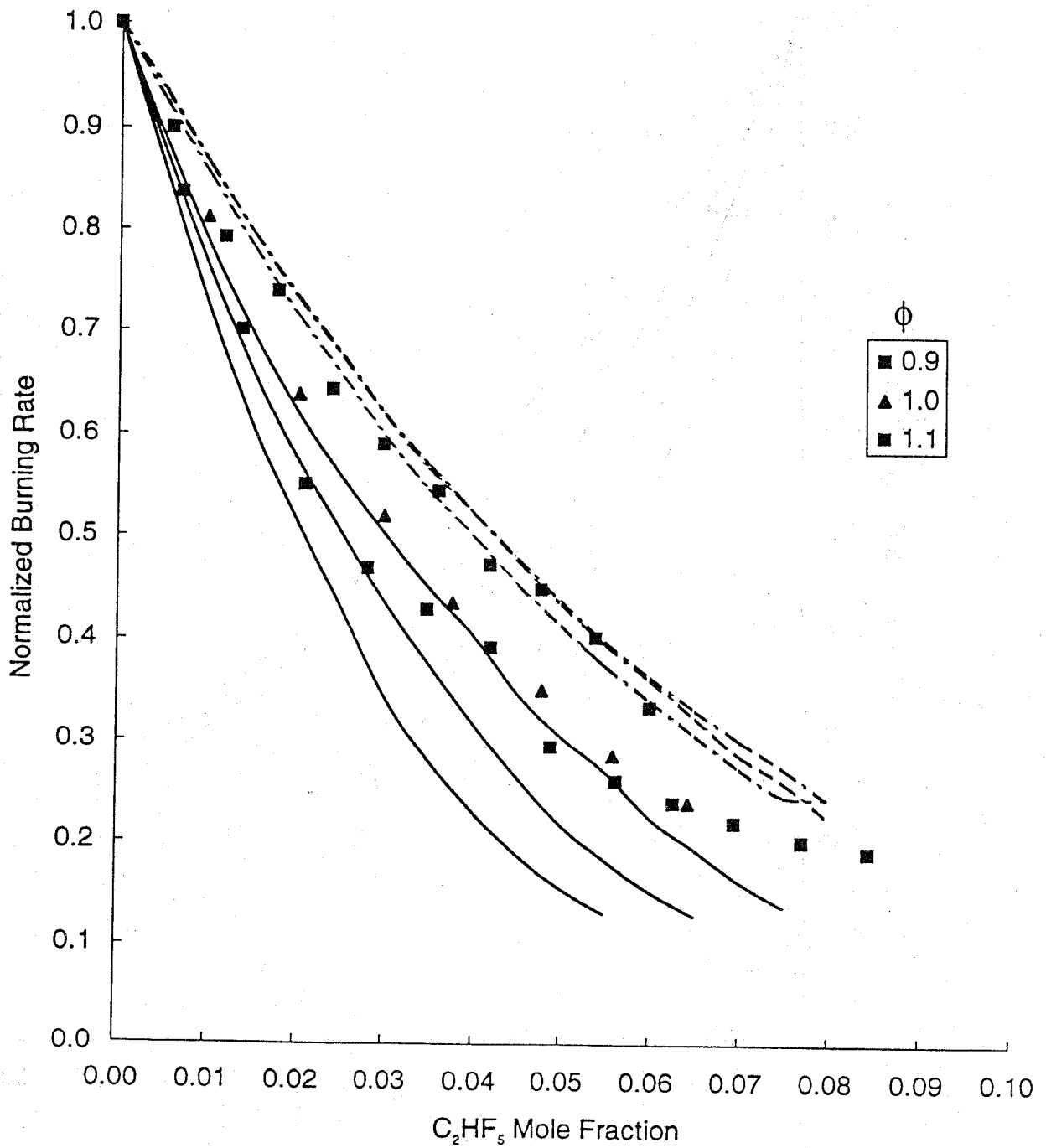


Figure 14. Normalized burning rate of premixed methane-air flame versus C_2HF_5 mole fraction at $\phi = 0.9, 1.0,$ and 1.1 . Symbols: exp. data; solid lines: numerical - full chemistry; dotted: inhibitor not reacting.

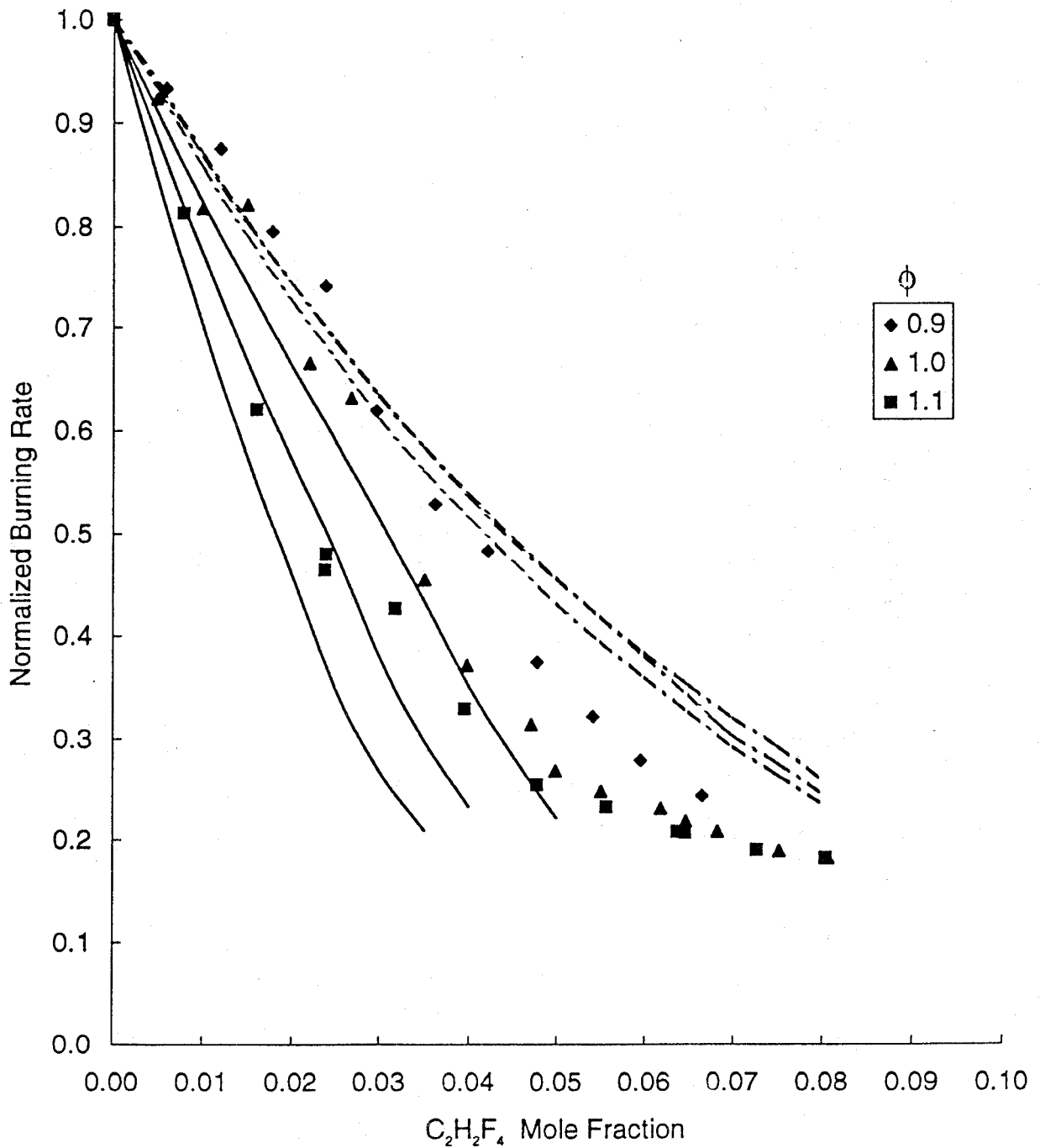


Figure 15. Normalized burning rate of premixed methane-air flame versus $C_2H_2F_4$ mole fraction at $\phi = 0.9, 1.0, \text{ and } 1.1$. Symbols: exp. data; solid lines: numerical - full chemistry; dotted: inhibitor not reacting.

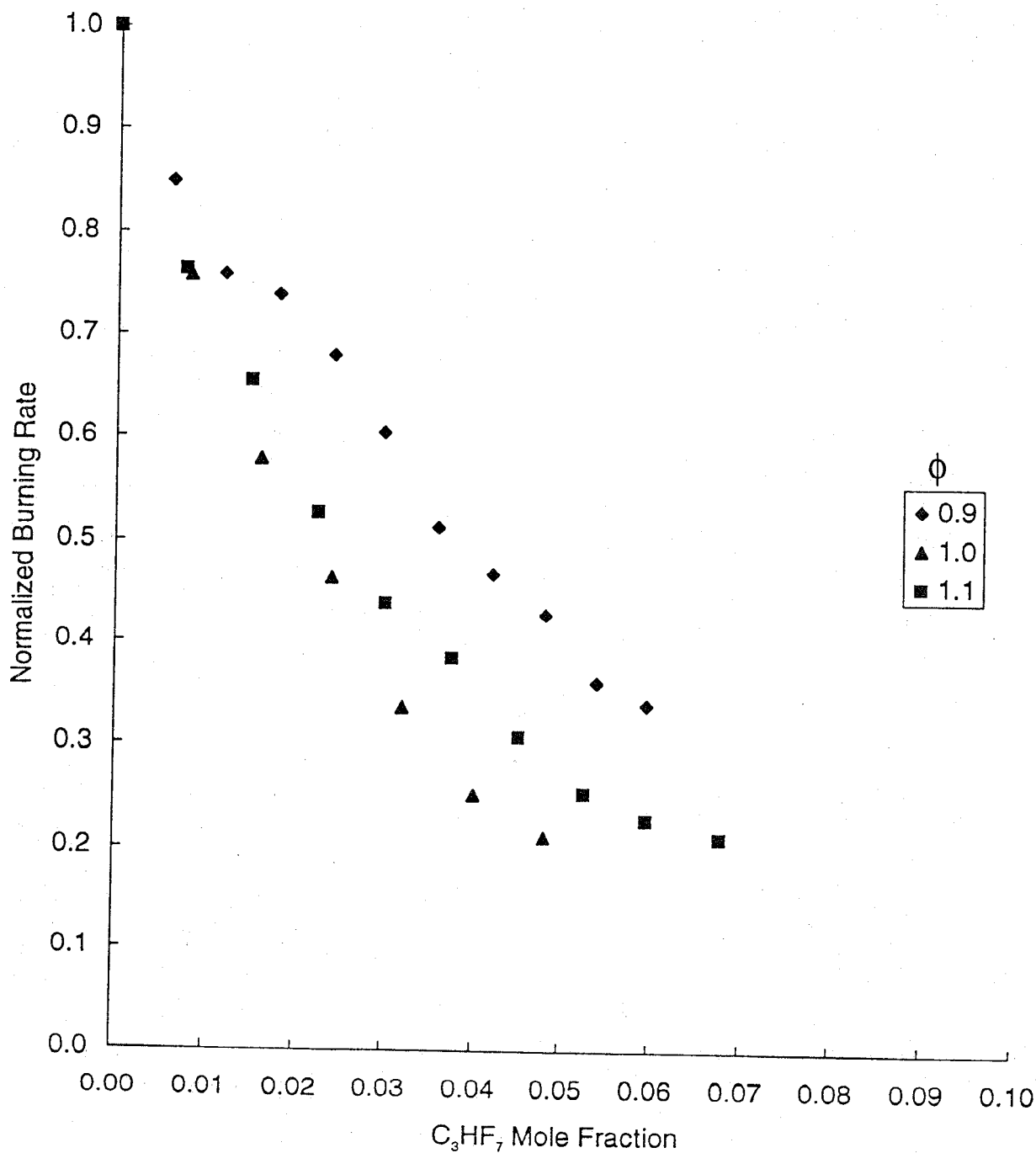


Figure 16. Normalized burning rate normalized by the uninhibited burning velocity at the same stoichiometry for the methane-air flame at fuel-air equivalence ratios of 0.9, 1.0, and 1.1 versus C_3HF_7 mole fraction.

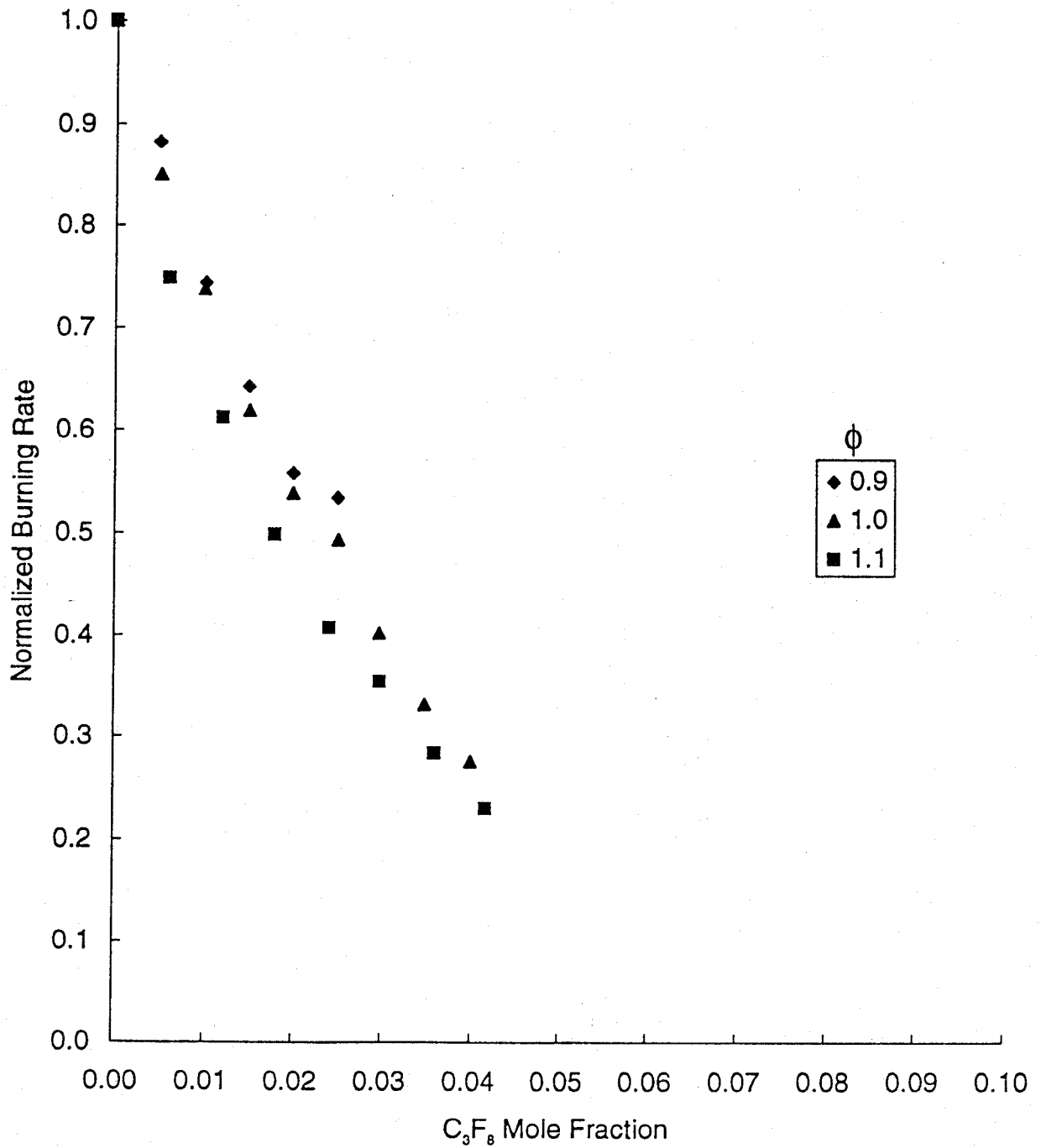


Figure 17. Normalized burning rate normalized by the uninhibited burning velocity at the same stoichiometry for the methane-air flame at fuel-air equivalence ratios of 0.9, 1.0, and 1.1 versus C_3F_8 mole fraction.

rate reduction is somewhat greater for the calculated flames as compared to the experiments, the model is able to reproduce many of the features of the flames. Both show a linear increase in the burning velocity with increased initial temperature and pressure, and similar behavior at all inhibitor concentrations.

While burning velocity comparisons are, by no means, a complete validation of the mechanism, they are an important first step. If the burning rate is wrong, the global reaction rate and flame thickness are probably wrong, and the predicted concentration profiles of the important species will be incorrect. Predicting the burning velocity is different from predicting the production of a species such as HF which has only a secondary effect on the heat release rate. Nonetheless, the reasonable agreement in the burning velocity results is reason to have more confidence in the predictive ability of the model, and to begin to use it to investigate HF formation in the present flames. Figure 21 shows the calculated species concentration profiles for methane-air flames with CF_4 , CF_3H , and CH_2F_2 at a mole fraction in the unburned gases of 4 %. The temperature and the mole fractions of CH_4 , agent, and HF are given as a function of position.

As the profiles for the agent mole fraction show, the agents CF_3H and CH_2F_2 behave similarly, whereas, CF_4 does not decompose appreciably in the 3 mm domain of the figure. The methane consumption is slightly slower in the inhibited flames, with CH_2F_2 slowing the consumption slightly more than CF_4 , but not as much as CF_3H . On the other hand, the temperature rise is greatest for the CH_2F_2 -inhibited flame and least for the CF_4 -inhibited flame. Clearly, the exothermicity of the reactions of fluorine increase the final temperature for an equivalent reduction in burning rate as compared to an agent which is nearly inert (CF_4). While CF_4 is predicted to form some HF, only a small fraction of that possible (about 15 %) forms within 3 mm. An important observation is that while the inhibitors CF_3H and CH_2F_2 require slightly higher temperatures to start to decompose than methane (*i.e.*, inhibitor decomposition occurs later), their consumption is complete at about the same point as for methane. Likewise, HF formation is nearly complete near end of the fuel consumption.

Figure 22 shows the results of similar calculations for a condition of 497 K and 659 kPa in the bomb. For these conditions, the final temperature is higher and the gradients of fuel, CF_3H , HF, and temperature are greater. Less carbonyl fluoride is formed, and it decomposes faster; however, the rate of formation of HF compared to the fuel decay is similar to the 298 K 101 kPa case.

The calculated flame structures for the two-carbon inhibitors show similar trends. Figure 23 presents these results for C_2F_6 , C_2HF_5 , and $\text{C}_2\text{H}_2\text{F}_4$ at 2 % in stoichiometric methane-air flames. The inhibitors again decompose later, but more rapidly, than the fuel, and HF formation is fast. The perfluorinated agents, in both cases, decompose the slowest yet provide the slowest temperature rise at the end of the flame. Decreased hydrogen content in the agent tends to favor higher concentrations of COF_2 as an intermediate.

Once the initial decomposition of the agent has occurred, the reaction of the intermediates and HF formation are rapid. This is clearly seen in Figure 24, where the temperature profile and the mole fractions of some intermediate species are illustrated for C_2HF_5 inhibition. Both the formation of fluorinated-species intermediates and their consumption occur over a narrow region of the flame.

Figure 25 shows the dominant reaction pathways indicated by the numerical calculations. The conditions shown correspond to inhibition by CF_3H under laboratory conditions in the nozzle burner (298 K, 101 kPa) and at elevated temperature and pressure in the bomb (497 K, 659 kPa). The mole fractions of inhibitor are 4 % and 5 % respectively. The arrows connect species of interest; next to the arrows are the second reacting species and the percent of the first reactant which goes through that route. The top number is the result for the atmospheric pressure, 298 K flames, while the lower number is the result for the higher pressure and temperature flame. With this chart, it is possible to study the reaction sequence for consumption of an inhibitor and its fragments, and the subsequent formation of unwanted by products. For example, the reactions which form HF are indicated in bold.

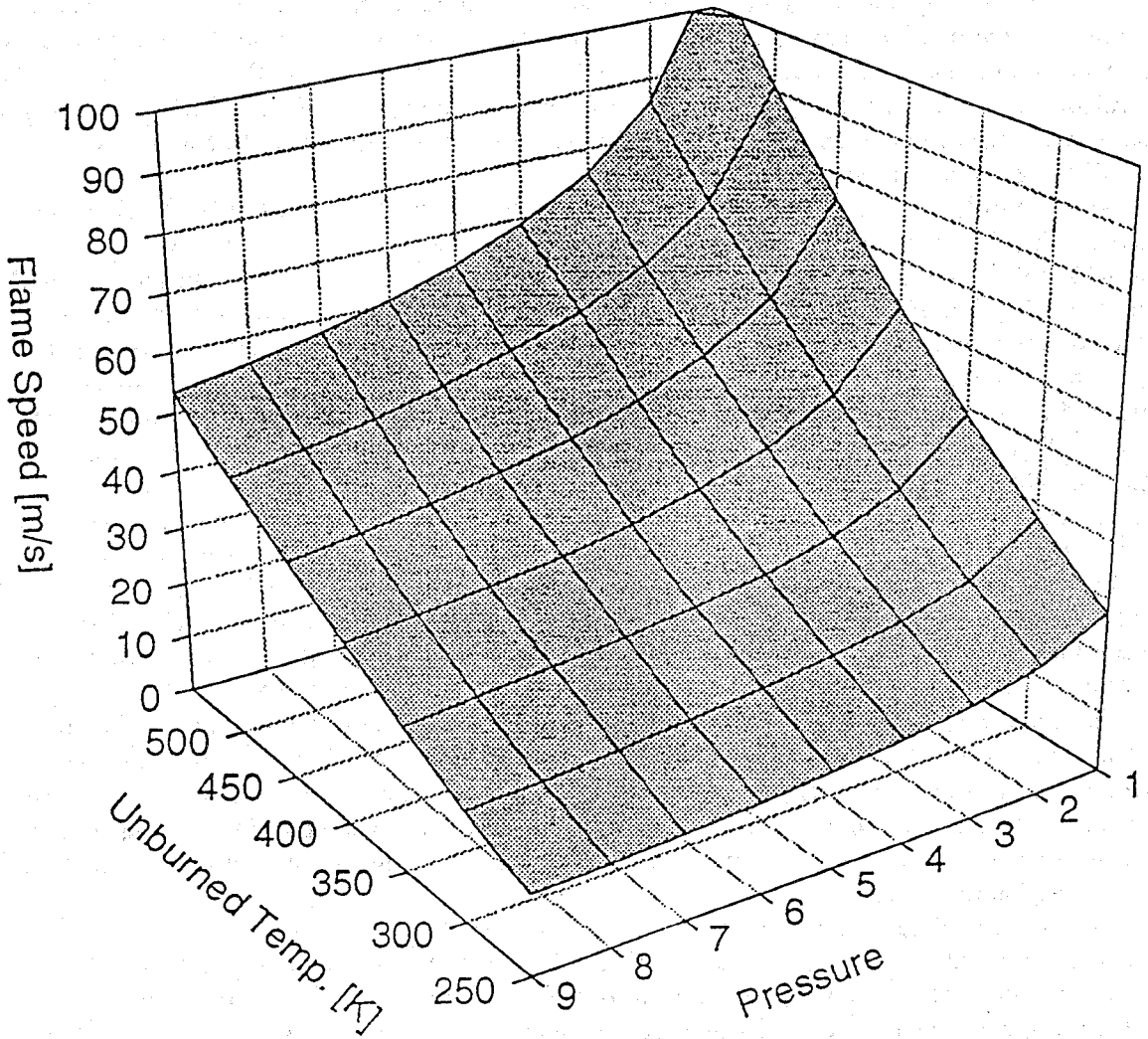


Figure 18. Curve fit to experimental burning rate velocity in combustion bomb (pressure in 10^5 Pa)

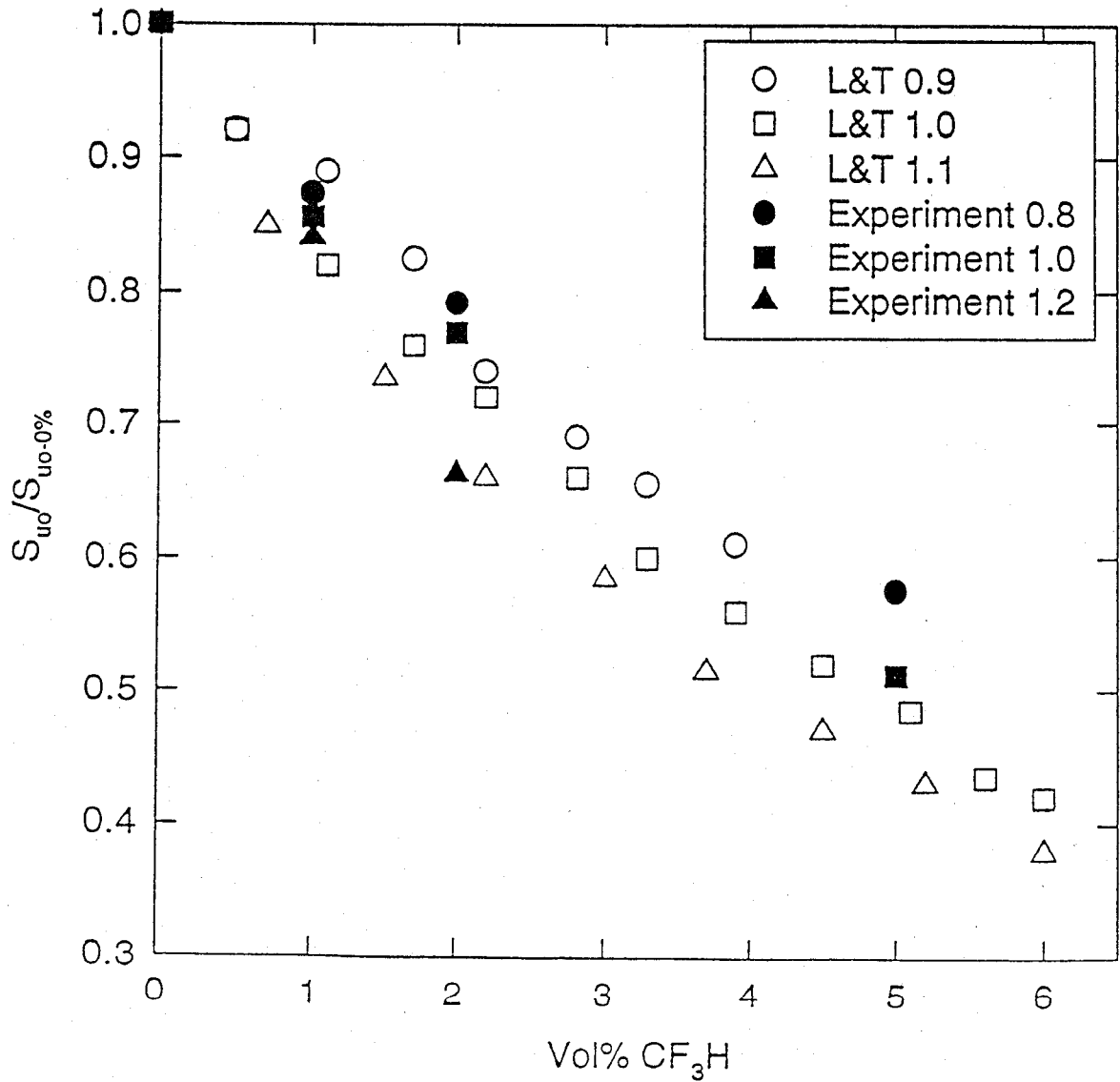


Figure 19. Normalized burning velocity of bomb experiments as a function of CF_3H mole fraction extrapolated to the conditions of the nozzle burner.

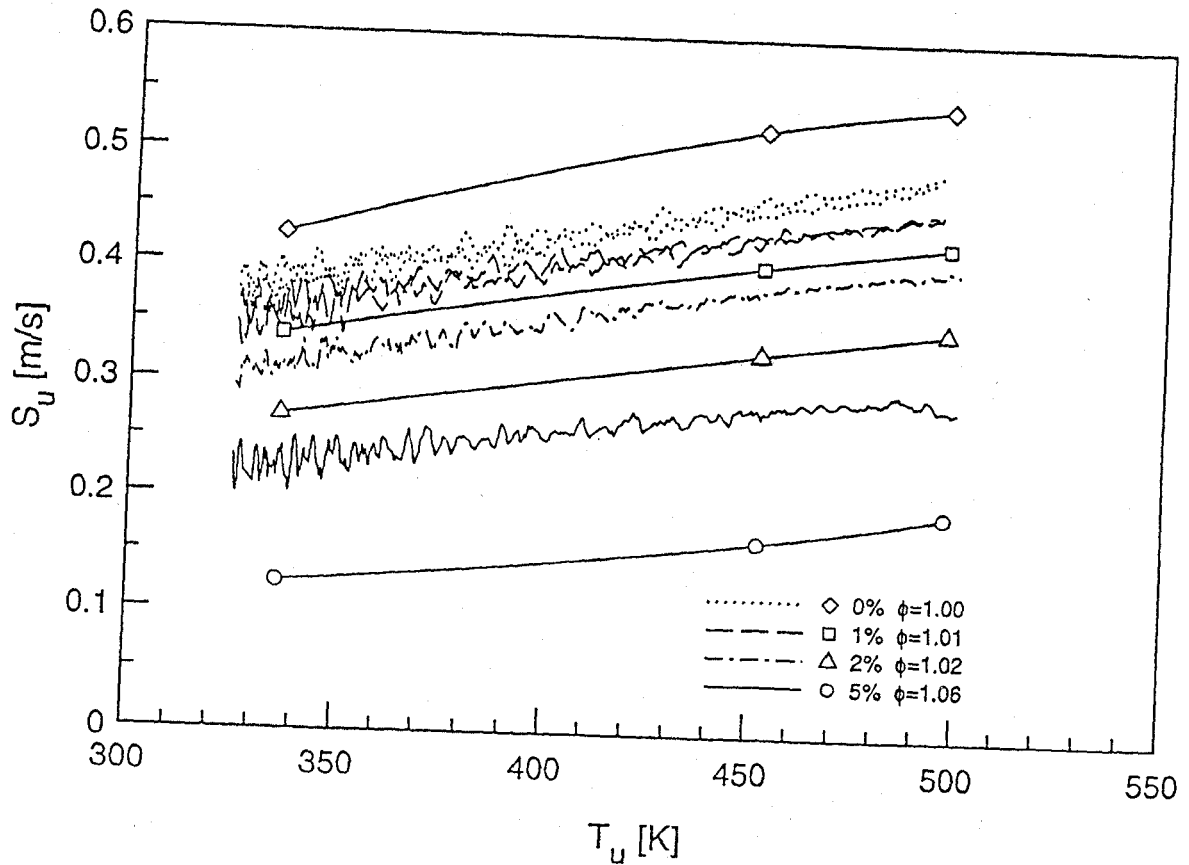


FIGURE #10 VanDerWege/Bush/Hochgreb/Linteris Combustion & Flame

Figure 20. Experimental versus calculated laminar flame speeds at a nominal equivalence ratio near 1.0 (0, 1, 2 and 5 % CF_3H in CH_4 -Air; $p_0 = 92.1$ kPa).

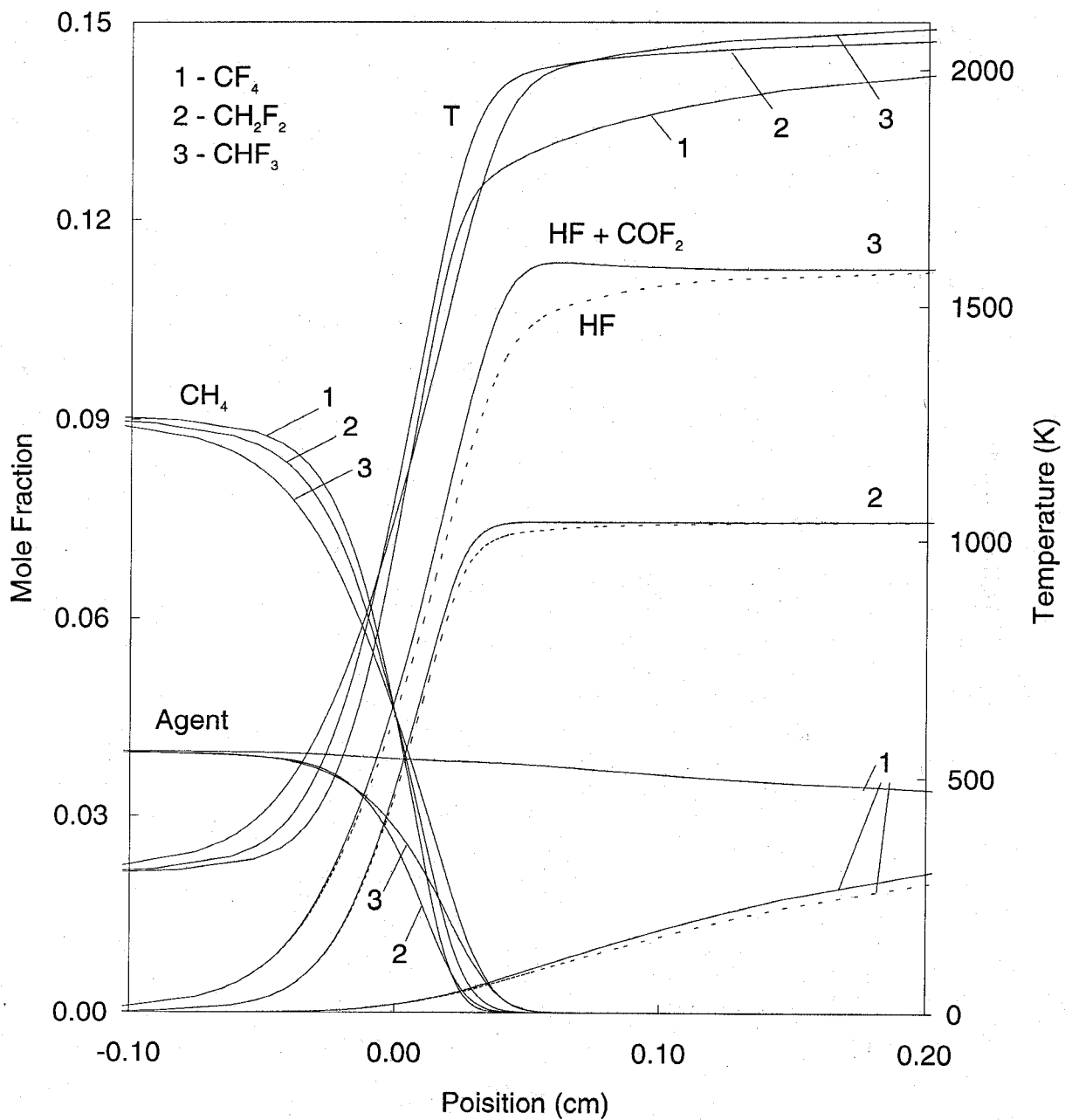


Figure 21. Calculated species mole fraction profiles for stoichiometric premixed methane-air flames with 4% CF_4 , CH_2F_2 and CHF_3 .

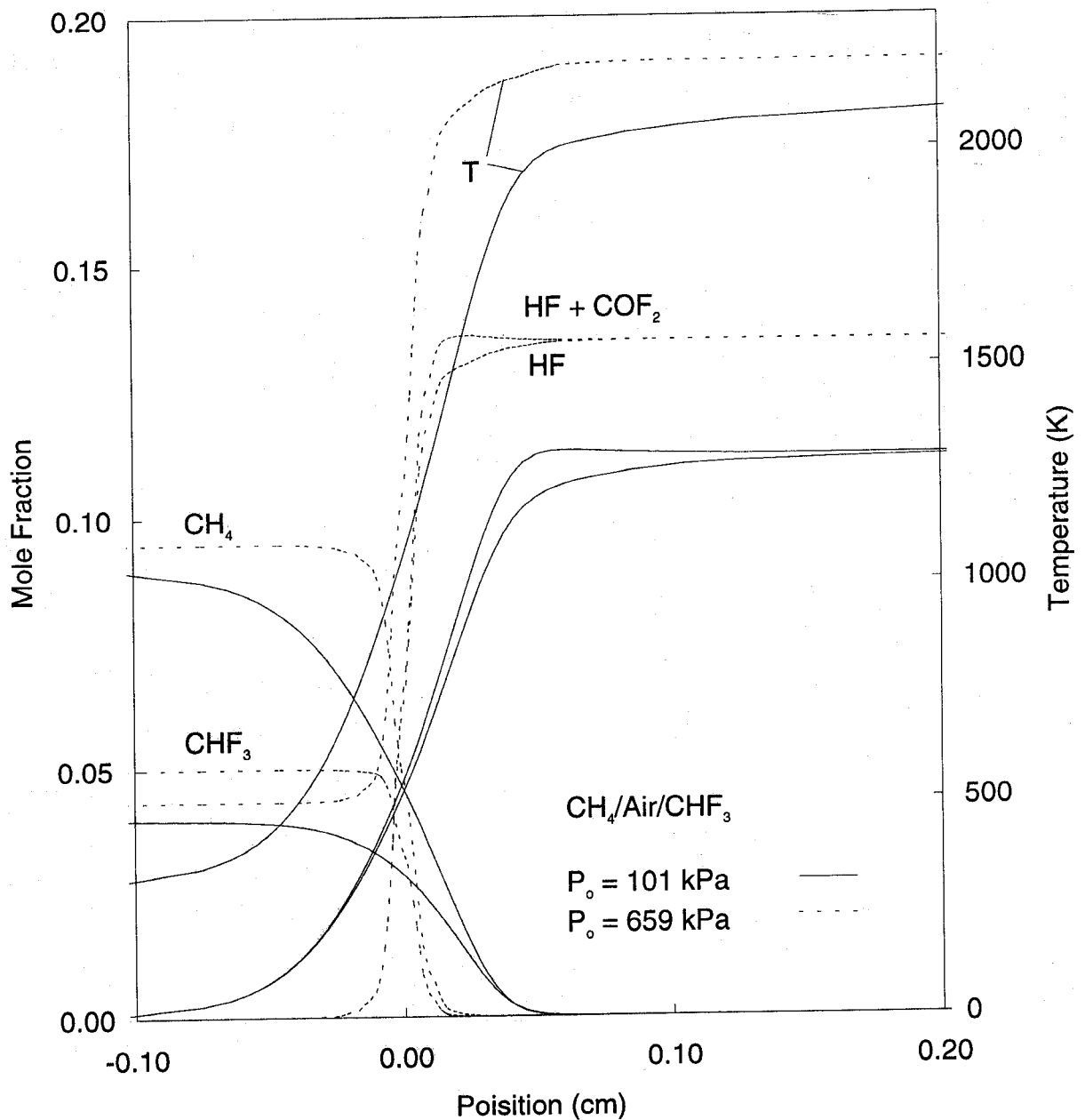


Figure 22. Calculated species mole fraction profiles for stoichiometric premixed methane-air flames with 4 % CHF₃ at 298 K, 101 kPa, and 5 % CHF₃ at 497 K and 659 kPa.

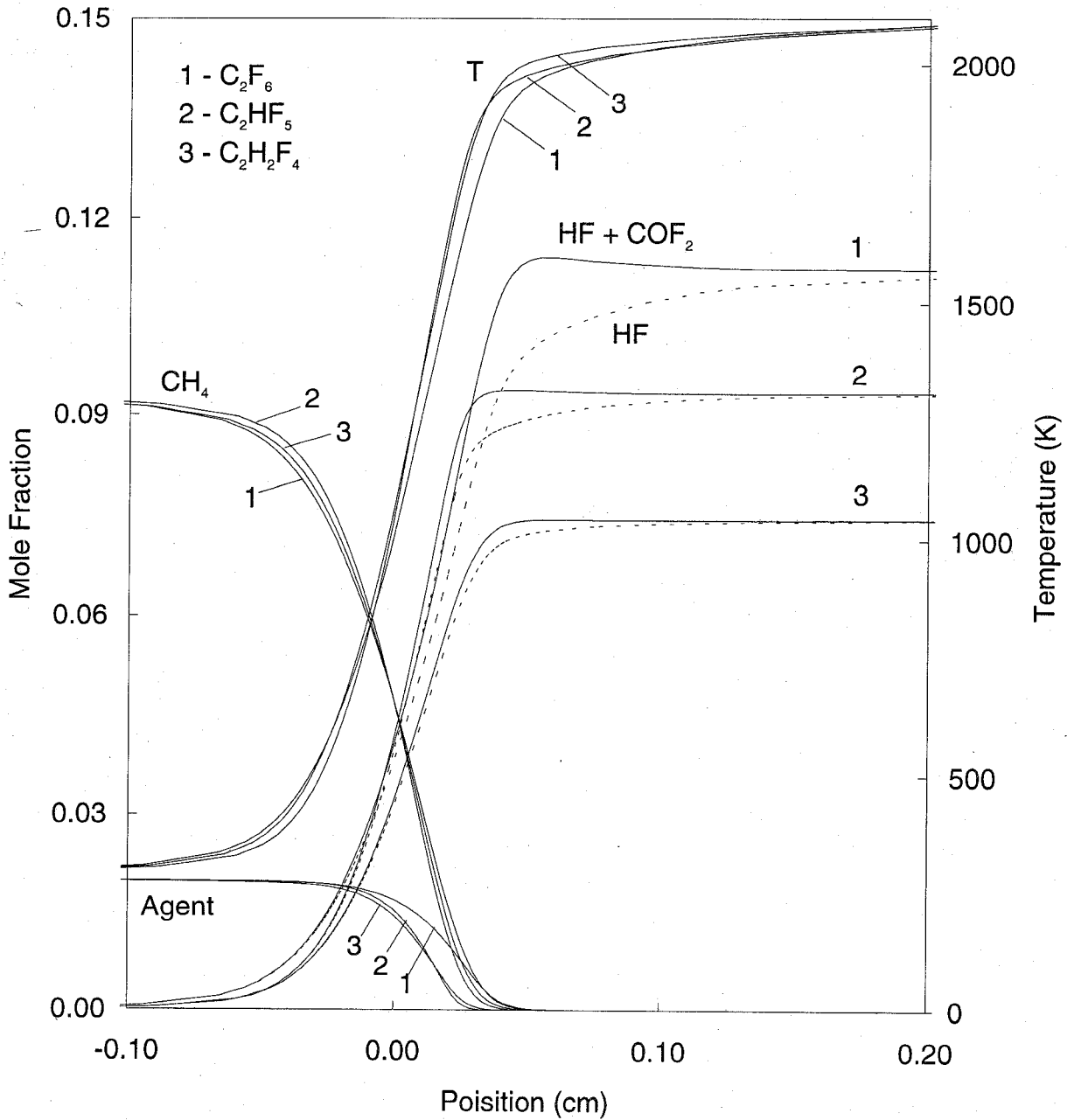


Figure 23. Calculated species mole fraction profiles for stoichiometric premixed methane-air flames with 2% C_2F_6 , C_2HF_5 and $C_2H_2F_4$.

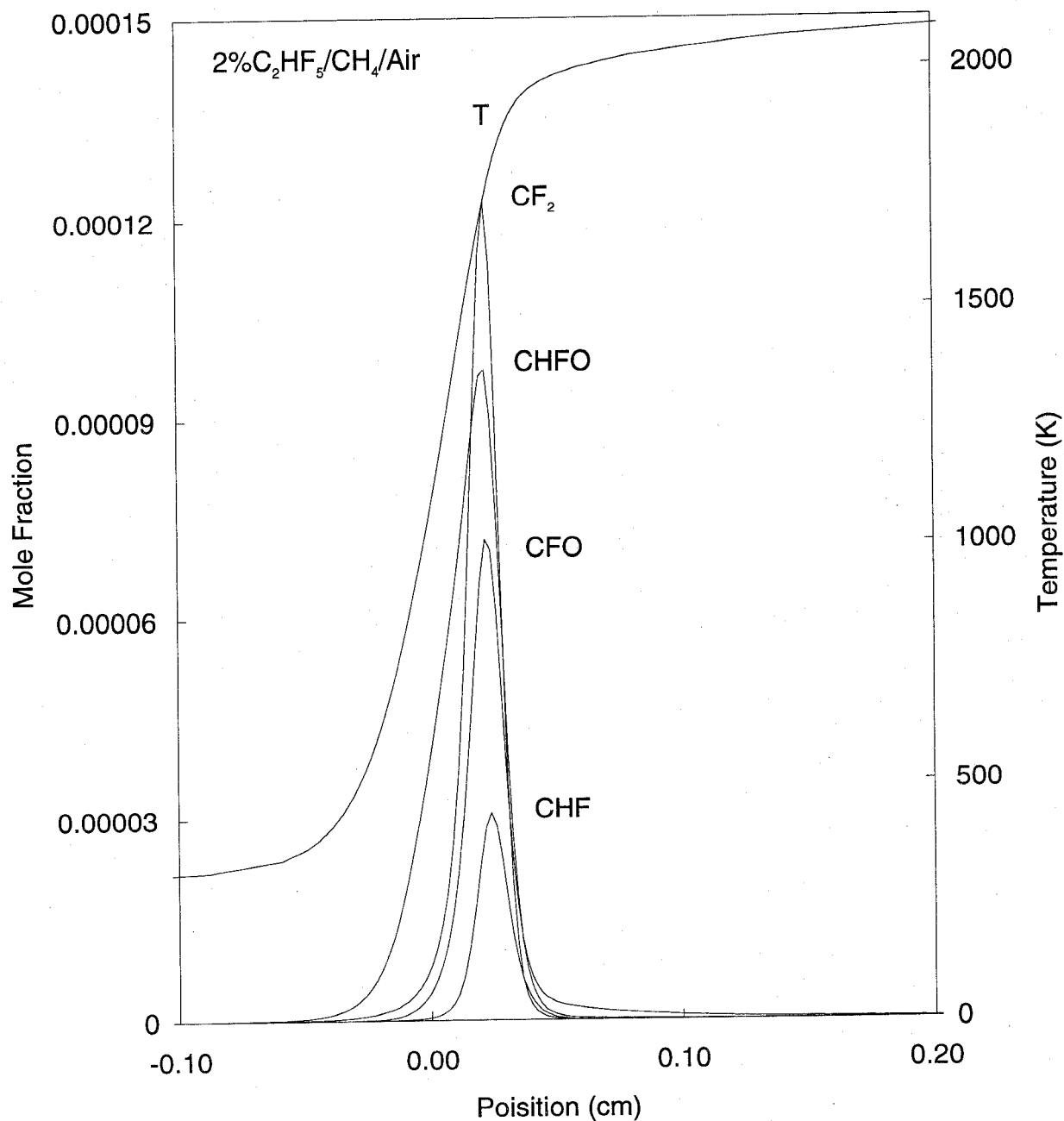


Figure 24. Calculated species mole fraction profiles of selected fluorinated intermediate species for stoichiometric premixed methane-air flames with 2 % C_2HF_5 .

Table 1. Reactions responsible for formation of HF in premixed stoichiometric methane-air flames of 2 % CHF₂-CF₃ and 4 % CF₃H at atmospheric conditions, and 5 % CHF₃ at 659 kPa and 497 K in the bomb

Reaction	Fraction of HF Formation
AGENT: CHF ₂ -CF ₃ , 2 %, φ = 1.0, P ₀ = 101 kPa	
CF ₂ +H↔CF+HF	0.16
H ₂ O+F↔OH+HF	0.10
CF:O+H↔CO+HF	0.10
CHF ₂ +H↔CHF+HF	0.06
CF ₃ +H↔CF ₂ +HF	0.06
CF ₂ :O+H↔CF:O+HF	0.06
CHF ₂ -CF ₃ ↔CF ₂ :CF ₂ +HF	0.06
CHF+H↔CH+HF	0.04
H ₂ +F↔H+HF	0.03
CH ₄ +F↔CH ₃ +HF	0.03
CH ₂ :CHF↔C ₂ H ₂ +HF	0.03
CF:O+OH↔CO ₂ +HF	0.02
CF:O+CH ₃ ↔CH ₂ CO+HF	0.02
CHF ₂ +OH↔CHF:O+HF	0.02
CF ₃ +OH↔CF ₂ :O+HF	0.02
CHF+H ₂ O↔CH ₂ O+HF	0.02
CH ₃ +CHF ₂ ↔CH ₂ :CHF+HF	0.02
CH ₃ +CF ₃ ↔CH ₂ :CF ₂ +HF	0.02
CF+H↔C+HF	0.02
CF+OH↔CO+HF	0.02
CHF:O+M↔CO+HF+M	0.01
AGENT: CHF ₃ , 4 %, φ = 1.0, P ₀ = 101 kPa	
CF ₂ +H↔CF+HF	0.16
H ₂ O+F↔OH+HF	0.13
CF ₃ +H↔CF ₂ +HF	0.13
CF ₂ :O+H↔CF:O+HF	0.08
CF:O+H↔CO+HF	0.08
CHF ₃ +M↔CF ₂ +HF+M	0.05
CH ₃ +CF ₃ ↔CH ₂ :CF ₂ +HF	0.05
CF ₃ +OH↔CF ₂ :O+HF	0.04
H ₂ +F↔H+HF	0.03
CH ₄ +F↔CH ₃ +HF	0.03
CF+H↔C+HF	0.02
CF+OH↔CO+HF	0.02
CH ₂ :CHF↔C ₂ H ₂ +HF	0.02
CF:O+OH↔CO ₂ +HF	0.02
CH ₂ :CF ₂ ↔C ₂ HF+HF	0.01
CF:O+CH ₃ ↔CH ₂ CO+HF	0.01
CHF:O+M↔CO+HF+M	0.01

Table 1. Continued

AGENT: CHF ₃ , 5 %, φ = 1.06, P ₀ = 659 kPa	
CF ₂ +H↔CF+HF	0.17
CHF+O+M↔CO+HF+M	0.11
H ₂ O+F↔OH+HF	0.10
CF ₃ +H↔CF ₂ +HF	0.10
CHF ₃ +M↔CF ₂ +HF+M	0.09
CF ₂ :O+H↔CF ₂ O+HF	0.07
CH ₃ +CF ₃ ↔CH ₂ :CF ₂ +HF	0.06
CF:O+H↔CO+HF	0.05
CH ₄ +F↔CH ₃ +HF	0.04
CF ₃ +OH↔CF ₂ :O+HF	0.04
H ₂ +F↔H+HF	0.04
CH ₂ :CHF↔C ₂ H ₂ +HF	0.03
CH ₂ :CF ₂ ↔C ₂ HF+HF	0.02
CHF+H↔CH+HF	0.02
CF:O+OH↔CO ₂ +HF	0.01

As can be seen in the figure, the higher pressure and temperature conditions decrease radical reactions of the inhibitor and its fragments and increase thermal decomposition reactions.

Table 1 lists the reactions which contribute 1 % or more to the formation of HF in flames inhibited by CF₃H, CH₂F₂, and C₂HF₅.

Clearly, the reactions which form HF are intimately related to the entire hydrocarbon oxidation mechanism. From these figures, it appears that once decomposition of the inhibitor molecule has been initiated, nearly every reaction of the intermediates forms HF or COF₂. This is expected since reaction of the inhibitor mostly involves removing fluorine from the carbon backbone, reducing fluorine to HF and oxidizing carbon to CO₂. It is important to note, however, that even for the one-carbon inhibitors, about a 20 % of the inhibitor rapidly pyrolyses to form larger (*i.e.*, two-carbon) fluorinated species, which are then decomposed in the flame.

10.5.7 Conclusions. The reduction in burning velocity has been determined experimentally and numerically for the inhibitors CF₃H, CH₂F₂, CF₄, C₂F₆, C₂HF₅, and C₂H₂F₄ in near-stoichiometric premixed methane-air flames at initial inhibitor mole fractions of 0 to 8 %, 298 K and 101 kPa. Even at this early stage of development, the NIST fluorine-inhibition mechanism predicts the burning velocity reduction quite well for these flames, and is a useful tool for understanding HF formation. Constant volume bomb experiments have extended the burning velocity measurements to a range of pressures of 2 to 7 bar and 330 to 500 K.

The following specific conclusions can be drawn concerning HF formation in these premixed flames:

1. Burning velocities are reduced in the inhibited flames by an amount greater than attributable to thermal dilution effects.
2. Of the six inhibitors for which calculations were performed, only CF₄ shows kinetic limitations to HF formation for premixed methane-air flames.

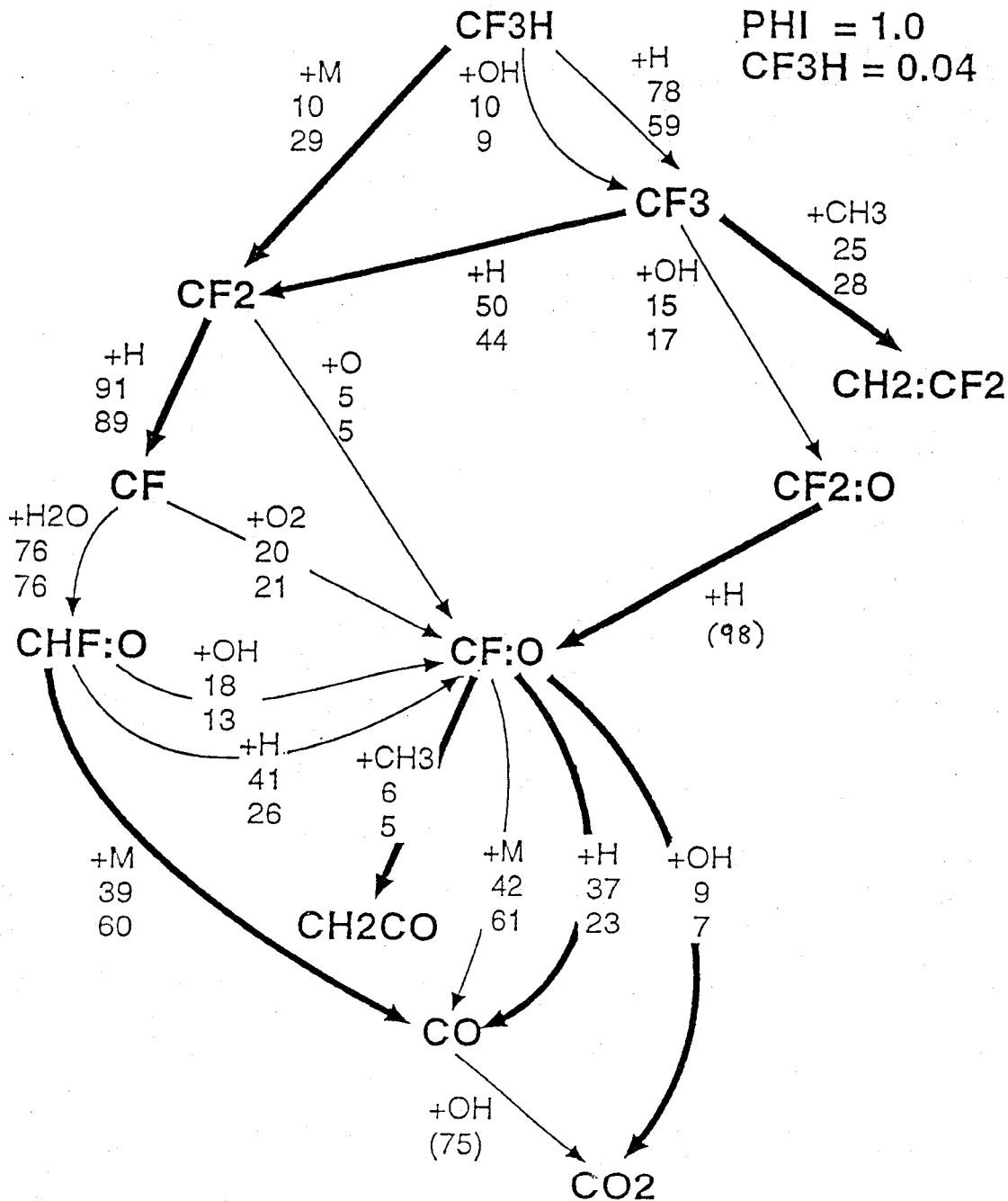


Figure 25. Dominant reaction pathways for decomposition of CF₃H in a stoichiometric premixed methane-air flame to which 4 % inhibitor has been added.

3. The inhibitors (except CF_4) are consumed in these flames as fast or faster than the fuel (methane) itself.
4. All of the fluorinated intermediates react rapidly and achieve only low concentrations except COF_2 which can persist in the product gases. Since COF_2 rapidly hydrolyses in the presence of water, its fate in the post-suppression gases will depend upon the availability of additional water from other sources besides the steady-state flame products.
5. HF is formed early in the flame, and persists at high concentrations as a final product. The amount of HF depends on the amount of hydrogen present (from the fuel and agent) and fluorine (from the agent).
6. Since the characteristic times for fuel consumption and HF formation are similar and fast, equilibrium conditions will be reached for all agents (except CF_4) in typical premixed flames.
7. Stable flames could not be obtained at fluorine loadings at or above the inhibitor concentration where the fluorine to hydrogen ratio in the flames is unity.
8. The agents appear to inhibit the flames primarily by reducing the hydrogen atom concentration well below the level which can be attributed to the temperature reduction of the flame by the agent.

10.6 Physical/Chemical Model

10.6.1 Steady-state - Premixed Flames. Although the premixed flame numerical modeling of the previous section can be used as the physical/chemical model to describe HF formation for the one- and two-carbon inhibitors, it is desirable to obtain simplifications to predict HF formation in these flames. Steady-state premixed flames are the simplest case to consider. Here, the reactants (fuel, air, and agent) are assumed to be premixed prior to interaction with the flame. This flame type most closely describes a flame ball expanding into a premixed combustible region as may occur in a dry-bay fire threat. In these cases, the mass flux of both fuel and agent into the reaction zone are well specified. As described in the section above describing the equilibrium calculations, the most abundant products of agent decomposition are CO , CO_2 , HF , and COF_2 . The model adopted in the present work assumes that the fluorinated agents decompose to the most thermodynamically favorable products and that finite rate kinetics are not important for HF formation. The validity of these assumptions are based on the extensive numerical modeling of premixed flames as described above (Linteris and Truett, 1995a, 1995b; Linteris, 1995a, 1995b). As will be shown below, predictions of HF formation in premixed flames based on thermodynamic equilibrium are in good agreement with measurements of HF in these flames. Hence, the model predictions for premixed flames consist essentially of the results of equilibrium calculations based on the fuel and agent species present in the flame.

10.6.2 Steady-state - Diffusion Flames. A calculation of the equilibrium concentration of HF and COF_2 in the products of a diffusion flame is not as straightforward as in a premixed flame since the amount of agent in the reactant zone is not known a priori. Consider the case of a co-flow diffusion flame in a chimney (as in Figure 26). Fuel is supplied by the center jet, and air diffuses inward, towards the high-temperature reaction zone where it is consumed. Addition of agent to the air stream

at a concentration less than the extinction concentration causes some of the agent to be consumed by the flame. Not all of the agent in the co-axial region is consumed, however; the amount consumed depends upon the relative flow rates of fuel and air. For example, if the outer chimney is very large, then only a small fraction of the agent in the coflowing region is consumed. Likewise, for a fire in a larger space, only inhibitor which is consumed in the flame will form HF. Thus it is necessary to estimate the flux of inhibitor into the reaction zone, since only this agent will decompose to form HF.

A model for acid gas formation has been developed based on a simple Burke-Schumann model (1928) of a co-flowing jet diffusion flame with fuel in the center and air co-axial. In the Burke-Schumann analysis, the fuel is assumed to be consumed at a reaction sheet, where fuel and oxidizer come together in stoichiometric proportions and the temperature reaches its highest value (which can be approximated by the adiabatic flame temperature of a stoichiometric premixed flame). The height of the flame is determined by the jet diameter and the rate at which the oxidizer can diffuse to the center-line of the fuel jet. The present flames differ in that the air stream contains inhibitor in addition to oxidizer.

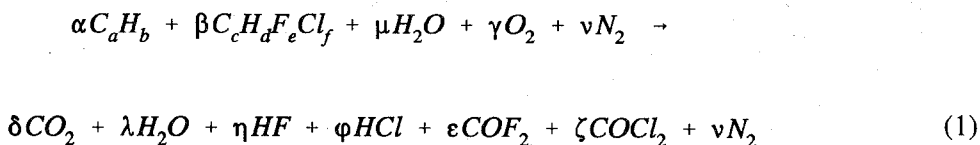
In the present analysis, the inhibitor is assumed to be consumed in the reaction zone as a reactive species. This assumption is based on premixed flame measurements and modeling (Linteris *et al.*, 1994). For both brominated and fluorinated carbon compounds, complete consumption of the inhibitor is typical. In many cases, the inhibitor is consumed faster than the fuel itself. Extensive thermodynamic equilibrium calculations of the composition of fuel-air mixtures in the presence of halogenated inhibitors also indicate complete exothermic conversion of the inhibitors to HF, CO₂, COF₂, and water.

The agent can be thought of as an additional fuel species, having its own oxygen demand, yet coming from the air side of the flame. It must diffuse to the hot reaction zone which serves as a sink for the inhibitor. Thus fuel, oxygen and inhibitor are consumed in the reaction zone in stoichiometric proportions, with the stoichiometry determined from a balanced chemical reaction to the most stable products.

Transport rates of inhibitor and oxygen are based on their relative rates of diffusion (Linteris and Gmurczyk, 1995) incorporating molecular weight effects. An implicit assumption in the present analysis is that the characteristic height for reaction of the fuel with oxygen is the same as the characteristic height for decomposition and reaction of the inhibitor. For a wide variety of flames and conditions, the consumption of the inhibitor occurs more rapidly with hydrogen and oxygen atoms than through thermal decomposition (Linteris and Truett, 1995a; Linteris, 1995a, 1995b). Given the inhibitors' preference for reactions with radicals and the high concentration of these species near the flame sheet, this assumption is reasonable.

Presently, it is also assumed that there is always sufficient air for complete combustion of the inhibitor and fuel. Hence, the estimate of HF formation is an upper limit since fuel rich flames will extinguish more easily and consequently produce less HF.

The global reaction representing a combustion process in a hydrocarbon/air/water environment in the presence of a halocarbon, leading to formation of combustion/inhibition products can be formulated as follows:



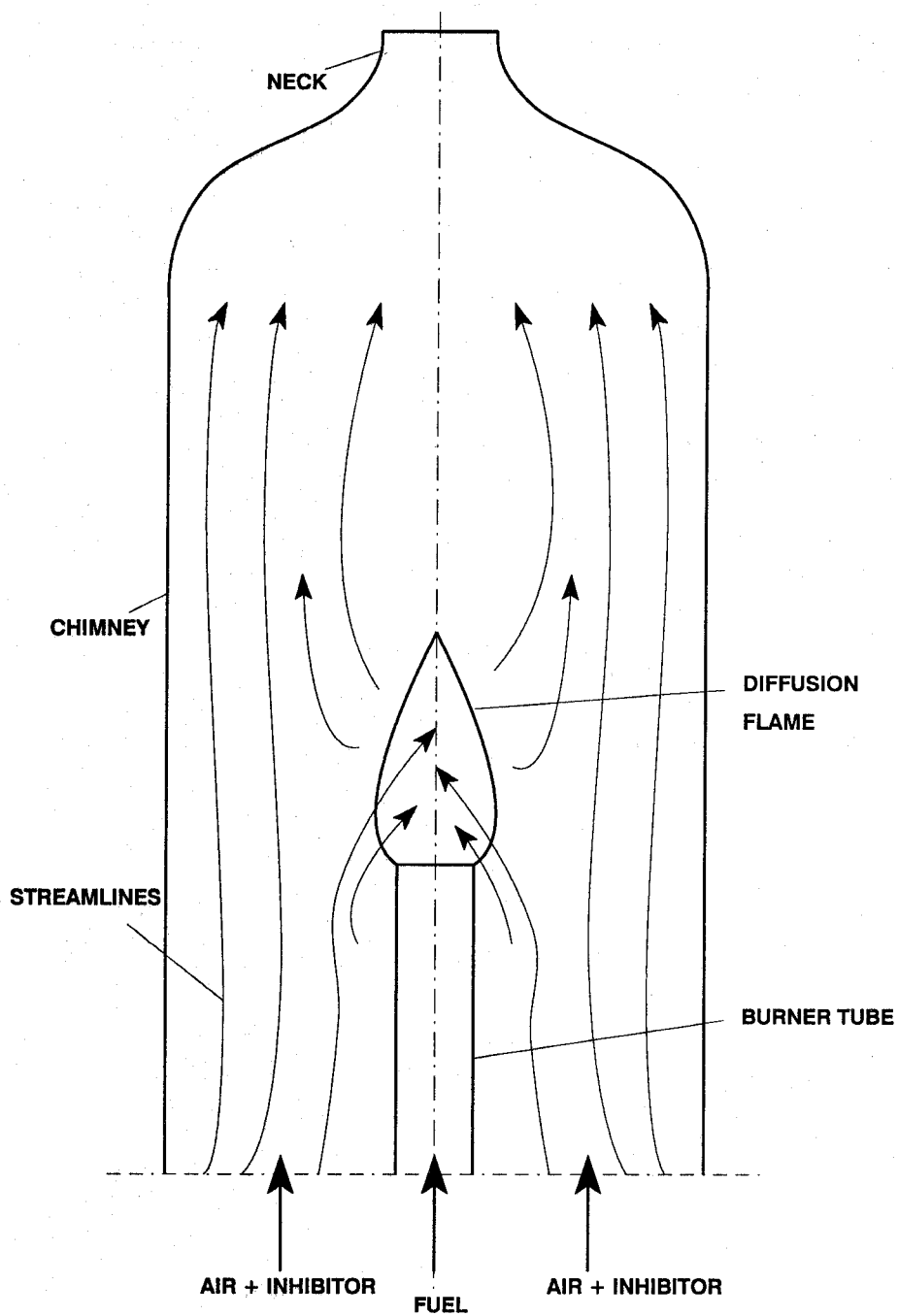


Figure 26. Illustration of the inhibitor and oxygen transport in a co-flow hydrocarbon-air diffusion flame.

where the greek symbols are the stoichiometric coefficients. In this reaction, chlorine is the second halogen, however, bromine or iodine can be used alternatively.

The fluxes of the inhibitor and water vapor to the reaction zone relative to the flux of oxygen are assumed to be proportional to the ratio of the diffusion coefficients and the concentrations, and are expressed as follows:

$$\frac{\beta}{\gamma} = \frac{[i]}{[O_2]} \times \frac{D_i}{D_{O_2}} \quad (2)$$

$$\frac{\mu}{\gamma} = \frac{[H_2O]}{[O_2]} \times \frac{D_{H_2O}}{D_{O_2}} \quad (3)$$

The molecular weight corrections for the diffusion rate of oxygen, inhibitor, and water vapor in nitrogen are:

$$D_{O_2}/D_{N_2} = \sqrt{((W_{O_2} + W_{N_2})/(W_{O_2} \times W_{N_2}))} \quad (4)$$

$$D_i/D_{N_2} = \sqrt{((W_i + W_{N_2})/(W_i \times W_{N_2}))} \quad (5)$$

$$D_{H_2O}/D_{N_2} = \sqrt{((W_{H_2O} + W_{N_2})/(W_{H_2O} \times W_{N_2}))} \quad (6)$$

where: D_{O_2} , D_{N_2} , D_{H_2O} , D_i are the diffusion coefficients and W_{O_2} , W_{N_2} , W_{H_2O} , W_i are the molecular weights of oxygen, nitrogen, water vapor, and inhibitor.

For a given fuel and inhibitor, all of the subscripts (a-f) are known, so that there are seven unknown coefficients on the right side of Equation 1 and five on the left, or twelve unknowns. There are six species balance reactions (for C, O, H, N, F, and Cl) and two mass flux equations (Equations 2 and 3). The mass input of fuel is known, as is the ratio of oxygen to nitrogen in the air. The final condition is obtained from a consideration of the equilibrium results described above. Two distinct cases exist: 1 - more hydrogen than halogen in the reaction zone, and 2 - less hydrogen than halogen in the reaction zone.

Case 1 occurs for low inhibitor loadings. Hydrogen in the product gases first goes to form HF until all of the halogen has been consumed, and any remaining hydrogen forms H_2O . The concentration of COF_2 is assumed to be zero for this case, providing the needed final relation.

In the second case, there is more halogen than hydrogen. In this case, no water forms since all of the hydrogen has been tied up as HF, and the excess halogen forms COF_2 . The solutions for these two cases are described below.

For the case of high halogen loading, or less hydrogen than halogen, the solution of the above equations yields the following relations describing both the flux of agent, water vapor, and oxygen into the flame (β , λ , and μ) and the amounts of product species. The fluxes of the reactants are given by:

$$\beta = \frac{\alpha(4a + b)}{\frac{4}{\rho r} + e + f - 4c - d} \quad (7)$$

$$\gamma = \frac{\beta}{\rho r} \quad (8)$$

$$\mu = \beta \rho^* \quad (9)$$

where:

$$\rho^* = \frac{\rho_{H_2O}}{\rho} \times \frac{r_{H_2O}}{r} \quad (10)$$

The fluxes of the products are expressed as follows:

$$\delta = 2\gamma - \alpha a - \beta c + \mu \quad (11)$$

$$\varphi = \delta + \alpha\left(\frac{b}{2} - a\right) + \frac{\beta}{2}(d + f + 2\mu - 2c - e) \quad (12)$$

$$\zeta = \frac{1}{2}[-\delta + \alpha\left(a - \frac{b}{2}\right) + \frac{\beta}{2}(2c + e + f - 2\mu - d)] \quad (13)$$

$$\varepsilon = \frac{1}{2}[\delta - 2\mu - \alpha\left(a + \frac{b}{2}\right) + \frac{\beta}{2}(e + f + 2\mu - d - 2c)] \quad (14)$$

$$\eta = -\delta + 2\mu + \alpha\left(a + \frac{b}{2}\right) + \frac{\beta}{2}(2c + d + e - 2\mu - f) \quad (15)$$

Note that all of the terms in the product coefficients contain α (either directly or through β), so that the amount of each product species depends upon the fuel flow rate (α).

For the condition of low halogen loading, or less hydrogen than halogen, the solution is given below:

$$\beta = \frac{\alpha(4a + b)}{\frac{4}{\rho r} + e + f - 4c - d} \quad (16)$$

$$\gamma = \frac{\beta}{\rho r} \quad (17)$$

$$\mu = \beta \rho^* \quad (18)$$

where:

$$\rho^* = \frac{\rho_{H_2O}}{\rho} \times \frac{r_{H_2O}}{r} \quad (19)$$

The fluxes of the products are expressed as follows:

$$\delta = \alpha a + \beta c \quad (20)$$

$$\varphi = \beta f \quad (21)$$

$$\eta = \beta e \quad (22)$$

$$\lambda = 2\left[\beta\left(\frac{1}{\rho r} - c\right) - \alpha a\right] + \mu \quad (23)$$

Thus, depending on the relative halogen/hydrogen ratio different pathways of formation of inhibition products are possible. When water vapor is absent in the system, the same system of equations is valid, but the terms represented by μ are equal to zero.

Basic features of the model are illustrated in Figure 27 for a steady-state propane-air cup burner diffusion flame with C_3F_8 in the air stream. In this figure, the fluxes of hydrogen and fluorine atoms into the reaction zone are depicted as a function of the C_3F_8 mole fraction in the air stream. At zero inhibitor mole fraction, all of the hydrogen input to the flame is converted to H_2O . As the inhibitor is added and fluorine becomes present in the reaction zone, hydrogen fluoride is formed preferentially over water (it is more stable). When all of the hydrogen has been consumed as HF, there is no water in the final products; any additional fluorine reaching the reaction zone shows up primarily as COF_2 .

The ratio of the halogen to hydrogen concentration in the reaction zone is a useful parameter, and is obtained from the equations above as follows:

$$\frac{[\text{Halogens}]}{[\text{Hydrogen}]} = \frac{\beta(e + f)}{\alpha b + \beta d + 2\mu} \quad (24)$$

The crossover point for the two curves in Figure 27 corresponds to a value of unity for this parameter, and represents the switch from the first to the second solution above. This point corresponds to a critical value of the inhibitor flux into the reaction zone β_{cr} which is equal to:

$$\beta_{cr} = \frac{\alpha b + 2\mu}{e + f - d} \quad (25)$$

As illustrated in Figure 27, the HF production cannot be greater than the hydrogen or fluorine flux to the reaction zone; also, the sum of HF and COF_2 (the only significant other final species for fluorine) cannot be greater than the fluorine flux. For C_3F_8 in a propane-air flame, all of the hydrogen comes from the fuel, so that at zero inhibitor concentration there is a non-zero hydrogen flux to the reaction zone and additional inhibitor in the air stream does not increase the hydrogen flux to the reaction zone (for other inhibitors, such as C_2HF_5 , increasing amounts of inhibitor slightly increase the hydrogen flux to the reaction zone).

Conversely, all of the fluorine comes from the inhibitor, so it increases nearly linearly with the inhibitor mole fraction X_i . Since COF_2 readily hydrolyses in water to form fluoride ion F^- , measurements of fluoride typically include that from both HF and COF_2 . In principle, the product gases from inhibited flames near extinction could contain fluorine from both HF and COF_2 . Interestingly, however, the experimental results for a number of fuels and agents (Bajpai, 1974) indicate that measured fluorine levels are rarely above the limit imposed by the hydrogen flux shown in Figure 27. These reduced fluoride levels may be due to kinetic limitations on the rate of inhibitor consumption and HF formation (Linteris, 1995).

For the present analyses, however, the predicted acid gas formation in inhibited flames is based on equilibrium thermodynamics assuming that HF (not COF_2) is the source. Provision is also made in the model for inclusion of an empirical parameter, based on the experimental results, which describes the observed deviation from the equilibrium prediction in diffusion flames for which experiments have been performed.

Based on the assumptions made in the stoichiometric model, a set of algebraic equations has been derived and a computer program has been developed to solve the set. The program uses as input: the atomic composition of a fuel and inhibitor, and the initial concentrations of the inhibitor, fuel, air, and the water vapor in the air and fuel stream. From these the estimated mole fractions of all reactants and products in the reaction zone are calculated. The program is particularly useful for parametric studies of the influence of each parameter on the predicted HF generation rate.

10.6.3 Transient State. The steady-state results are used to obtain results for transiently suppressed flames. In the present analyses, the inhibitor concentration in the air stream is assumed to increase linearly in time up to the extinction concentration for the particular flame (although any known profile of concentration versus time may be used). At each value of the inhibitor concentration, the

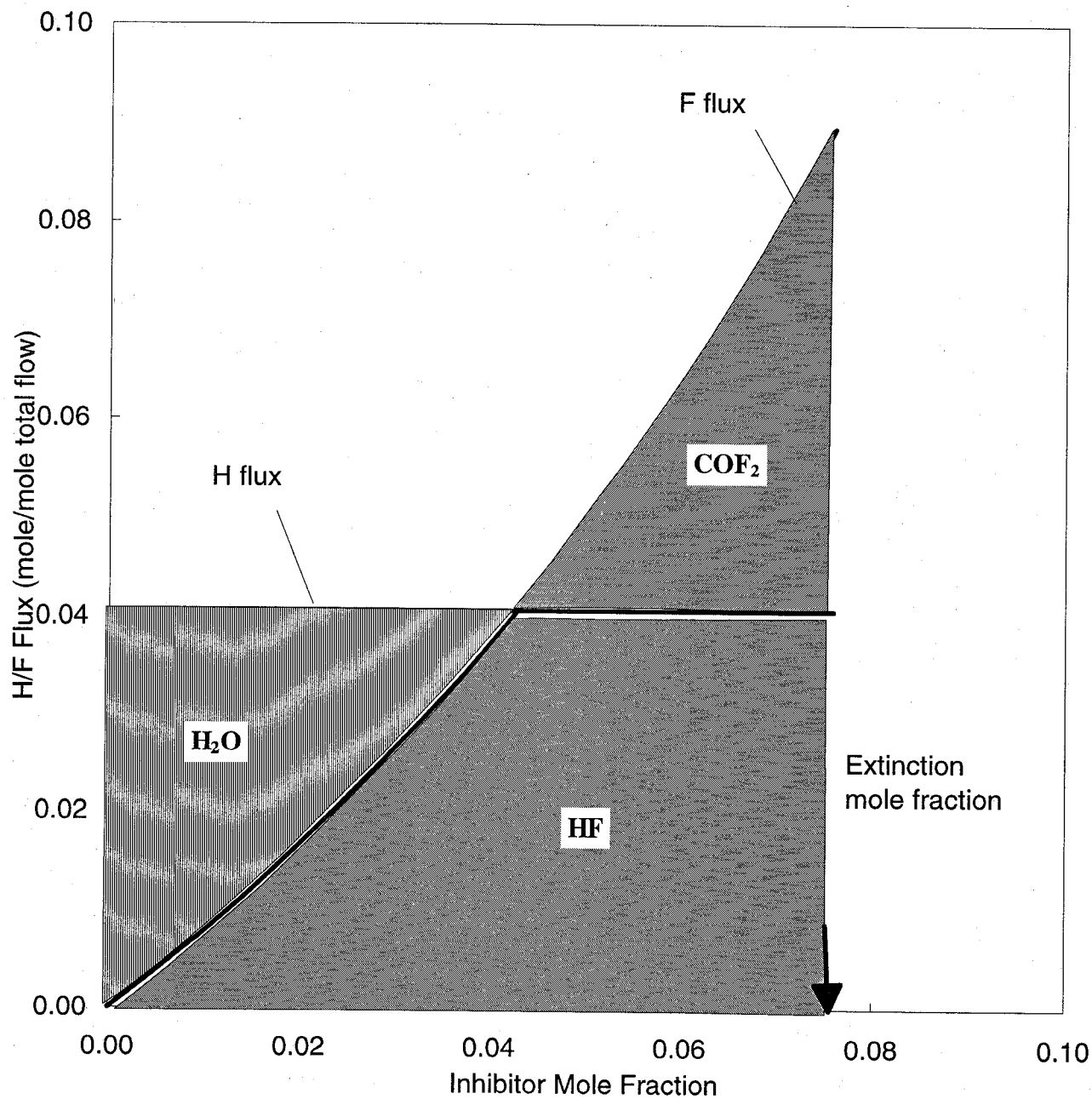


Figure 27. Stoichiometric model prediction of hydrogen and fluorine flux to the reaction zone of a propane-air diffusion flame. The fate of the hydrogen and fluorine are indicated at each inhibitor concentration.

production rate of HF is determined from the steady-state equilibrium model described above, providing a plot of the HF generation rate as a function of time. Integration of this curve provides the total HF formed during suppression of the flame. The inhibitor concentration as a function of time is provided as input, as is the concentration of inhibitor necessary to extinguish the flame.

10.7 Experiments

Laboratory experiments for HF formation were performed using several burner types, which shared some components. Three diffusion flame experiments were constructed: a propane-fueled cup burner, a propane-fueled jet burner, and a heptane-fueled cup burner. These three were used in steady-state, and the propane cup burner was also used for transient experiments. Premixed flames were used both for numerical model validation (the experiment for which is described above) and for HF measurements in steady-state. The following sections describe these experiments.

10.7.1 Propane Diffusion Flame Tests for HF. Two burner types are used for the gaseous diffusion flame experiments. The first is modelled after the cup burner described by Booth *et al.*, (1973) and Bajpai (1974). The experimental arrangement is shown in Figure 28. The burner consists of a 28 mm diameter pyrex cup positioned concentrically in a 120 mm diameter 450 mm tall chimney at about 150 mm from the base. In these experiments with propane, the cup burner was modified for use with a gaseous fuel. The cup is filled with 1 mm diameter glass beads and covered with a stainless steel screen. The second burner consisted of a 25 cm long pyrex tube with a 0.50 mm diameter opening positioned concentrically and at the same height as the cup burner, with the same chimney. The cold flow Reynolds number based on the exit velocity in the tube is 1050. This second burner, referred to here as the jet burner, is designed to provide turbulent mixing of the inhibitor in the air stream with the fuel. Although a higher jet Reynolds number would have been desirable to achieve turbulent mixing, the flame is very close to blow-off at flows with a Reynolds number of 2000, and very little inhibitor can be added before blow-off occurs. Consequently, at these flows, it is difficult to study the effects of air stream inhibitor concentration on HF formation.

The air used is shop compressed air, filtered and dried as described below. The fuel gas is propane (Matheson, CP grade) at flow rate of 0.114 l/min at 21 °C. Gas flows are measured with rotameters (Matheson 1050 series) which are calibrated with bubble and dry (American Meter Co. DTM-200A and DTM-325) flow meters. Inhibitor gases are of different purities from various suppliers.

Before measuring HF in the product gases, the concentration of inhibitor in the air stream necessary to extinguish the flame is determined. The inhibitor is then added to the co-flowing air stream at a concentration of either 50 % or 90 % of the extinguishing concentration, and the product gases are sampled for acid gas. In one series of experiments with the cup burner, the inhibitor is added to the gaseous propane stream at 70 % of the concentration which would extinguish the flame.

10.7.2 Liquid Heptane Diffusion Tests for HF. The cup burner apparatus was also used in its more usual configuration with a liquid fuel. For the purposes of this research, it is necessary to know the fuel consumption rate. To accomplish this, the overflow fuel feed system (Figure 29) was developed. In this system, a syringe pump (Harvard Apparatus Model 975) delivers the fuel at a known volumetric flow rate to the flame and the overflow tube. The flow is set to be greater than the expected fuel consumption rate of the flame, and the height of the fuel overflow tube is adjusted to provide the proper height of fuel in the cup. An electronic laboratory balance (Mettler PE360) connected to a

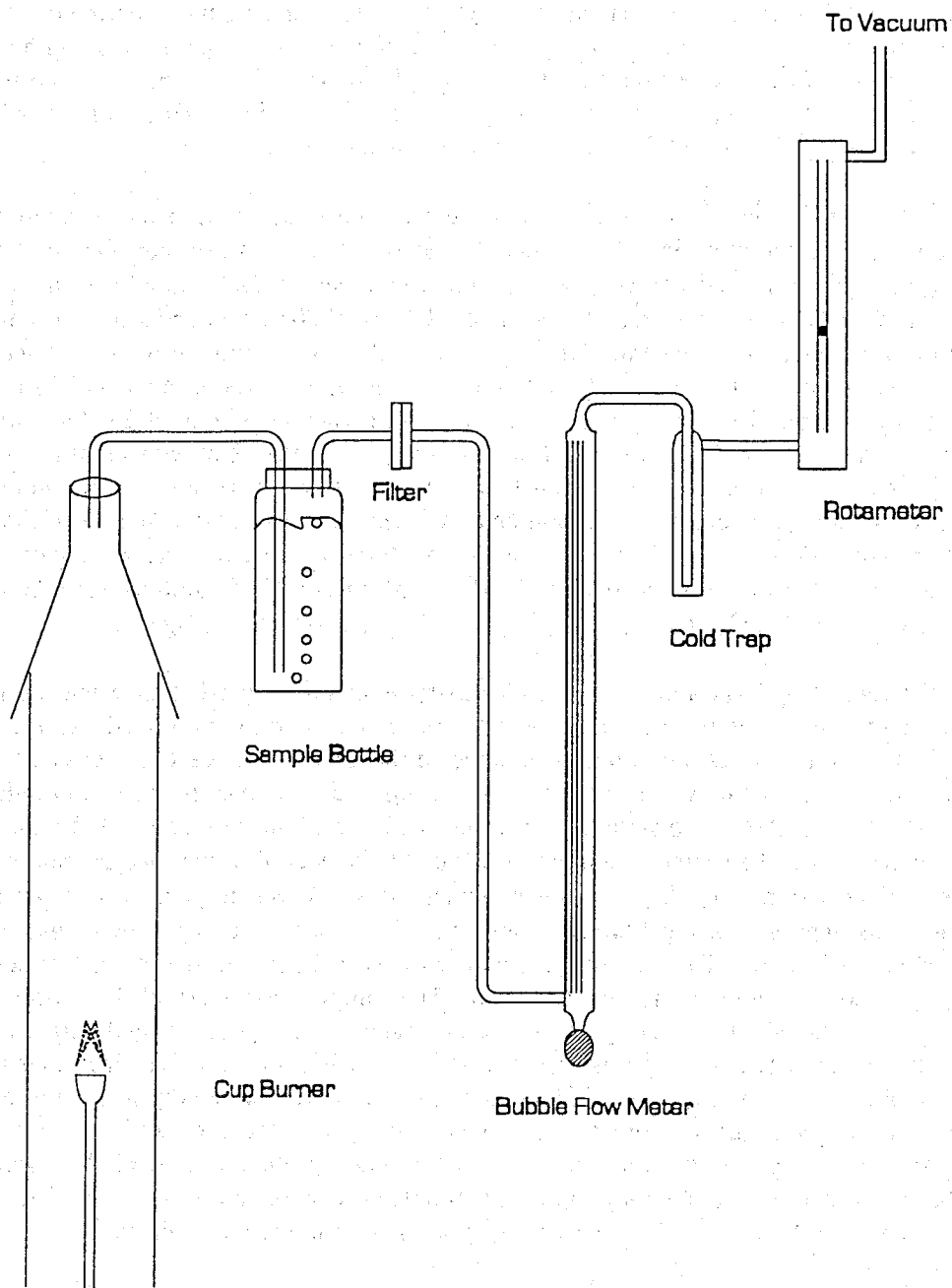


Figure 28. Experimental apparatus for co-flow diffusion flame studies of acid gas formation in inhibited propane-air diffusion flames.

computer data acquisition system, measures the mass of liquid emerging from the overflow tube. By subtracting the measured overflow rate from the supplied flow rate, the fuel consumption rate of the burner is determined. The fuel in the cup burner is adjusted to a height 1 mm below the cup rim, and this level is maintained through manual periodic adjustments during the experiment.

Heptane was used as the fuel for the liquid cup burner tests. The air cleaning and gas supply systems were identical to those described above for the premixed flame burning rate measurements. The air flow was 20.7 l/m, and the agents tested were CHF_3 , C_2F_6 , C_2HF_5 , C_3F_8 , C_3HF_7 , at flow corresponding to 50 % and 90 % of the extinction concentration.

10.7.3 Premixed Flame Tests for HF. For the premixed flame tests of HF formation the same nozzle burner as in the burning velocity measurements is used. The burner consisted of a Mache-Hebra (1941) nozzle burner 27 cm long, with an inner diameter of 22 mm and wall thickness of 1.5 mm. A contraction at the top to a nozzle diameter of 1.02 (+/- 0.005 cm) occurs over a length of 3 cm. The burner tube is located concentrically in a 40 cm tall quartz chimney with an inner diameter of 7.6 cm, with contraction at the top to a 3 cm diameter. The burner produces conical flames with a height of 1.3 cm and base of 1.0 cm diameter. Air flows in the annular region at 25 l/m, while the reactant gas stream to the burner is about 2 to 5 l/m, depending upon the agent concentration and equivalence ratio. The flame height is maintained constant while the flows of oxidizer, fuel, and agent are varied to produce the desired agent concentration and equivalence ratio. The sampling of the product gases is done at the contraction in the top of the chimney as described below. The gas handling system for the premixed burner is also described below. Methane (Matheson UHP) and propane are used as the fuels, and CHF_3 , C_2F_6 , C_2HF_5 , C_3F_8 , C_3HF_7 , and CF_4 are used as the agents.

10.7.4 HF Sampling Technique. A wet chemistry technique is used to measure the HF concentrations in the exhaust gases from the co-flow diffusion flames and the premixed flames. A quartz probe (6 mm O.D., 4 mm I.D., 20 cm long) is centered in the neck and extracts a measured fraction of the product gases (approximately 0.5 to 5.5 %). A vacuum pump draws the gases through polyethylene sample lines to one 250 ml polyethylene impinger and one 25 ml impinger filled with water which trap the acid gases. The second impinger was found to collect less than one percent of the total HF, but was retained for most of the experiments nonetheless. Desiccant-packed tubes or a cold finger dry the sample gas upstream of a calibrated rotameter. The steady-state experiments had sample gas flow rates of about 200 ml/m. To increase the quantity of HF collected in the short, transient experiments, the sample flow was increased to about 1.2 l/m. The sample flow is established for a total collection time of one to four minutes. The quartz probe and sample lines were washed with water which was returned to the impinger. The sample was tested for F- using ion-selective electrodes (Orion model 96-09). It should be noted that since COF_2 is known to hydrolyze rapidly in the presence of water, this technique for acid gas measurement includes F- from both HF and COF_2 . To reduce the effects of sampling losses reported by other investigators, a quartz probe and polyethylene sample lines were used, the distance from the chimney top to the bubbler was kept small (~ 10 cm) and the sample lines were washed with the bubbler fluid immediately after the sample was collected.

10.7.5 Transient State Measurements. The experimental arrangement for the transient experiments is identical to the steady-state propane-air diffusion flame experiments described above. In these experiments, the agent is added to the air flow at a concentration increasing linearly in time up to a value 25 % above the cup burner extinction concentration. The concentration ramp, implemented through computer control of the mass flow controllers, allowed effective ramp times from 5 seconds to any number of minutes. The amount of HF formed is lower than in the steady-state experiments due to the short time for interaction prior to flame extinguishment. To insure that a sufficient amount of

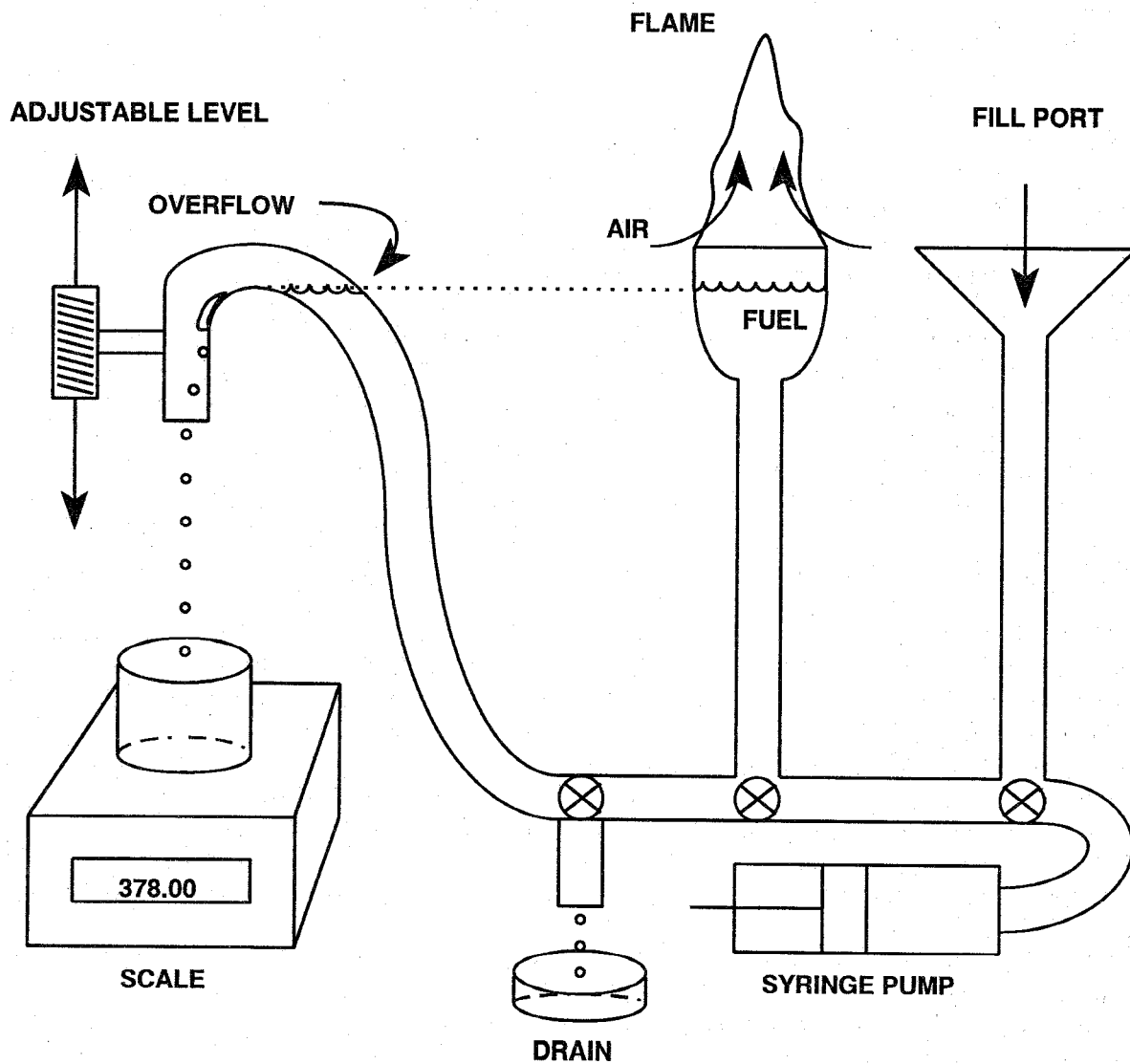


Figure 29. Experimental apparatus for co-flow diffusion flame studies of acid gas formation in inhibited heptane-air diffusion flames.

HF is collected, a higher sample gas flow is used (about 7 % of the total flow), and a second bubbler ensures that no HF is untrapped. In the experimental procedure, the gas sample flow is started, the inhibitor is ramped up in concentration to 125 % of the flame extinguishment concentration and the flame extinguished. The sample flow continues 30 seconds after extinguishment and is stopped. The sample probe consequently extracts a measured fraction of the total product gas flow, from which the total HF formed is determined.

10.8 Results

10.8.1 Steady-state - Premixed Flames. The amounts of HF measured in steady-state premixed flames are presented in Figures 30 and 31. Figure 30 shows the results for the inhibitors CF_4 , CHF_3 , C_2F_6 , and CH_2F_2 in premixed methane-air flames, and Figure 31 shows the results for the species C_2HF_5 , C_3F_8 and C_3HF_7 for propane-air flames. In these figures, the experimental results are indicated by the points, while the solid lines show the predicted HF mole fractions based on the results of equilibrium calculations. The quantities of HF produced per mole of fuel are plotted versus agent mole fraction in the reactant stream. An increase in the inhibitor mole fraction produces a linear increase in the HF generation, and there is a linear dependence on the number of fluorine atoms in the inhibitor molecule. The flames with propane show higher HF production rates per mole of fuel than do the methane-air flames, since combustion of one mole of propane requires 24 moles of air, compared to about 10 moles for methane. Since the inhibitor mole fraction is based on the sum of air and inhibitor, the resulting molar flow of inhibitor per mole of fuel is greater in the propane flames as compared to the methane flames.

For the present flames, the hydrogen to fluorine ratio is always greater than one, so that fluorine in the inhibitor molecule essentially appears only as HF in the product gases. As described above in the discussion of premixed flame modeling, the inhibitor molecule is consumed rapidly and completely in these flames to form HF. Thus, for these flames, the predicted HF molar flow in the product gases can be predicted solely from the inhibitor molar flow rate in the reactant stream and the number of fluorine atoms in the inhibitor. As the figures show, the assumption of complete inhibitor reaction to HF provides a predicted HF generation rate in good agreement with the results of experiments for all of these agents except CF_4 . It is interesting to note that we were not able to produce stable flames at inhibitor loadings near or above the point of unity hydrogen to fluorine concentration in the reactant stream for any agent.

Figure 32 shows the dependence of the quantity of HF generated from C_2F_6 in the premixed methane/air flame versus equivalence ratio of the mixture. Over this narrow range of equivalence ratio, the predicted HF is in good agreement with the measured values.

As Figure 30 shows, the amount of HF formed in CF_4 -inhibited premixed methane-air flames is less than half that predicted by equilibrium thermodynamics, and decreases as the inhibitor loading increases. In order to investigate this further, experiments were performed with premixed methane-air flames in which the oxygen mole fraction was changed to vary the peak final temperature of the flame.

Figure 33 shows the fractional conversion of CF_4 to HF (and COF_2) as a function of the calculated final flame temperature. As indicated, a change of final temperature of only a few hundred K produces a change in the fractional conversion of CF_4 from about 15 to 70 %. Consequently, this type of behavior was investigated numerically in premixed methane-air flames for the other inhibitors, but a strong temperature dependence for the rate of inhibitor decomposition was not observed. The

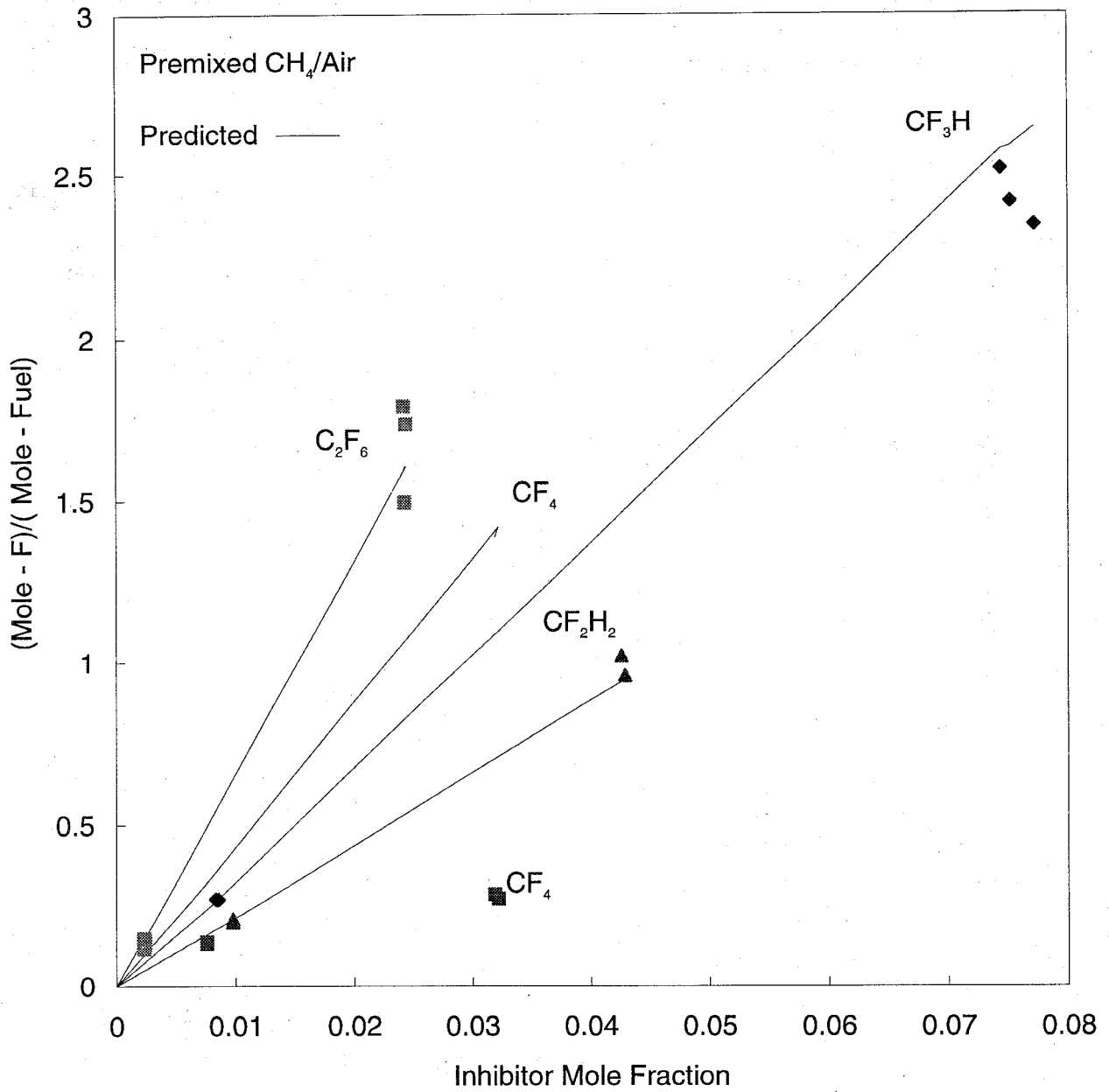


Figure 30. Measured and predicted HF in premixed methane-air flames with C_2F_6 , CF_4 , CHF_3 , CF_2H_2 .

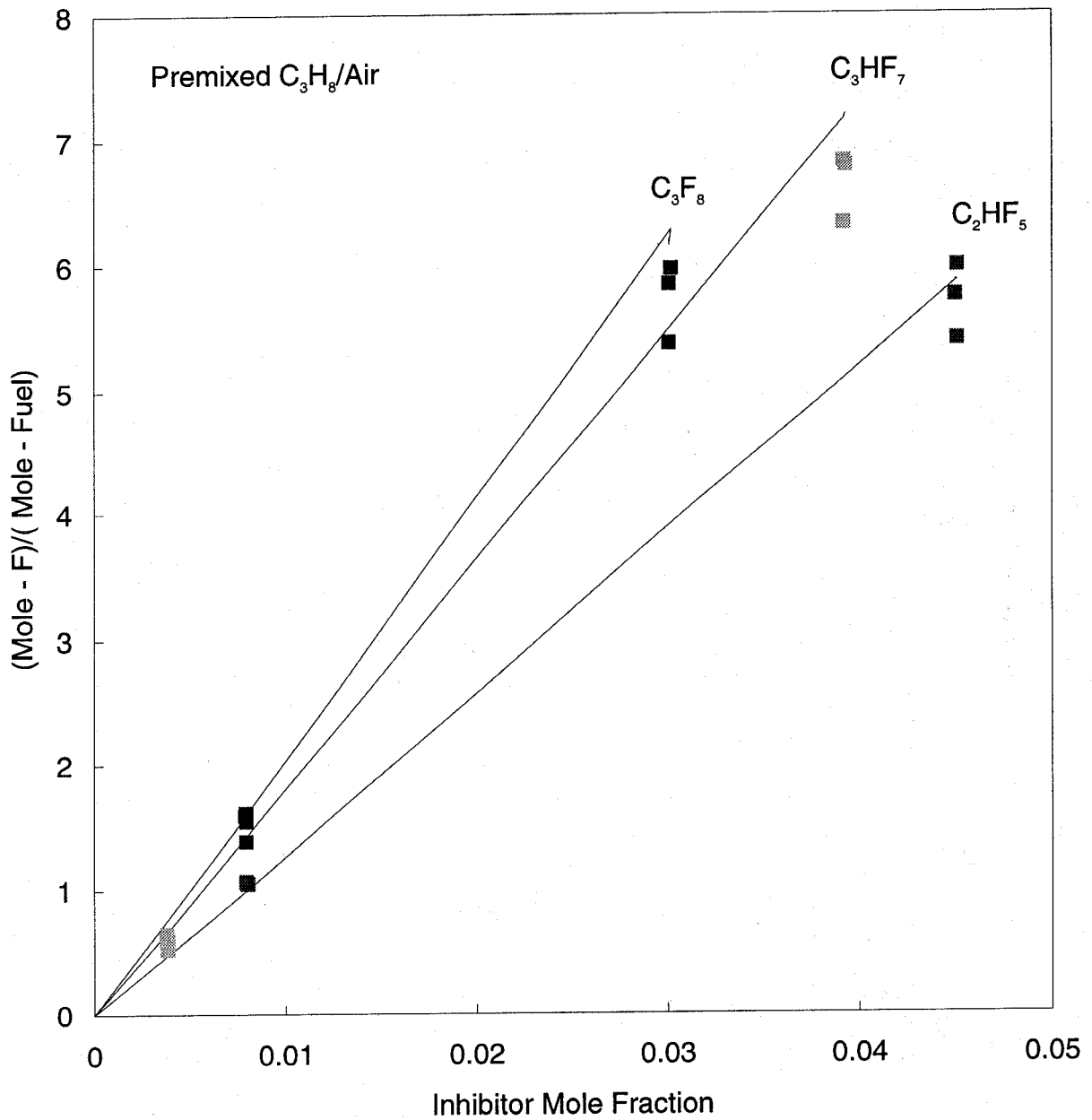


Figure 31. Measured and predicted HF in premixed propane-air flames with C_3F_8 , C_3HF_7 , C_2HF_5 .

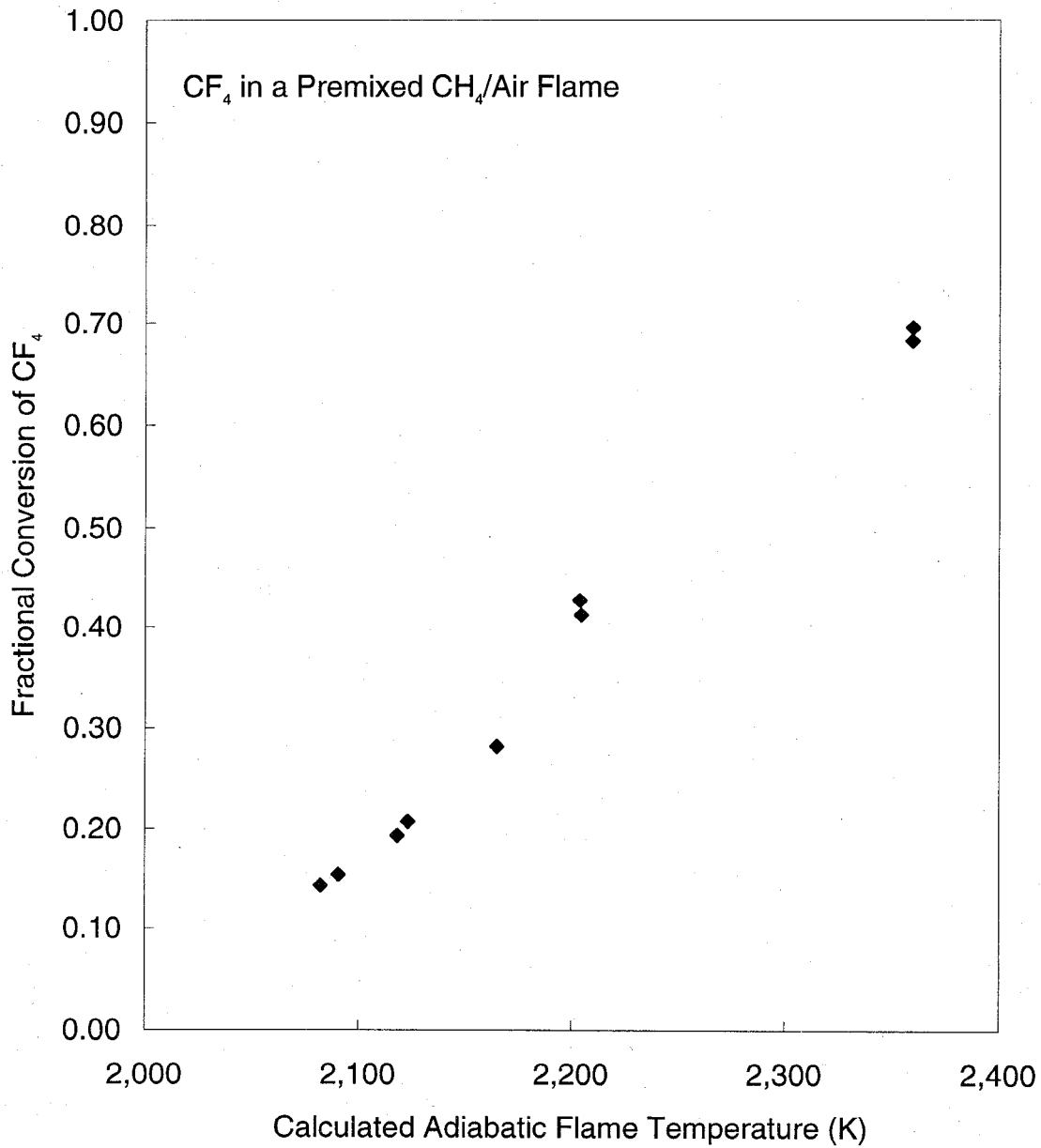


Figure 32. Fractional conversion of fluorine in CF₄ to HF in a premixed methane-air flame as a function of the calculated adiabatic flame temperature.

possibility of the effect of temperature should be kept in mind when extending the results of this study to other conditions.

It has been shown that for all of the hydrofluorocarbons tested in premixed flames, including CH_2F_2 , CF_3H , C_2HF_5 , and C_3HF_7 , the agent completely decomposed and formed species which appeared as fluoride ion in the bubbler (*i.e.*, either HF or COF_2). This indicates that kinetic limitations are not important for these agents in these flames, and that the assumption of chemical equilibrium provides estimates of HF formation that are consistent with the experimental results. This behavior is also observed for the perfluorinated agents C_2F_6 and C_3F_8 . It is important to note that all of these flames had fluorine to hydrogen ratios in the flame greater than unity. Indeed, it was not possible, in either the nozzle burner (which has narrow stability limits) or in a premixed, water-cooled, flat-flame McKenna burner (which has wide stability limits), to stabilize any premixed flame at hydrogen to fluorine ratios of one or less. Thus it appears that at agent loadings where premixed flames burn, there is nearly complete destruction of the agent and subsequent formation of HF or COF_2 .

10.8.2 Steady-state - Gaseous Diffusion Flames. In the propane-air diffusion flames, the acid gases produced are measured at inhibitor concentrations of 50 % and 90 % of the concentration of inhibitor found to extinguish the flame when the inhibitor is added to the co-flowing air stream in the cup burner and jet burners. Table 2 lists the extinction concentrations for each agent for inhibitor added to the air stream of both burners. As the table indicates, the jet burner flame typically requires about 50 % less inhibitor in the air stream to extinguish the flame than the cup burner, even for identical fuel and air flows, although there are notable exceptions: CF_3Br , which requires about one fifth as much inhibitor in the jet burner than in the cup burner, and $\text{C}_2\text{H}_2\text{F}_4$ and the $\text{CH}_2\text{F}_2/\text{C}_2\text{H}_2\text{F}_4$ mixture which had nearly the same extinction concentrations. In addition to providing the necessary extinction conditions for specification of inhibitor flows at 50 % and 90 % of extinction, these results also demonstrate the sensitivity of the extinction conditions to the burner geometry.

The HF production in steady-state propane air diffusion flames was measured for the agents C_2F_6 , C_3F_8 , C_4F_{10} , C_4F_8 , C_2HF_5 , C_3HF_7 , $\text{C}_2\text{H}_2\text{F}_4$, C_2HClF_4 , $\text{C}_3\text{H}_2\text{F}_6$, $\text{CF}_2\text{H}_2/\text{C}_2\text{HF}_5$, CHF_2Cl , CF_3Br , and CF_3I ; the results are presented in Figures 34 to 46, respectively. The symbols represent the experimental data, while the lines marked F and H represent estimates of the fluxes of fluorine and hydrogen into the reaction zone based on the stoichiometric model described above.

Figure 39, for example, shows the measured and estimated HF production rates in a propane-air diffusion flame for C_2F_6 in the cup and jet burners. The curve labeled F' in Figure 39 is the maximum fluoride atom molar flux into the reaction sheet of the diffusion flame calculated using the stoichiometric model described above. The curve labeled F in Figure 39 is the fluoride molar flux when the diffusion rate of the inhibitor relative to oxygen is not modified to account for preferential diffusion of oxygen. These unprimed curves are expected to more closely describe near turbulent mixing as occurs in the jet burner.

Qualitatively, the curves F and F' are seen to increase with increasing inhibitor concentration in air, and the molar flux of inhibitor into the reaction zone is lower when a lower rate of diffusion is used for the inhibitor. The curves labeled H and H' (coincident for C_2F_6) show the estimated hydrogen atom flux into the reaction zone as a function of inhibitor concentration in the air stream. Since this inhibitor does not contain hydrogen, all of the hydrogen is from the propane, and increasing inhibitor in the air stream does not increase the hydrogen flux into the flame. One would expect that the HF production rate would not be greater than the estimated flux of F or H into the reaction zone. For this inhibitor, the flame appears to be hydrogen limited above about 5 % C_2F_6 in the air stream; however, when there is not enough hydrogen, the most stable product is COF_2 , which is known to rapidly hydrolyze in the presence of water, and would also appear as F- in the bubbler. Consequently,

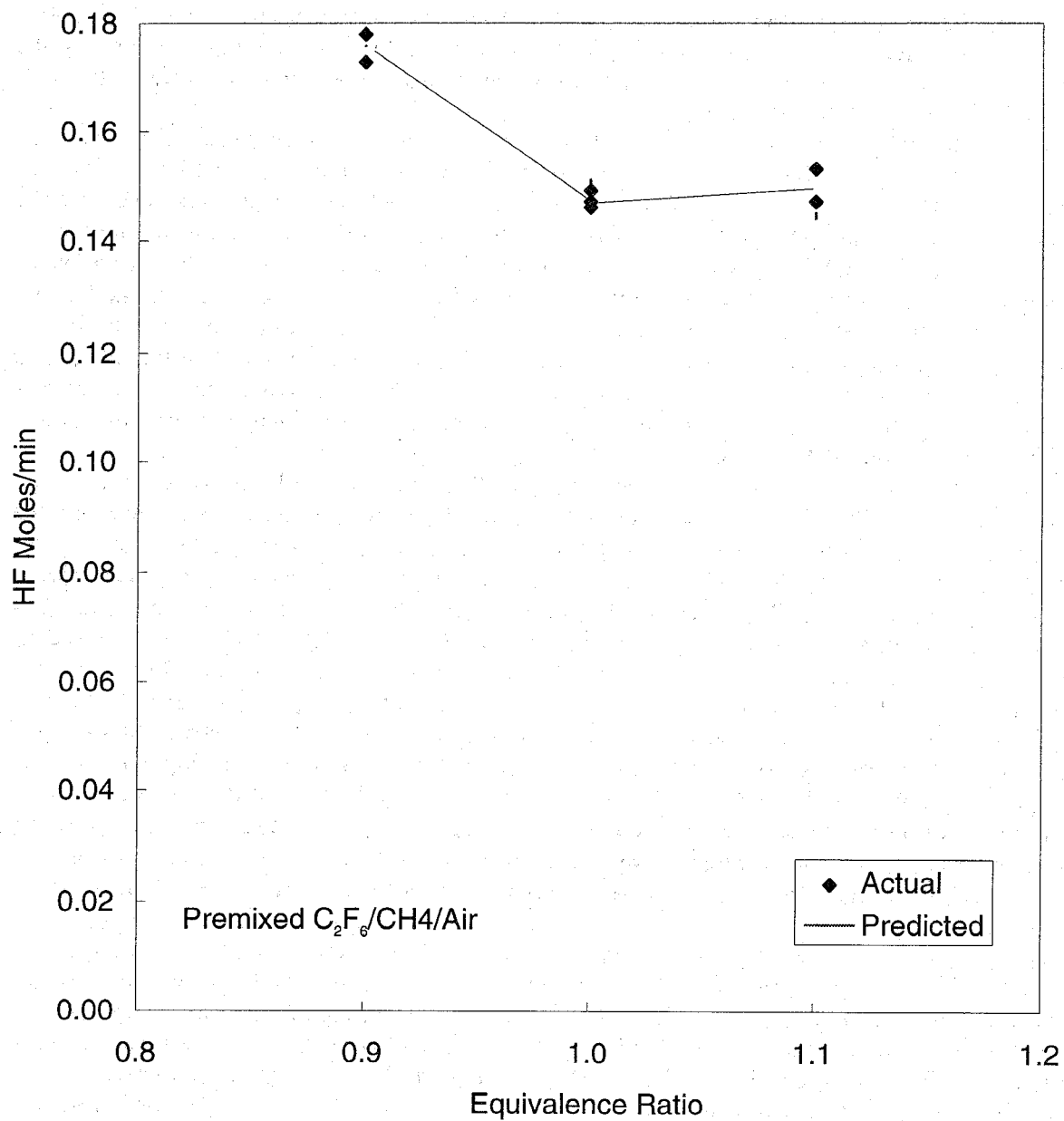


Figure 33. Measured and calculated HF production from C_2F_6 in a premixed methane-air flame for $\phi = 0.9, 1.0, \text{ and } 1.1$.

this hydrogen limit may or may not exist (depending upon whether the kinetics are fast enough to form COF_2 in the hydrogen-limited case).

Also shown in the figure are the experimentally measured HF production rates for the jet and cup burners (labeled c and j respectively) at 50 % and 90 % of the extinction concentration of C_2F_6 . As indicated, the measured quantities of HF are lower than both the fluorine and hydrogen limits, and the measured values are closer to the estimated limits when the effects of preferential diffusion (H' and F') are included as described above.

Although the cup and jet burner results are plotted together, the phenomenological behavior of jet burner is distinctly different from that of the cup burner. Because the flame of the jet burner first stabilizes as a co-flow diffusion flame anchored at the outlet of the jet, the heated gases have a much lower Reynolds number, keeping the flow laminar. As inhibitor is added to the air stream, the flame grows in length (as it would in increasing the fuel flow rate). Eventually, the flame lifts off the burner surface by about 5 cm to form a lifted jet diffusion flame. With further inhibitor addition, the flame eventually blows off. These blow-off concentrations are referred to as the extinction concentrations (see Table 1) and are found to be much lower (about half) of the values determined for the cup burner. In the tests at 50 % extinction, the flow is laminar, whereas at 90 % of extinction, the flow is nearly turbulent and the flame is lifted. Transport of the agent into the flame is estimated in the stoichiometric model assuming molecular diffusion.

The goal of these experiments is to compare the model's prediction of HF formation for a diffusion flame where more vigorous mixing occurs, and identify if the enhanced mixing increases the HF production. Figures 34 to 45 show that HF production in the turbulent burner at 90 % of extinction is higher relative to the model prediction than the cup burner results at 90 % (except for C_2F_6 and C_4F_8), but that the jet burner HF production rates are still not above the estimate of the fluorine flux based on equal transport for O_2 and the inhibitor (the curve labeled F). When viewed as in Figures 34 - 45, the behavior of the alternative inhibitors falls into three categories. In the first category are the inhibitors C_2F_6 , C_3F_8 , C_4F_{10} , C_3F_8 , C_2HF_5 , and C_3HF_7 (Figures 34 - 39). For these inhibitors, at the highest inhibitor concentration tested (cup burner at 90 % of extinction) the estimated hydrogen flux into the reaction zone is lower than the fluorine flux. The ratio of hydrogen to total halogen flux ranges from 0.31 to 0.68, and the H flux is not a strong function of the inhibitor concentration. For these inhibitors, the HF produced does not increase significantly when the inhibitor concentration in the air stream increases above that necessary for a hydrogen/fluorine ratio in the reaction zone of about unity (the region of where the lines marked F and H or F' and H' cross in Figures 34 to 43).

A second category includes those inhibitors ($\text{C}_2\text{H}_2\text{F}_4$, C_2HClF_4 , $\text{C}_3\text{H}_2\text{F}_6$, and $\text{CH}_2\text{F}_2/\text{C}_2\text{HF}_5$; Figures 40 to 43) for which the estimated H and X fluxes are closer, with H/X ratios of 0.68 to 0.85. For these inhibitors, the amount of HF produced increases with increasing inhibitor concentration in the air, but the highest concentration tested corresponds F/H ratio of about unity in the reaction zone. The last category consists of CF_3Br and CHClF_2 (Figures 44 and 45) for which the estimated hydrogen flux is much higher than halogen flux (in a ratio of 2.3 and 1.1, respectively), and there is estimated always to be more hydrogen than halogen in the reaction zone. For these agents, the HF produced is always increasing with higher agent concentration in the air stream. Although the stoichiometric model is simple and is only expected to provide an upper limit on the amount of HF formed, it is instructive to investigate the possible reasons that the measured HF production rates might be lower than the estimates. Lower HF may be measured in the experiments due to experimental difficulties, for example: loss of HF to the chimney walls, loss in the sampling system, HF undetected by the ion-selective electrodes, or imperfect mixing in the product gases. Based on parametric tests, however, these loss mechanisms are found to be minor. The predicted values of the

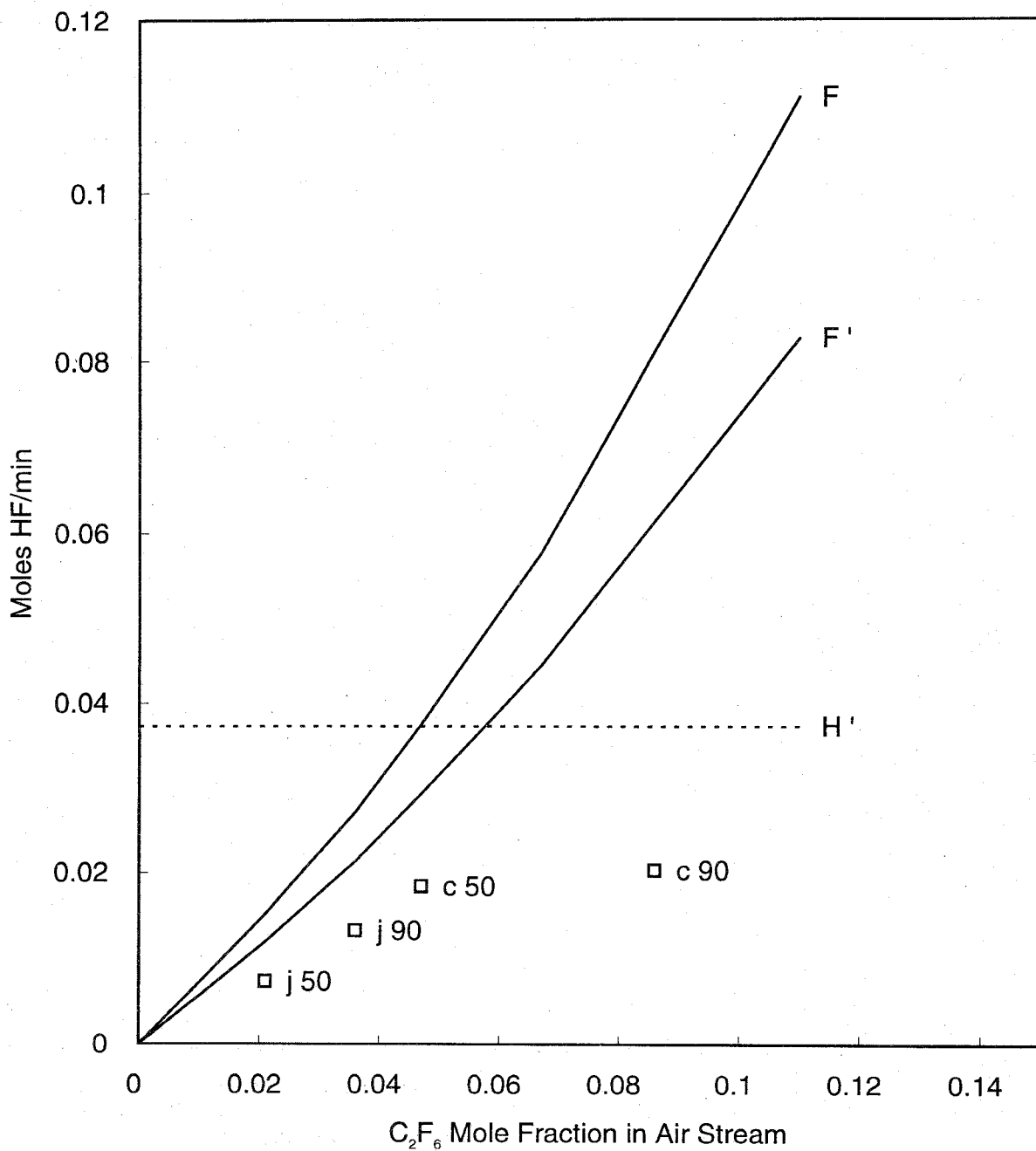


Figure 34. Measured HF production rates in co-flow propane-air diffusion flames inhibited by C_2F_6 with estimated fluorine and hydrogen fluxes to the reaction zone.

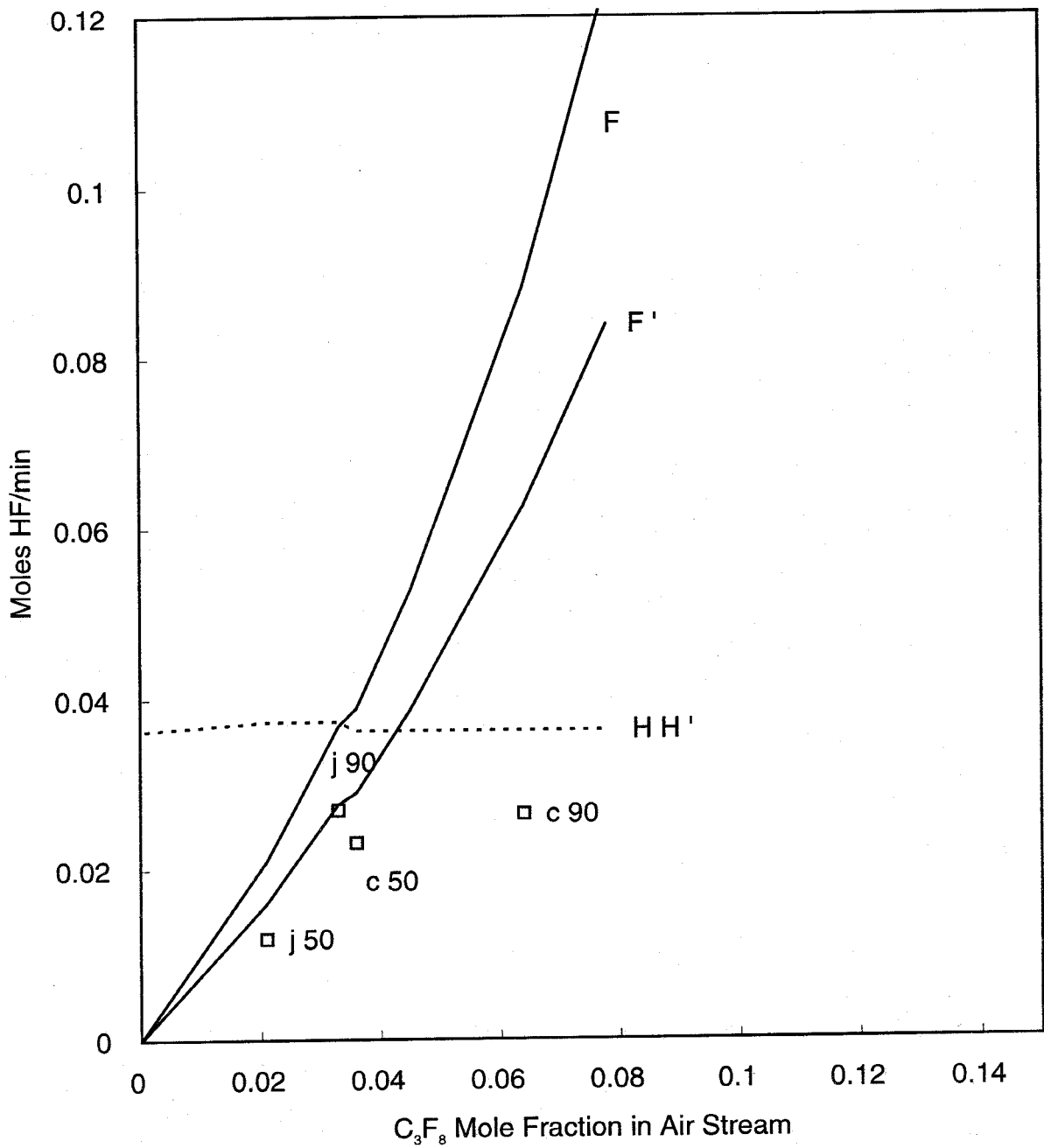


Figure 35. Measured HF production rates in co-flow propane-air diffusion flames inhibited by C₃F₈ with estimated fluorine and hydrogen fluxes to the reaction zone.

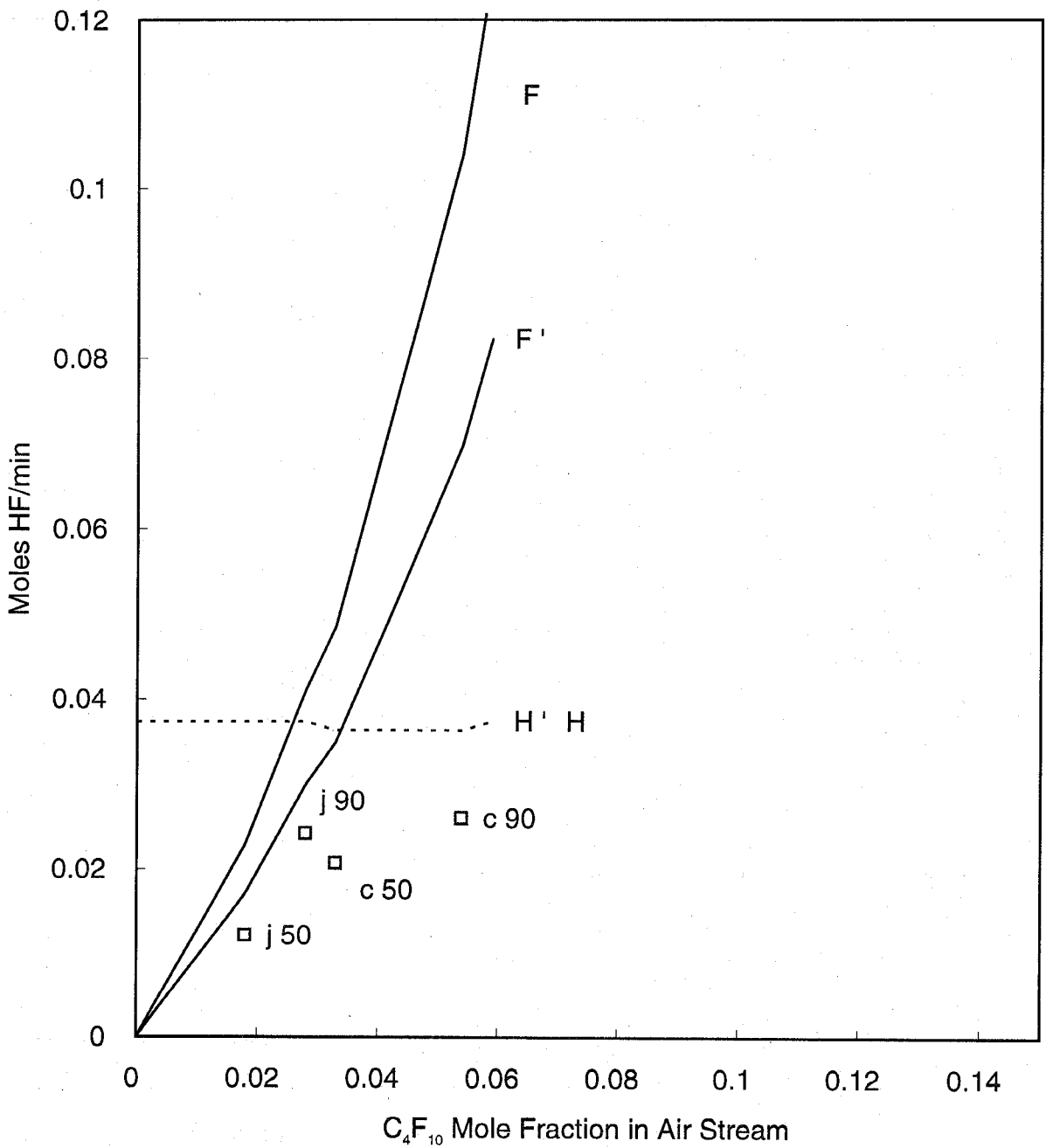


Figure 36. Measured HF production rates in co-flow propane-air diffusion flames inhibited by C_4F_{10} with estimated fluorine and hydrogen fluxes to the reaction zone.

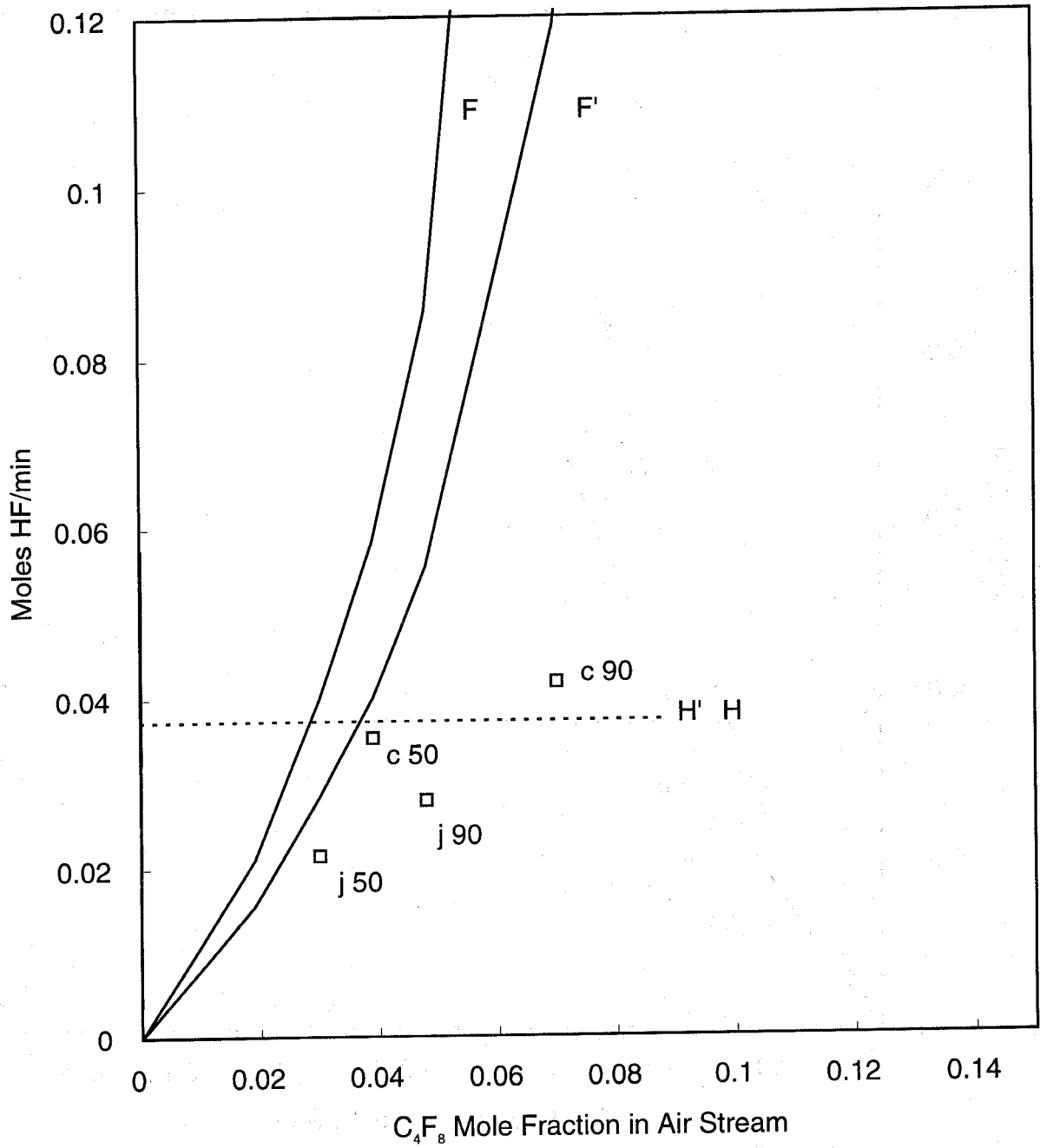


Figure 37. Measured HF production rates in co-flow propane-air diffusion flames inhibited by C₄F₈ with estimated fluorine and hydrogen fluxes to the reaction zone.

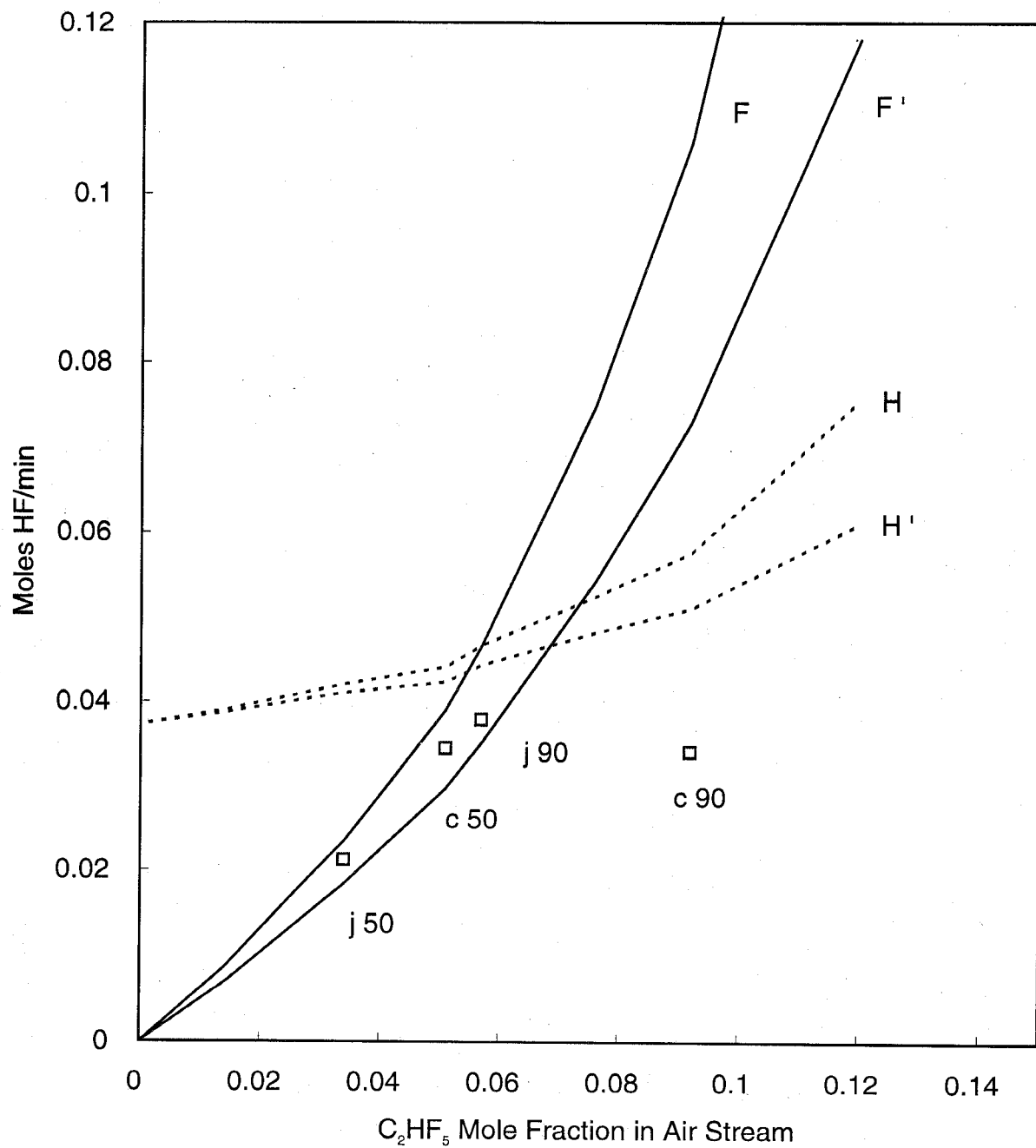


Figure 38. Measured HF production rates in co-flow propane-air diffusion flames inhibited by C₂HF₅ with estimated fluorine and hydrogen fluxes to the reaction zone.

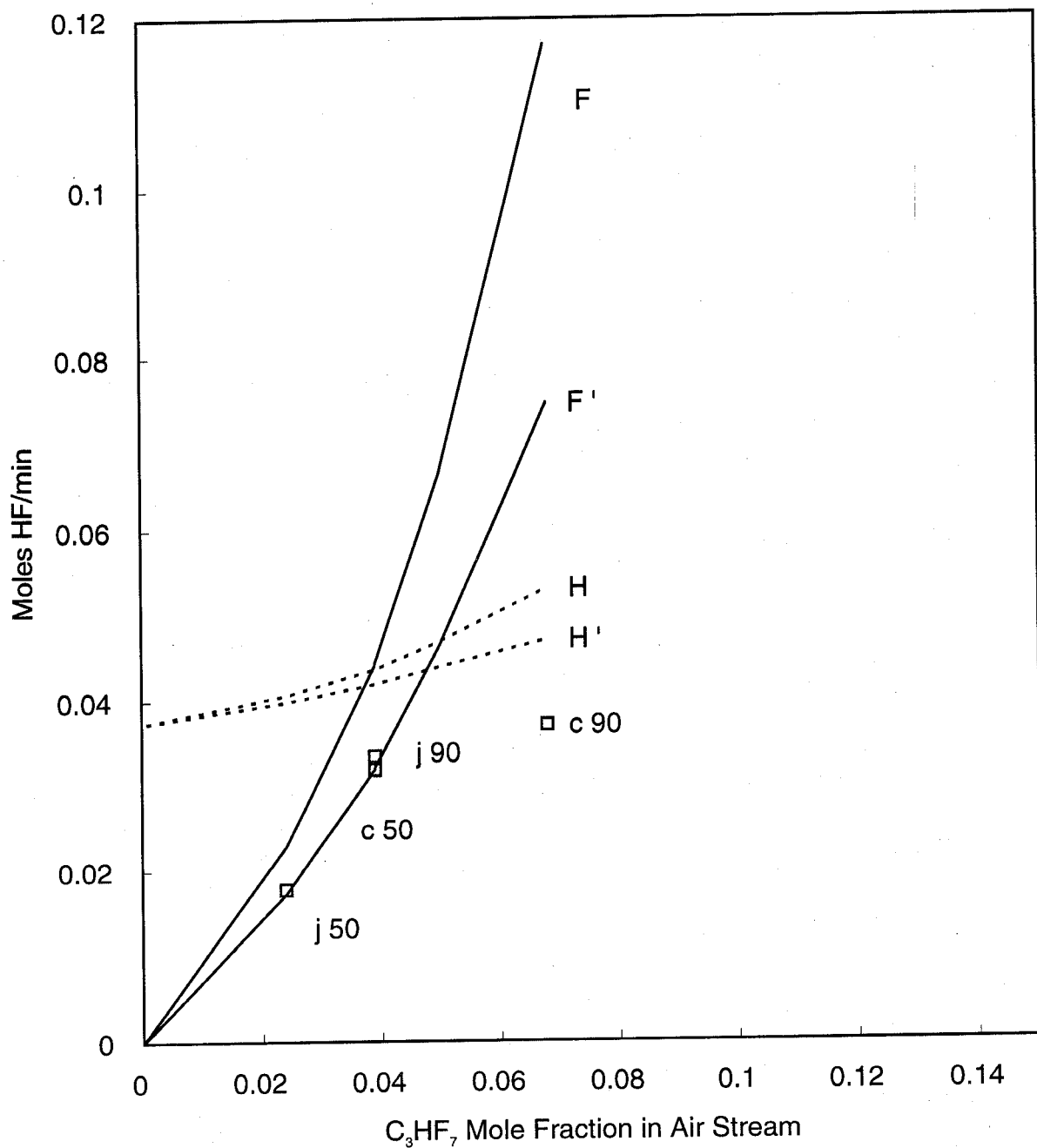


Figure 39. Measured HF production rates in co-flow propane-air diffusion flames inhibited by C_3HF_7 with estimated fluorine and hydrogen fluxes to the reaction zone.

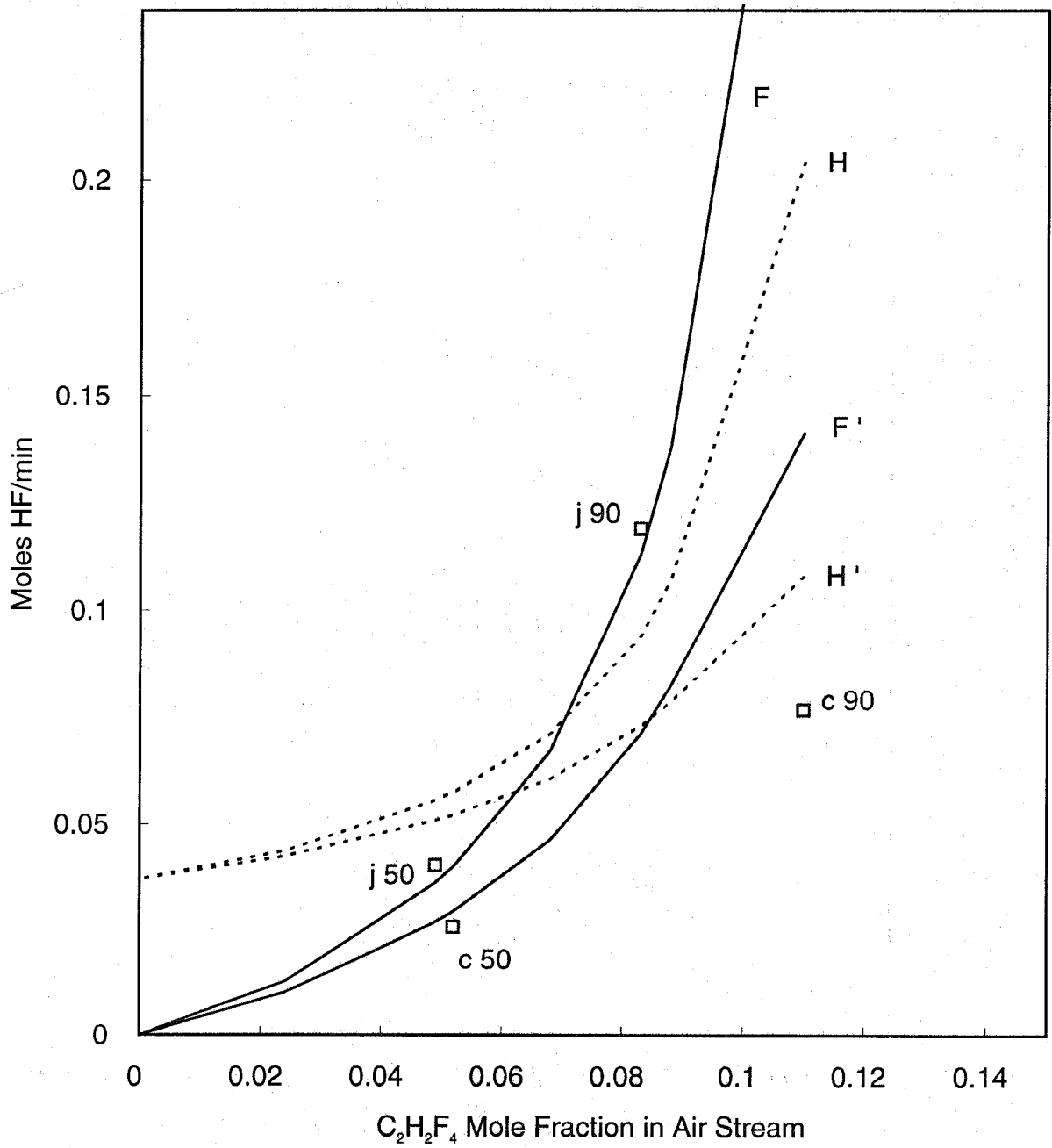


Figure 40. Measured HF production rates in co-flow propane-air diffusion flames inhibited by C₂H₂F₄ with estimated fluorine and hydrogen fluxes to the reaction zone.

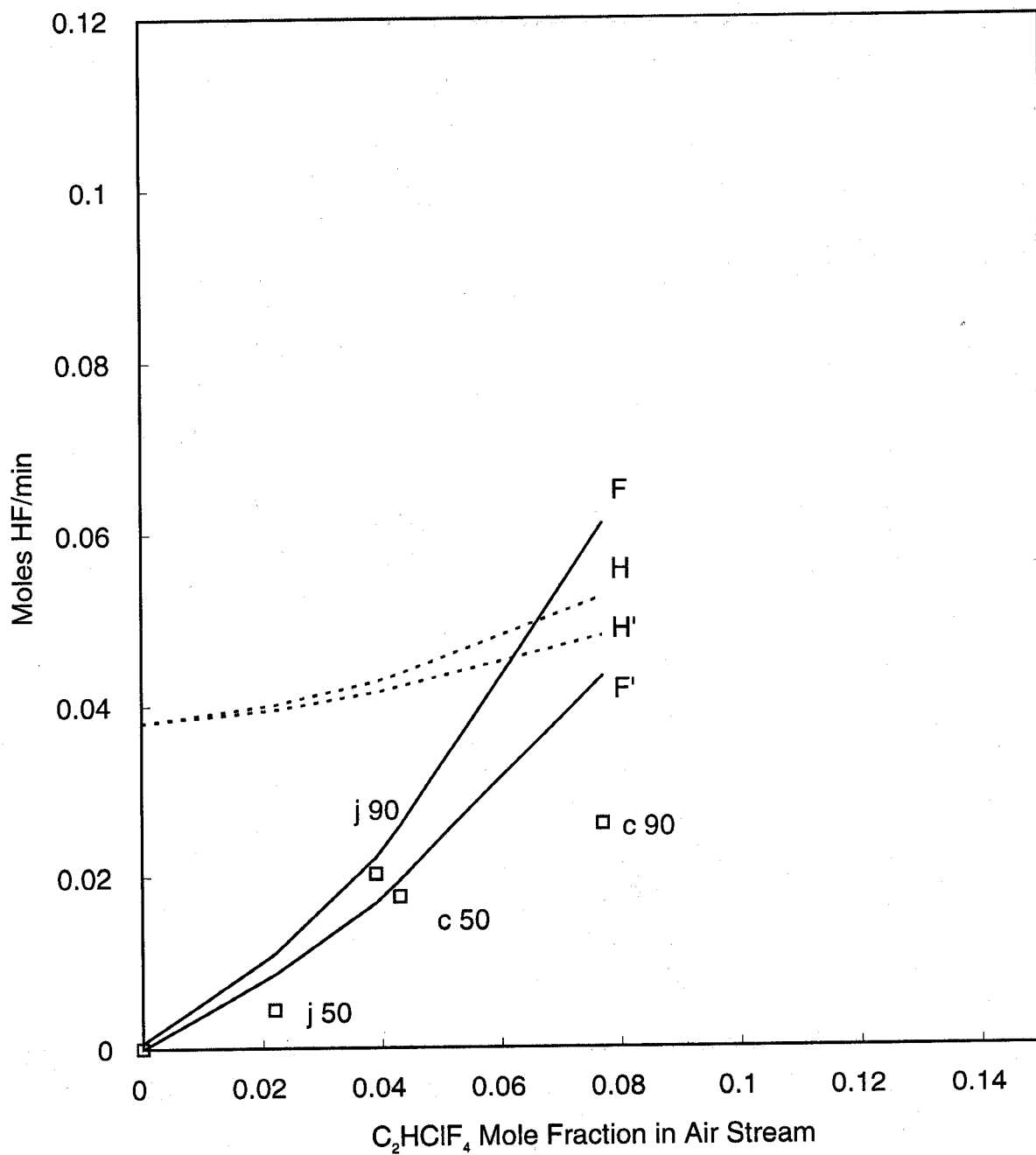


Figure 41. Measured HF production rates in co-flow propane-air diffusion flames inhibited by C_2HClF_4 with estimated fluorine and hydrogen fluxes to the reaction zone.

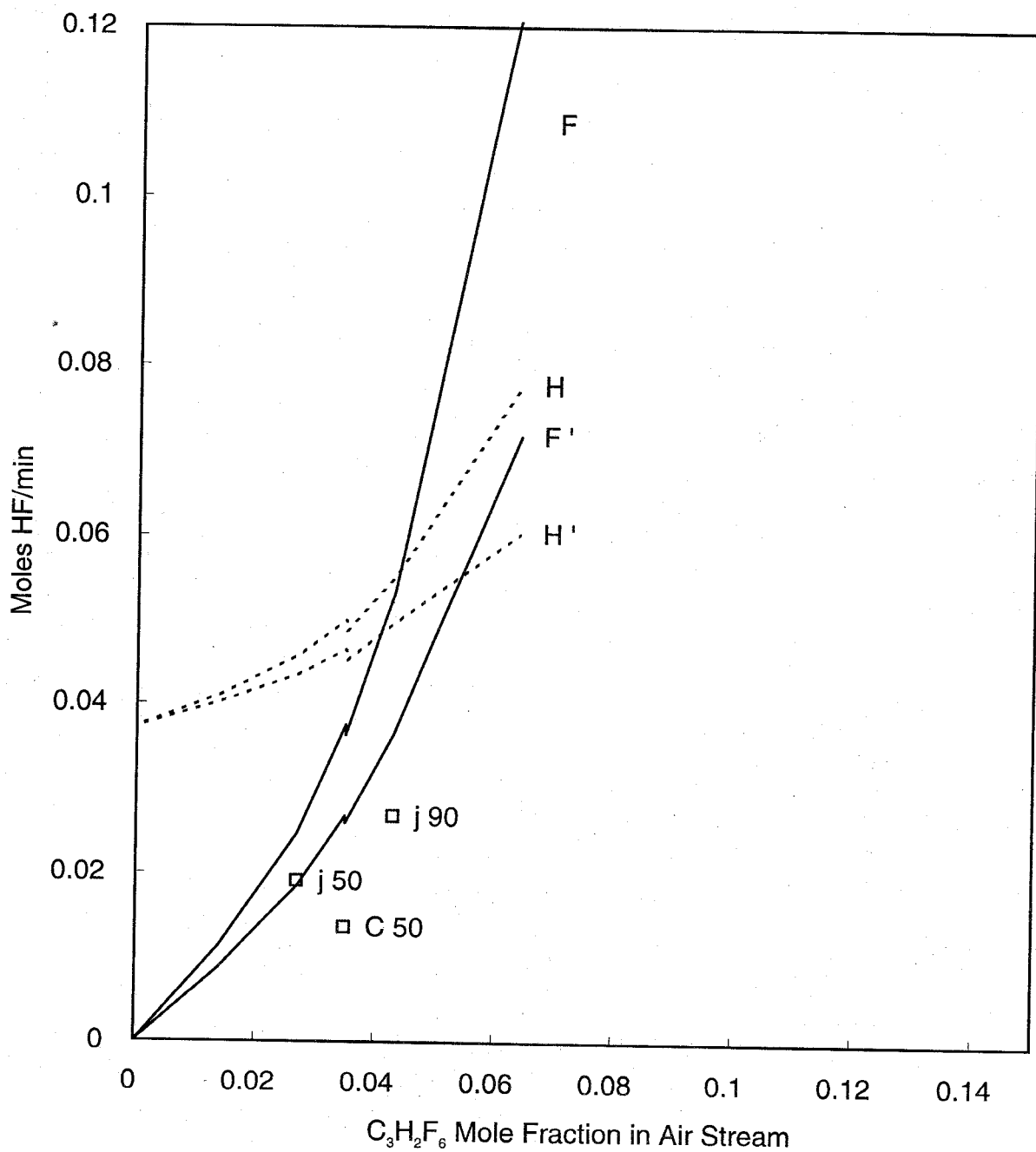


Figure 42. Measured HF production rates in co-flow propane-air diffusion flames inhibited by $C_3H_2F_6$ with estimated fluorine and hydrogen fluxes to the reaction zone.

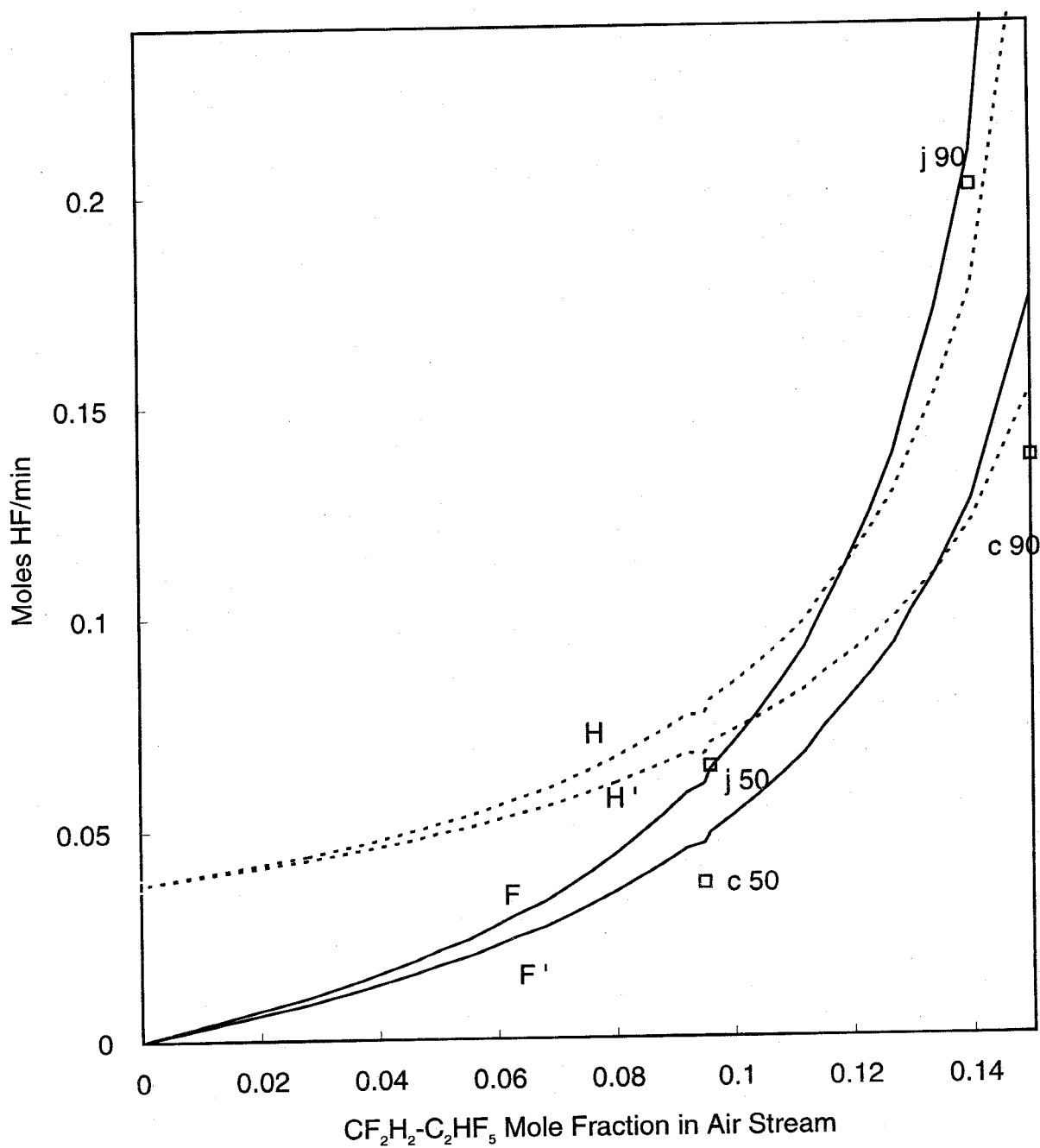


Figure 43. Measured HF production rates in co-flow propane-air diffusion flames inhibited by CF₂H₂-C₂HF₅ with estimated fluorine and hydrogen fluxes to the reaction zone.

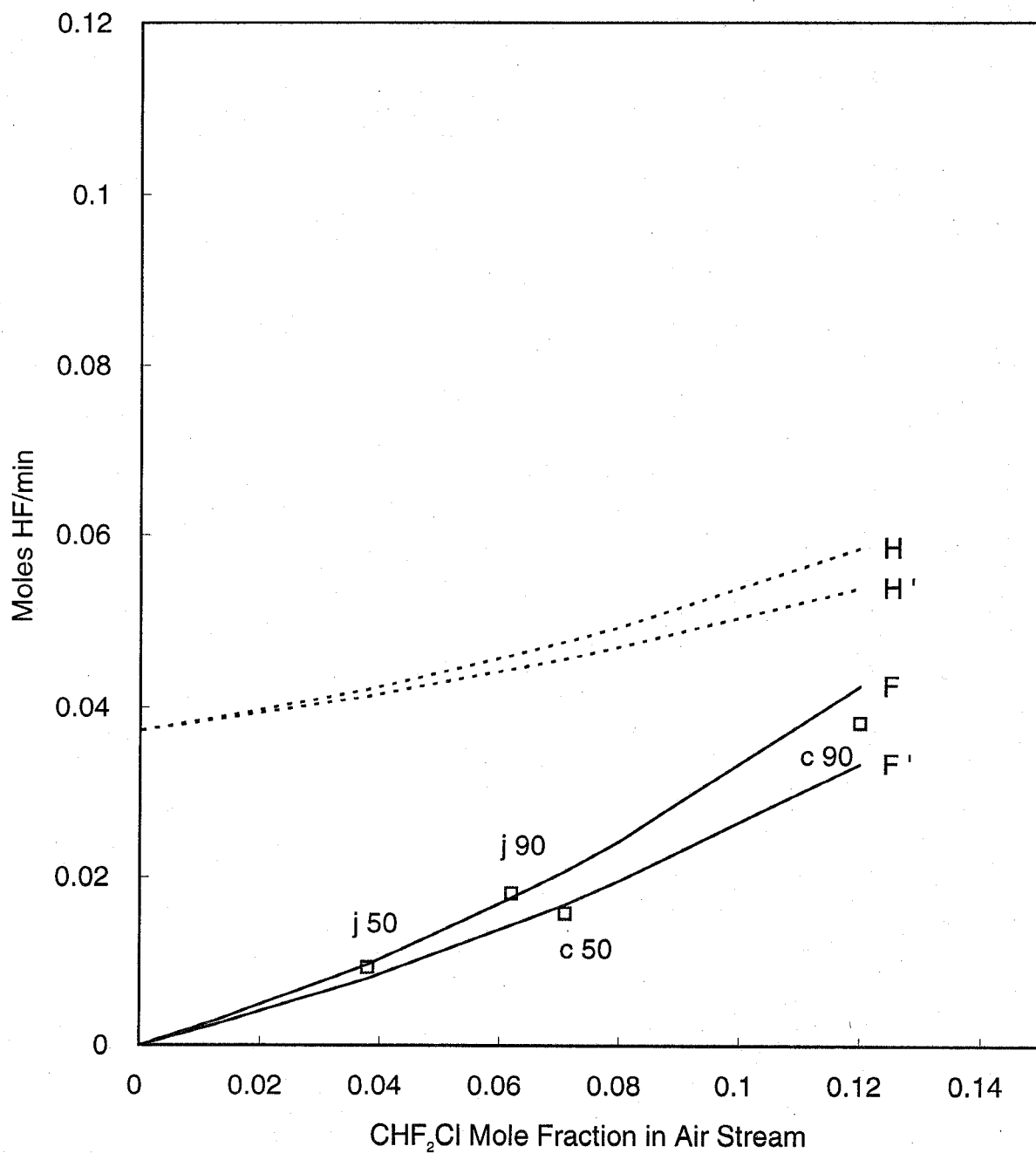


Figure 44. Measured HF production rates in co-flow propane-air diffusion flames inhibited by CHF₂Cl with estimated fluorine and hydrogen fluxes to the reaction zone.

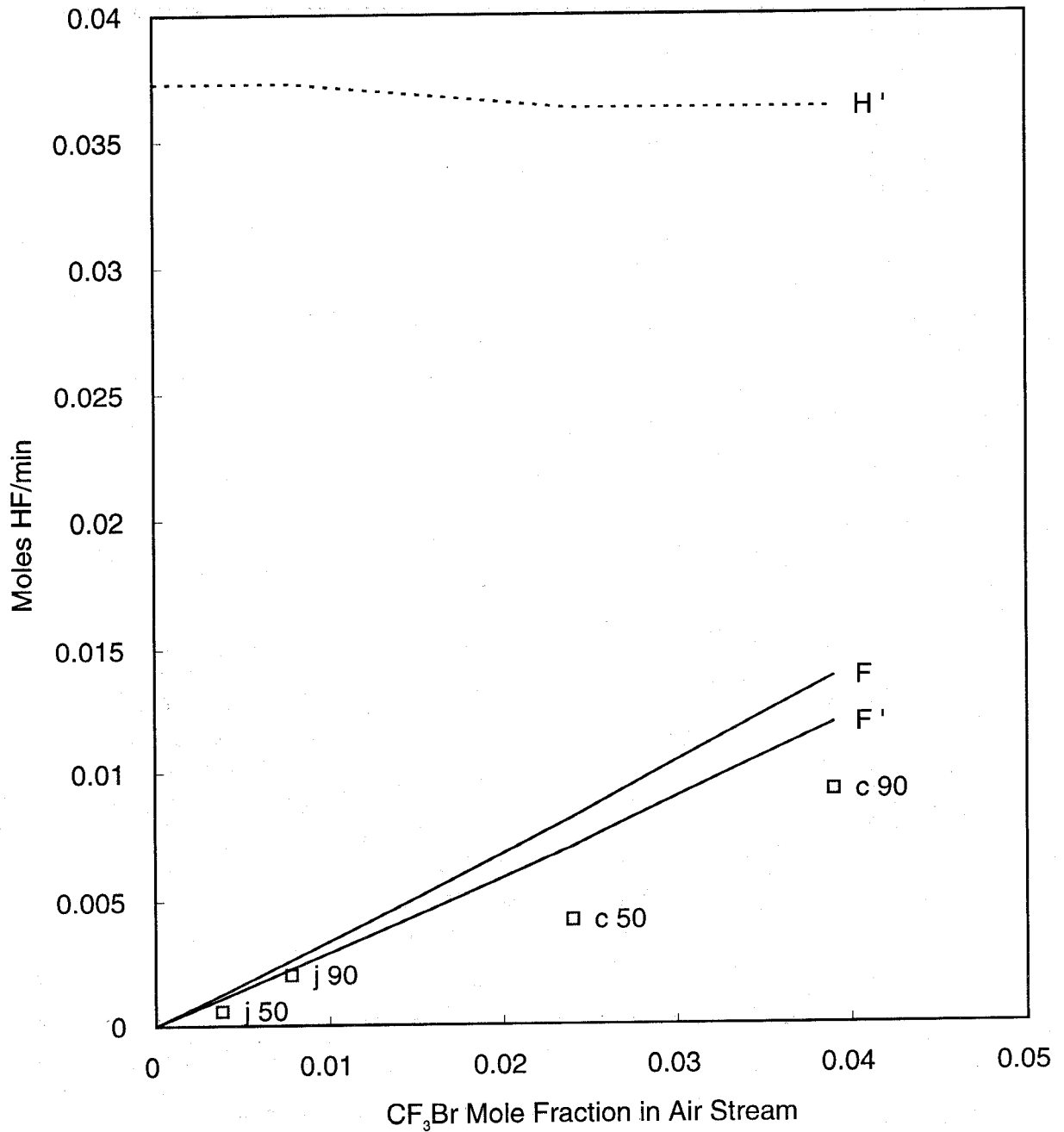


Figure 45. Measured HF production rates in co-flow propane-air diffusion flames inhibited by CF₃Br with estimated fluorine and hydrogen fluxes to the reaction zone.

Table 2. Extinction conditions for halon alternatives added to the air stream of co-flow propane-air cup burner and jet burner flames

Inhibitor	Extinction Concentration in Air (mole percent)	
	jet	cup
C_2F_6	3.8	9.4
C_3F_8	3.8	7.5
C_4F_{10}	3.2	5.0
C_4F_8	5.1	7.6
C_2HF_5	6.2	10.2
C_3HF_7	4.2	7.6
$C_2H_2F_4$	9.5	11.1
C_2HClF_4	4.2	8.6
$C_3H_2F_6$	4.0	7.2
CH_2F_2/C_2HF_5	15.5	15.2
CF_3Br	0.8	4.3
$CHClF_2$	6.7	13.8

HF production do not include chemical kinetic limitations; this is believed to be the likely source of the discrepancy.

The experimental results are typically within 30 % of the prediction for the hydrogenated fluorocarbons, which is good considering the simplicity of the model. Perfluorinated agents produce HF at rates significantly less, up to 50 %, than predicted based on equilibrium thermodynamics. These agents are believed to react more slowly in the flame. A detailed understanding of the apparent chemical kinetic limitations to HF formation for the perfluorinated agents at all concentrations as well as for hydrofluorocarbons at high fluorine loading should be possible using a recently developed chemical kinetic mechanism for fluorine inhibition of hydrocarbon flames (Burgess *et al.*, 1994) together with a diffusion flame model. For the present analyses, however, the predicted acid gas formation in inhibited flames is based on equilibrium thermodynamics assuming that HF (not COF_2) is the source.

The measured HF for CF_3I is shown in Figure 46. For CF_3Br , the experimental results are about 30 % lower than the prediction, although both are significantly lower than for the HFCs. On the other hand, CF_3I makes about twice as much HF as is predicted by the model (which was not developed for CF_3I), or about three times as much HF as CF_3Br in these diffusion flames. The reasons for this is believed to be due to the relative weakness of the C-I bond in CF_3I . It is likely that CF_3I enters the hot region near or above the flame and undergoes thermal decomposition much more easily than the other agents tested, so that the net amount of HF formed is higher (and higher than predicted from the model which assumes no additional decomposition in the region above the flame).

10.8.3 Steady-state - Liquid Diffusion Flames. For the liquid-fueled cup burner experiments the consumption rate of the fuel is found to be a strong function of the inhibition concentration. Figure 47 shows the measured burning rate (g/s) for heptane as a function of the C_2HF_5 mole fraction in the air stream. The measured HF formation rates for liquid cup burner flames of heptane are shown in Figures 48 to 51 for C_2HF_5 , C_3HF_7 , $C_2H_2F_4$, and C_3F_8 . As in Figures 34 to 46, the solid lines

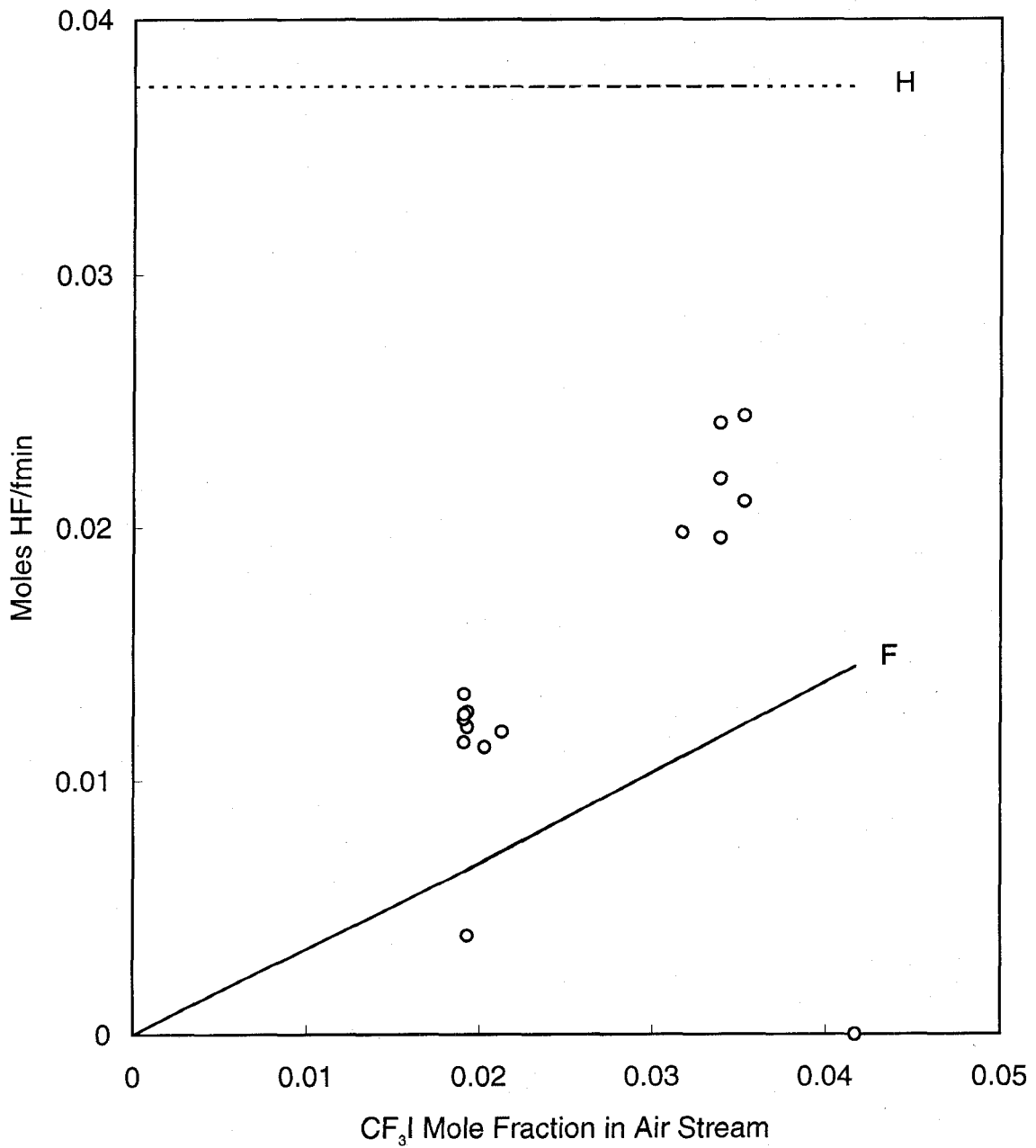


Figure 46. Measured HF production rates in co-flow propane-air diffusion flames inhibited by CF₃I with estimated fluorine and hydrogen fluxes to the reaction zone.

indicate the predicted flux of F and H into the flame. The measured HF production rate for these steady-state flames is within 16 % of the lower of the F or H flux for all of the inhibitors except C_2HF_5 . For this agent, the measured HF production rate is about 30 % higher than the estimated hydrogen flux, and is well predicted by the fluorine flux. The reasons for this discrepancy are unclear, but may be related to details of the reaction mechanism for this particular agent and fuel. It is important to emphasize that the "hydrogen limit" is really a kinetic argument. As illustrated in Figure 27, when there is not enough hydrogen to form HF as an equilibrium product, the thermodynamically-favored product is COF_2 . This species also appears in the bubbler as fluoride ion, and is thus indistinguishable from HF. Thus, when the hydrogen to fluorine ratio drops below unity, the argument is that the kinetics slow down such that the stages of inhibitor consumption which form either COF_2 or HF are impeded. Given the premixed modeling results described above, as well as the experimental results for inhibitor addition to premixed flames, this interpretation seems appropriate.

Nonetheless, it is remarkable that the rather simple stoichiometric model is still able to predict the HF formation within 30 % for this liquid pool flame when the agent is present at 90 % of the extinction value and the heat feedback and kinetics are affected to such an extent that the burning rate is reduced by about a factor of 2.5. This lends support for the basic assumptions in the model that the products are controlled primarily by the quantities of hydrogen and fluorine in the flame, and that these are controlled primarily by the fuel type and consumption rate and the inhibitor type and mole fraction in the air stream. The final assumption of equal characteristic flame height for both fuel and inhibitor consumption also appears to be good.

10.8.4 Transient-state - Gaseous Diffusion Flames. As described above, HF formation in the propane-air cup burner flames was also measured when the inhibitor was added in a transient fashion, rather than in steady-state, and the flames were extinguished. The concentration of inhibitor varied linearly from zero to 125 % of the extinction concentration, and the injection rate of inhibitor was varied to produce flame-extinguishment times of 5 to 18 seconds. Experiments were conducted for the agents C_2HF_5 , C_3HF_7 , C_3F_8 .

The results are shown in Figures 52 - 54 respectively, where the total mass of F- produced during the extinction event is plotted as a function of the extinction time. Also indicated in the figures are the predicted HF formed using the stoichiometric model assuming equilibrium products (solid lines), and using the model in which the steady-state HF production rates are determined from empirically determined deviations from full equilibrium based on the steady-state results. As the figures show, in either case, the model is able to predict the results within the experimental scatter. The uncertainty in Figures 52 to 54 is essentially shown by the experimental variation for similar conditions. Most of this variation is believed to occur from differences in the mixing of product gases with co-flowing air in the chimney prior to sampling. While the degree of mixing varies from run to run, the magnitude of the fluctuations are difficult to specify due to the turbulent nature. The relatively short experiment times (only a factor of three or four greater than the mixing times) accentuates the problem. Unfortunately, signal averaging (which would be achieved through longer experimental times) is not possible as in the steady-state experiments.

10.9 HF Production in Larger Scale Tests

The stoichiometric model developed above from consideration of laboratory flames allows an estimation of the HF generation based on the fuel consumption rate and transport of the agent in the flame. However, the quantities of acid gases formed in a large-scale suppressed fire will depend upon

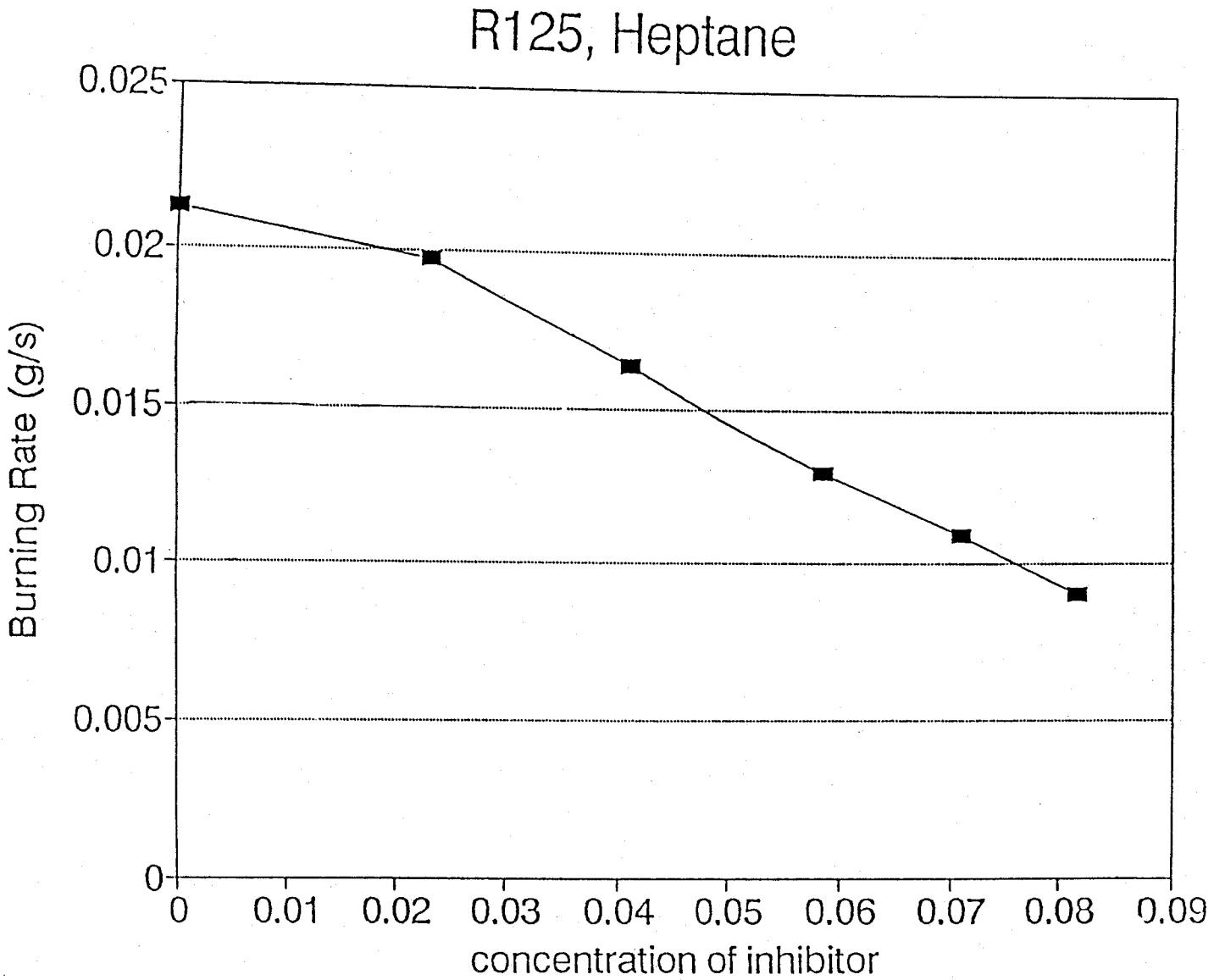


Figure 47. Burning rate of heptane in cup burner as a function of C_2HF_5 mole fraction in the air stream.

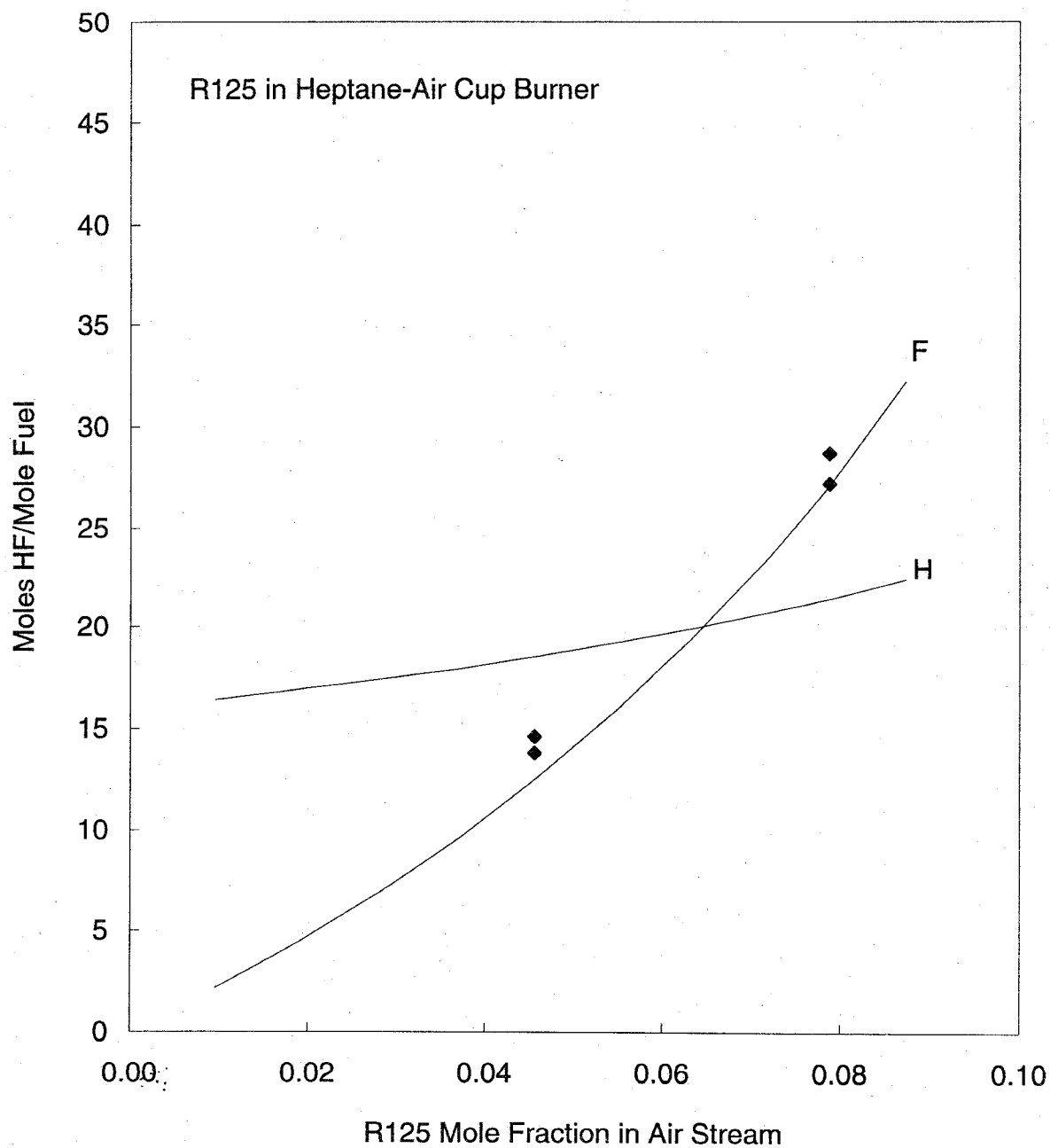


Figure 48. Measured HF production rates in co-flow heptane-air diffusion flames inhibited by C_2HF_5 with estimated fluorine and hydrogen fluxes to the reaction zone.

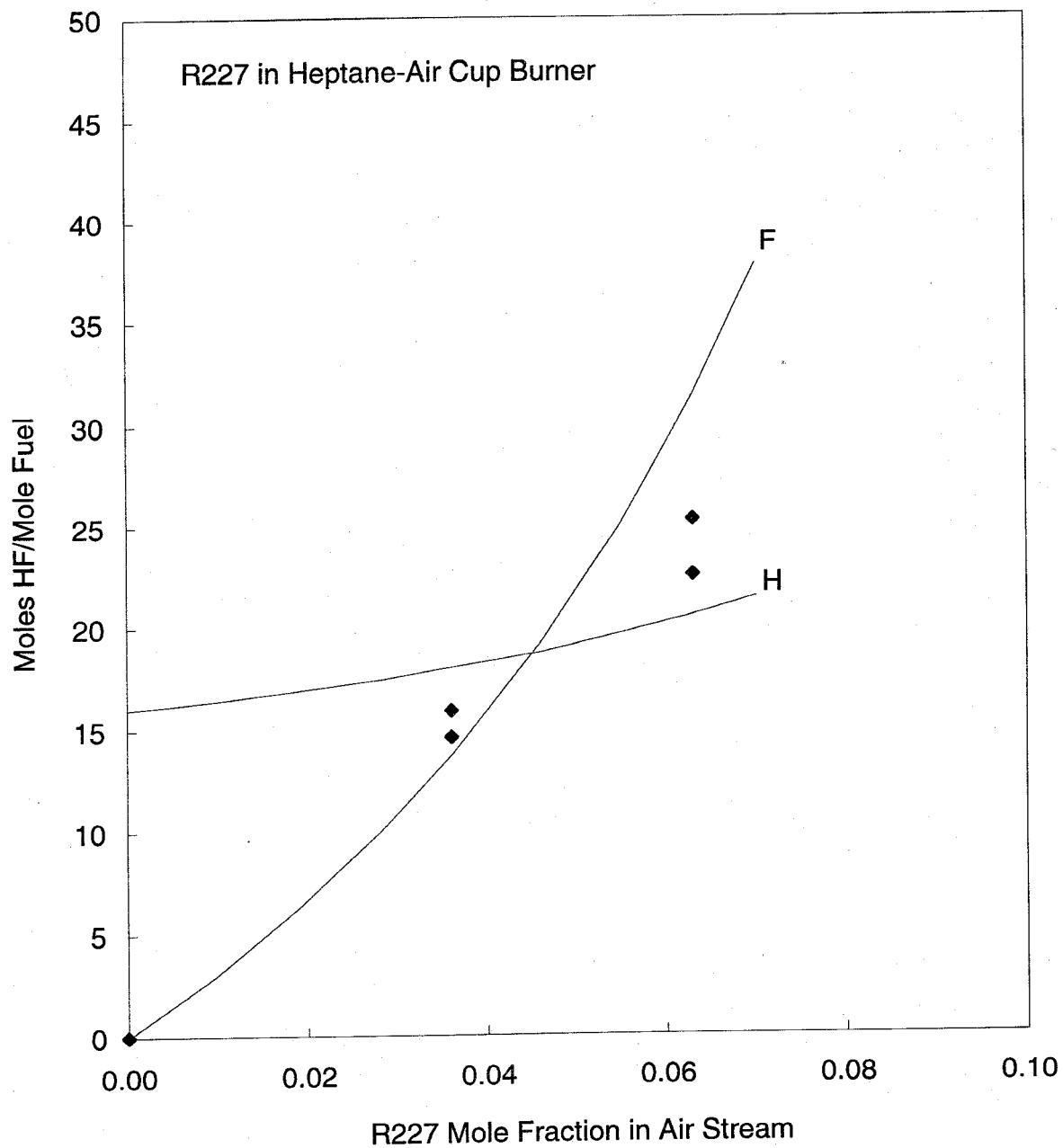


Figure 49. Measured HF production rates in co-flow heptane-air diffusion flames inhibited by C_3HF_7 with estimated fluorine and hydrogen fluxes to the reaction zone.

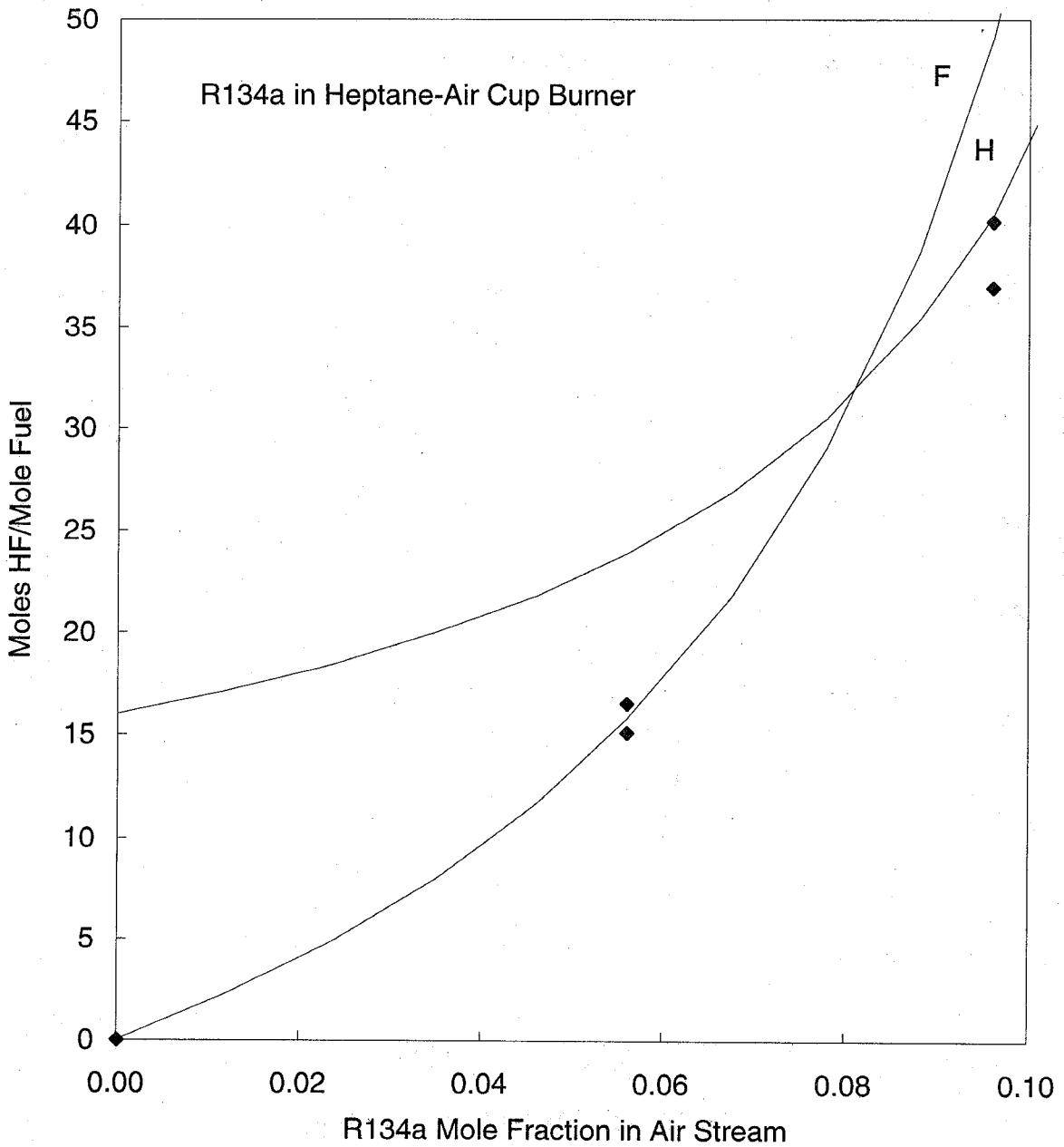


Figure 50. Measured HF production rates in co-flow heptane-air diffusion flames inhibited by $C_2H_2F_4$ with estimated fluorine and hydrogen fluxes to the reaction zone.

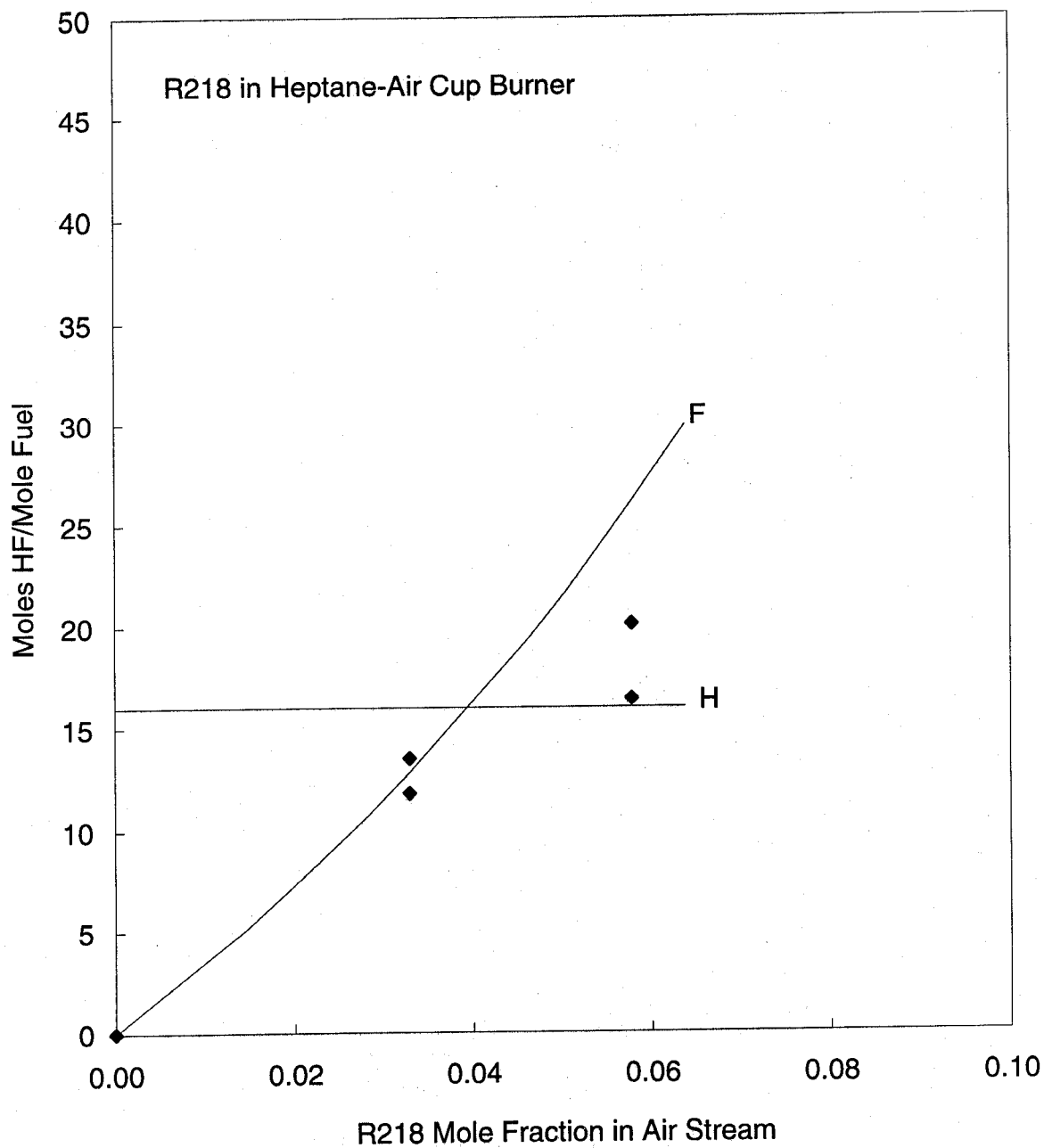


Figure 51. Measured HF production rates in co-flow heptane-air diffusion flames inhibited by C_3F_8 with estimated fluorine and hydrogen fluxes to the reaction zone.

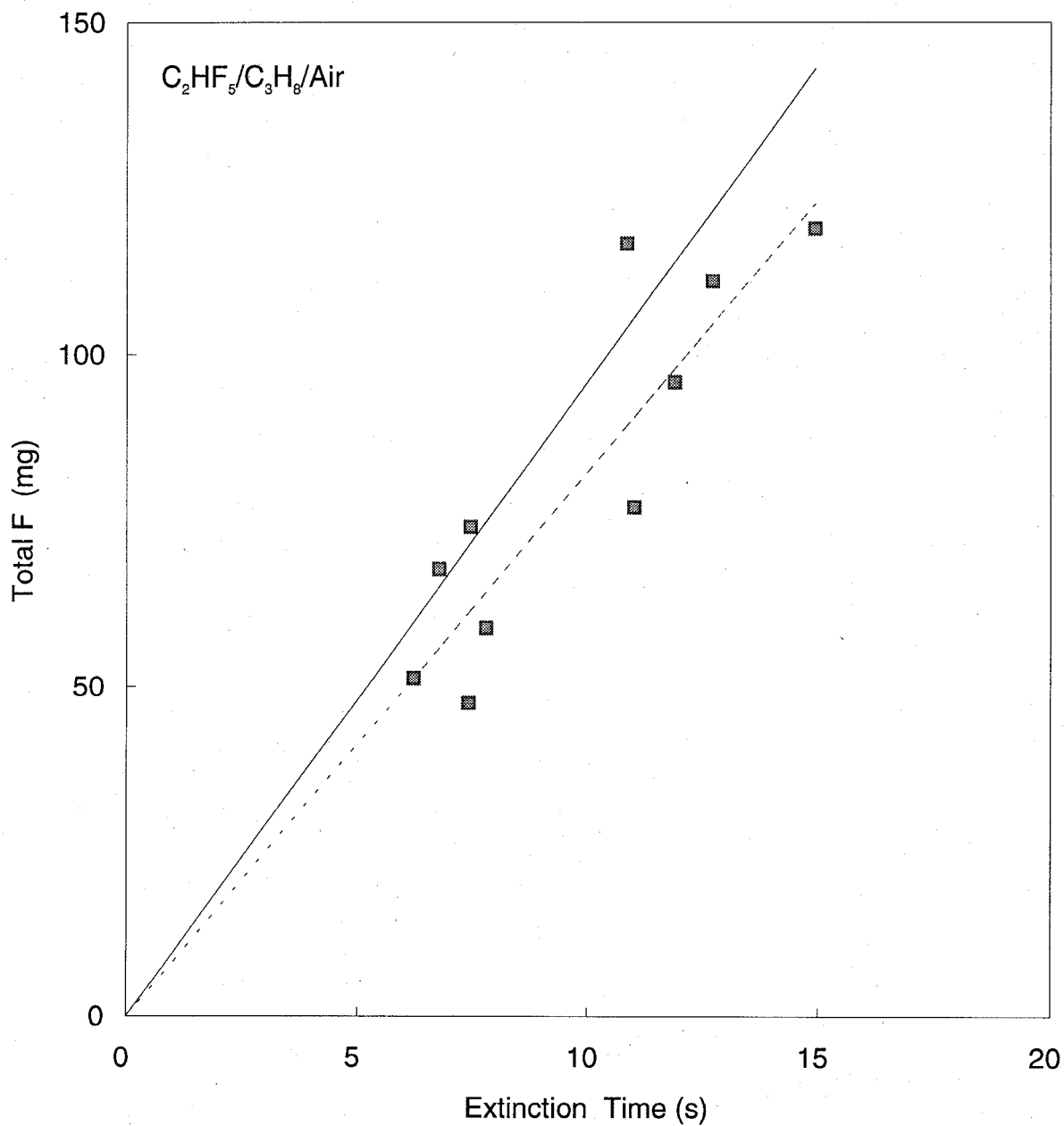


Figure 52. Total fluoride produced (points) during suppression of a cup burner propane-air diffusion flame for various extinction times, together with model predictions (solid line: calculations; dotted line: steady-state results).

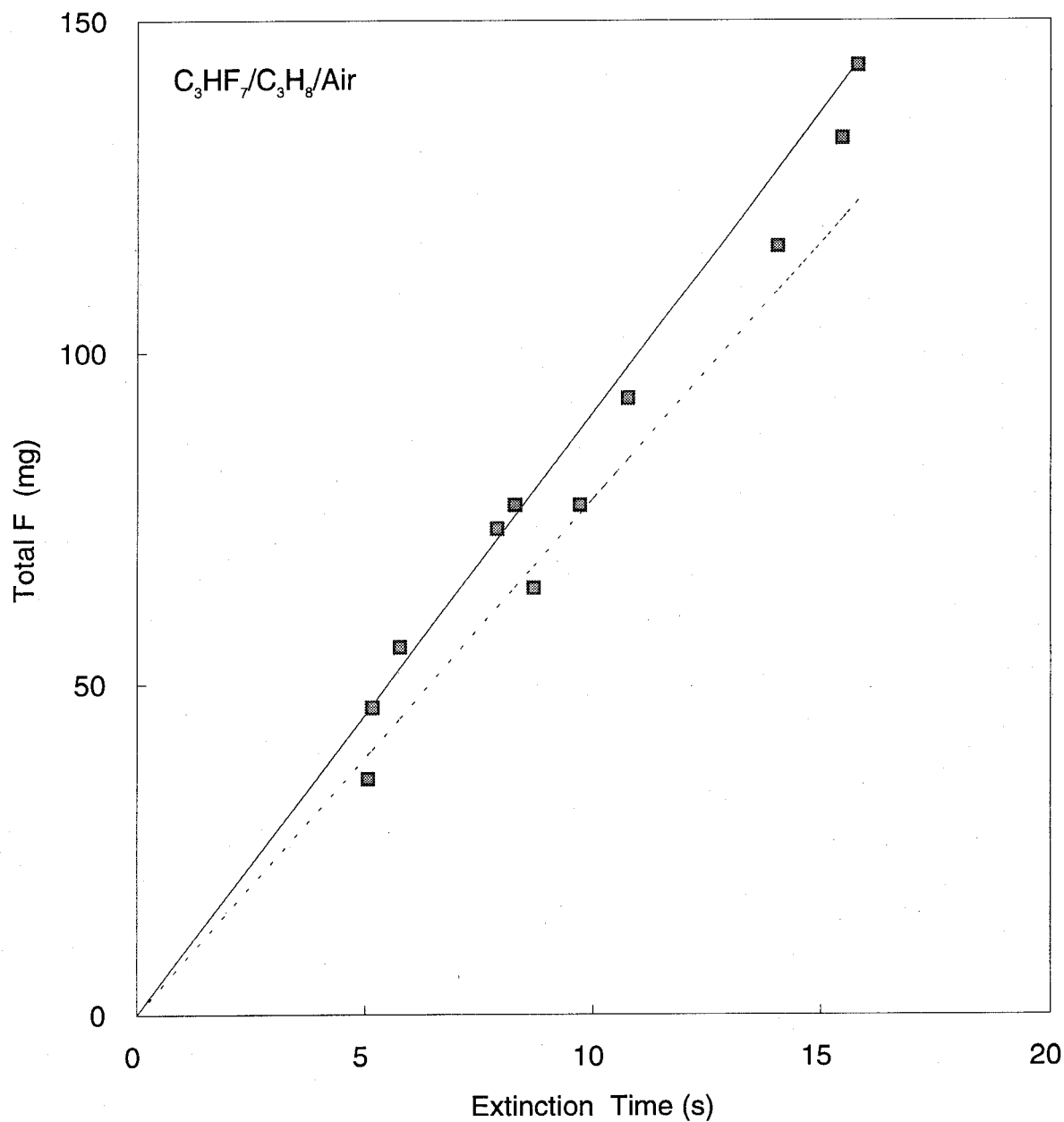


Figure 53. Total fluoride produced (points) during suppression of a cup burner propane-air diffusion flame for various extinction times, together with model predictions (solid line: calculations; dotted line: steady-state results).

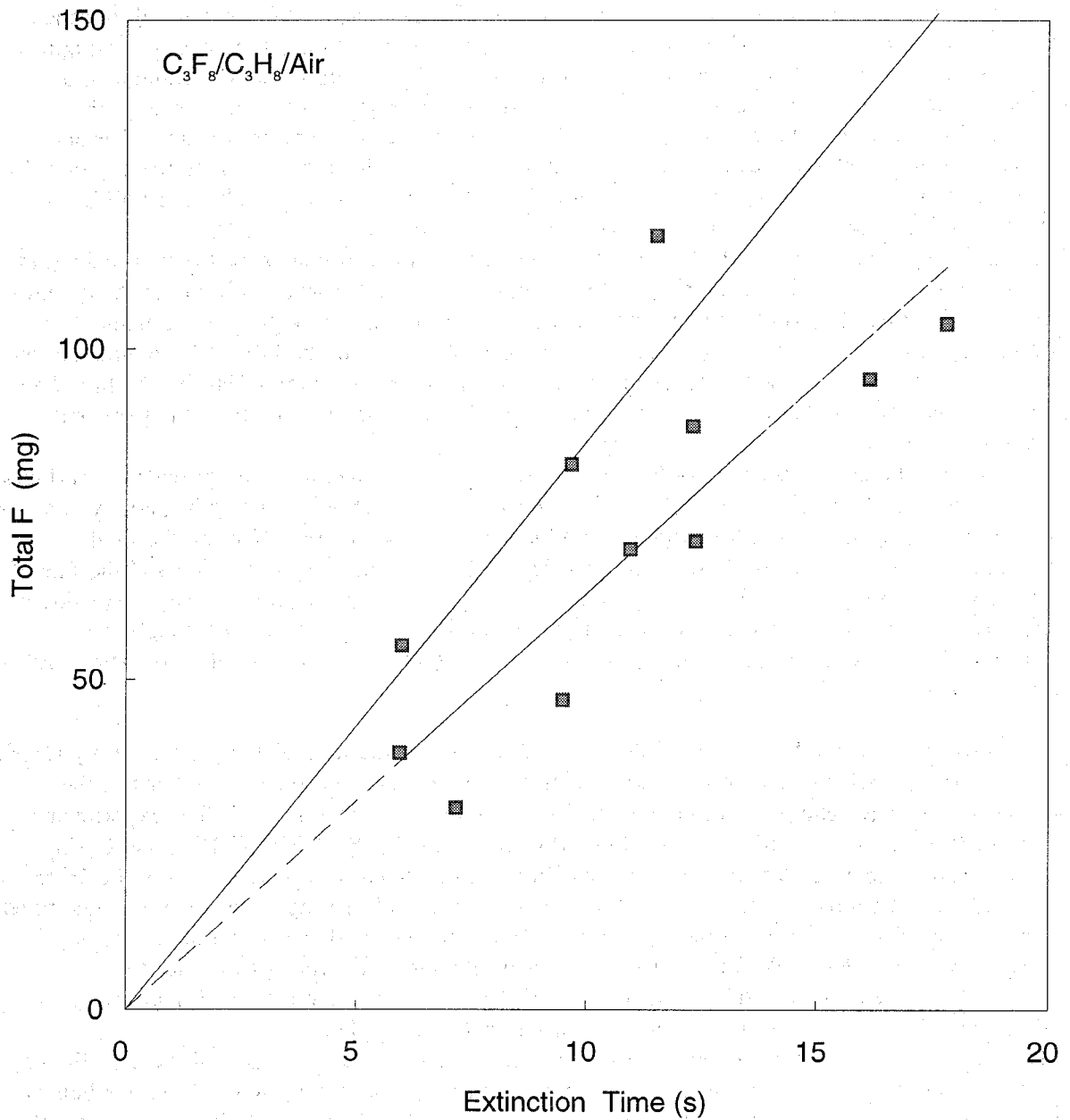


Figure 54. Total fluoride produced (points) during suppression of a cup burner propane-air diffusion flame for various extinction times, together with model predictions (solid line: calculations; dotted line: steady-state results).

the properties of the fire itself, characteristics of the agent delivery system, and fate of the acid gases after their formation. The fire is essentially the source term for acid gas formation, since high temperatures are required for rapid agent decomposition. The amount of HF formed will depend upon the fire size, fuel type, and flame type (premixed or diffusion). In addition, ease of extinguishment of the fire will be crucial, since for a given inhibitor, different fire types will extinguish at different concentrations for the same inhibitor. An additional feature of larger scale fires is the presence of hot surfaces. These could provide a high enough local temperature to cause thermal decomposition of the inhibitor molecule, and possibly result in HF formation. Given the apparent lack of decomposition of the inhibitor in the hot post-combustion region above the laboratory diffusion flames, this is not believe to be a major source for HF formation.

Flame extinguishment ease will be affected by the stabilization mechanisms, the flow field, and sources of re-ignition. The characteristics of the agent delivery system which will affect the quantity of HF formed include the agent type and the concentration at which it extinguishes the flame. The rate of introduction of the agent is important, as are the mixing rates in the protected volume and the delivery rate to the stabilization region of the flame. Finally, after formation of HF by the fire, the dispersion of the acid gas throughout the protected space and on surfaces will affect its peak and average concentrations.

The space volume as compared to the fire size, the ventilation rate, and the presence of surfaces for acid gas condensation will influence the HF concentrations, which will vary both spatially and temporally. The rate of air mixing in the protected space may have a large effect on the final measured HF concentrations. Both the characteristics of the agent delivery to the fire and the fate of the HF after fire suppression - while greatly affecting the quantities of HF formed, may vary widely for different applications. Because this potentially wide variation, they are difficult to specify. Nonetheless, it is of great interest to attempt to predict HF formation in larger-scale tests using the present model.

10.9.1 Comparison with Predictions. Extensive intermediate-scale tests of HF production by CF_3Br and halon alternatives have been reported by Sheinson *et al.*, (1994). In order to further test the present model, we have attempted to predict the HF formed in their experiments. The experiments consisted of 0.23 and 1.1 m^2 heptane pool fires extinguished by CF_3Br , CHF_3 , C_2HF_5 , and C_4F_{10} . The agents were injected at varying rates and to different final inhibitor concentrations in the 56 m^3 protected space. The reported HF concentrations represent the peak measured values at a single fixed location. The results of their experiments (for the 0.23 m^2 pools) are shown in Figure 55, which provides the measured HF mole fraction (in ppmv) as a function of the fire out time for the four agents. Although the experimental data represent different agent injection rates and final design concentrations of inhibitor, we have included all of the data in a single plot.

The large scatter in the experimental results probably occurs from the effects of these additional parameters. Of these three parameters, injection rate, design concentration, fire-out time, we believe the latter to be most important in determining the HF production and have made it the independent parameter. The results of the stoichiometric model predictions based on achievement of full equilibrium are given by the solid line. Each of the four lines in the figure refers to the predicted HF for one of the agents CF_3Br , CHF_3 , C_2HF_5 , and C_4F_{10} ; the symbol at the end of the line serves to identify the line with the proper data. In these calculations, the model predicts the total mass of HF produced. In order to allow a comparison, it is necessary to assume a spatial distribution of HF. Although there will be gradients of HF concentration in the room, uniform distribution has been assumed. As the figure shows, the predicted HF concentration agrees well with the experimental results. Having gained confidence in the ability of the model to predict some experimental results, we now proceed to investigate the effect of several parameters on HF production in suppressed fires.

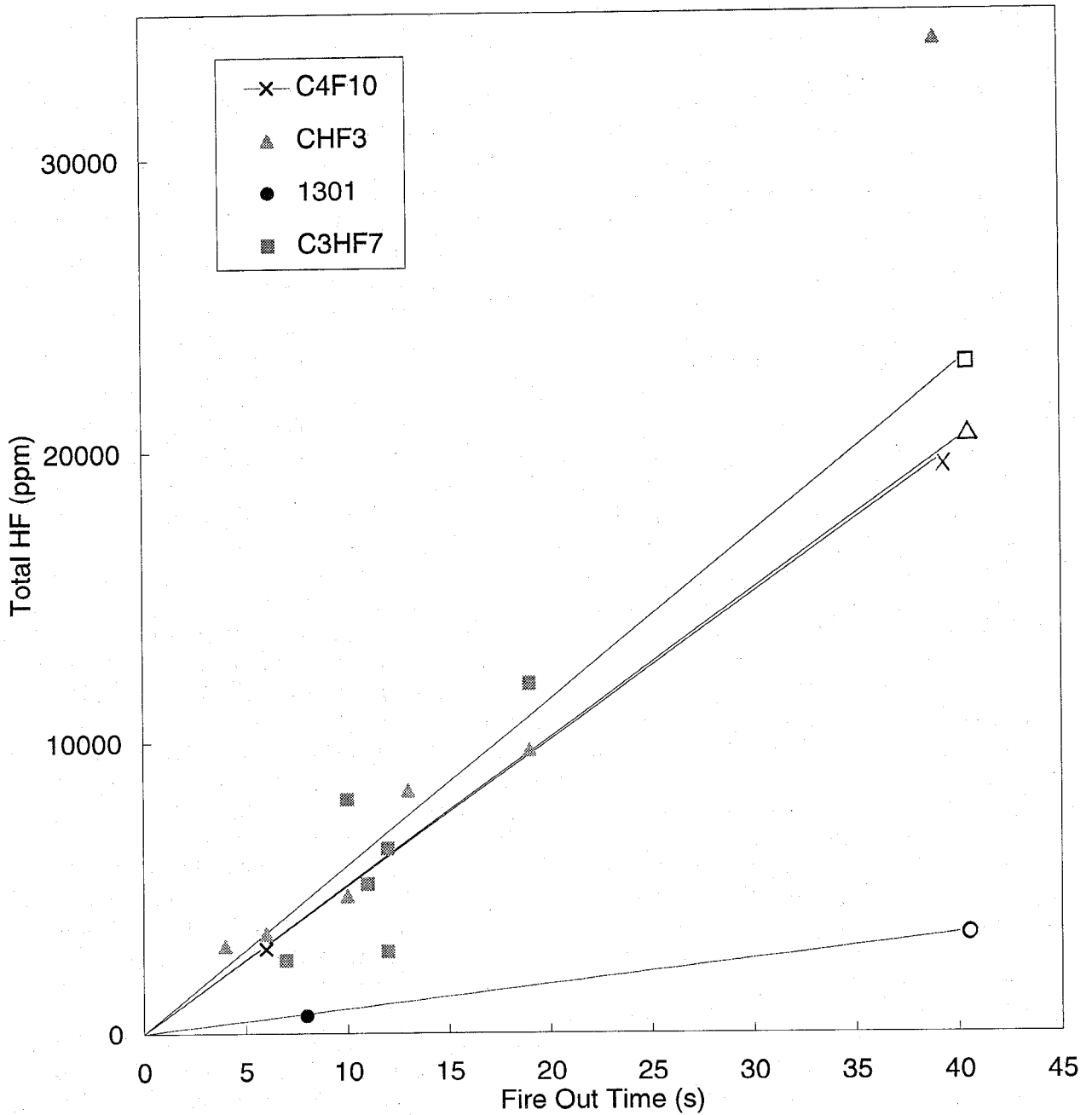


Figure 55. Experimental data of Sheinson *et al.* for intermediate-scale tests of HF production in heptane pool fires, with the model predictions for CF₃Br, CF₃H, C₂HF₅, and C₄F₁₀.

10.10 Parametric Analysis

The effect of various parameters on the production of HF can be examined using the stoichiometric model. First, it should be emphasized that in the present model, the HF generation rate is linearly proportional to the fuel consumption rate. Hence, in all subsequent figures in this section, the HF generation rate is normalized by the fuel consumption rate, so that this parameter need not be specified for each figure. Analyses are presented for the six inhibitors C_2HF_5 , C_3HF_7 , $C_2H_2F_4$, C_2F_6 , C_3F_8 , and CF_3Br as well as the four hydrocarbon fuels methane, propane, heptane, and JP8.

It has been assumed in these calculations that the extinction occurs at the cup burner extinction concentration for the particular fuel with dry air. Clearly, extinction at an inhibitor concentration larger or smaller than the cup burner value will affect the generation of HF; this is treated in a final figure.

10.10.1 Results. In Figures 56, 57, and 58 we examine the influence of inhibitor type, inhibitor concentration, fuel type, and the presence of water vapor in the air on the HF generation rate, all for steady-state flames. These calculations refer to a condition where the agent is added at a concentration lower than the extinction concentration, so that the flame continues to burn, but produces copious amounts of HF. These figures are shown to illustrate the influence of the fuel and agent type, inhibitor concentration, and moisture content of the air on steady flames. The results will be extended to transiently suppressed fires in subsequent figures.

Figure 56 shows the calculated steady-state HF production rate (g-HF/g-fuel) as a function of the agent mole fraction in the air stream for the one-carbon suppressants CF_3Br and CHF_3 , the two-carbon suppressants C_2F_6 , C_2HF_5 , and $C_2H_2F_4$, and the three-carbon suppressants C_3HF_7 and C_3F_8 . The results are calculated for heptane, and the calculations are performed for dry air. As the figure shows, the each curve has a distinctive change in slope (which occurs at the inhibitor concentration where the flux of fluorine into the flame equals that of hydrogen). The curves are grouped according to the number of carbon atoms in the inhibitor, which correlates with the number of fluorines and the molecular weight, both of which influence the flux of fluorine into the flame, and hence the HF generation rate. Surprisingly, for agents which extinguish the flame at approximately the same concentration, for example C_3F_8 and C_3HF_7 , the agent with more hydrogen atoms is predicted to make more HF. This occurs because above a certain concentration (about 3.5 % agent in the figure), the HF production is limited by hydrogen, not fluorine. The agent CF_3Br makes less HF because at a given mole fraction, the molecule carries fewer fluorine atoms into the flame than the larger halocarbons, and because it puts the flame out at a much lower concentration.

Each curve is truncated at the extinction concentration in a heptane cup burner flame for that inhibitor. The area under each curve from zero inhibitor up to the extinction concentration represents the total HF formed for an extinguished flame (in g-HF/g-fuel consumed). If the fuel consumption rate is larger or the inhibitor injection rate is slower, the total fuel consumed during the extinction event is larger, and the HF formed is proportionally greater.

The effect of water vapor in the air stream is indicated in Figure 57 which shows the steady-state production rate of HF as a function of inhibitor mole fraction for CF_3Br , C_3F_8 , and C_2HF_5 . Curves are shown for dry air (dotted lines) and for air with 2.3 mole percent water vapor (solid lines), corresponding to 100 % R.H. at 25 °C, and assuming that wet and dry flames extinguish at the same concentration. The effect of water vapor is small when the agent concentration is low, since under these conditions, the limitation on the amount of HF is the fluorine flux into the flame, not the

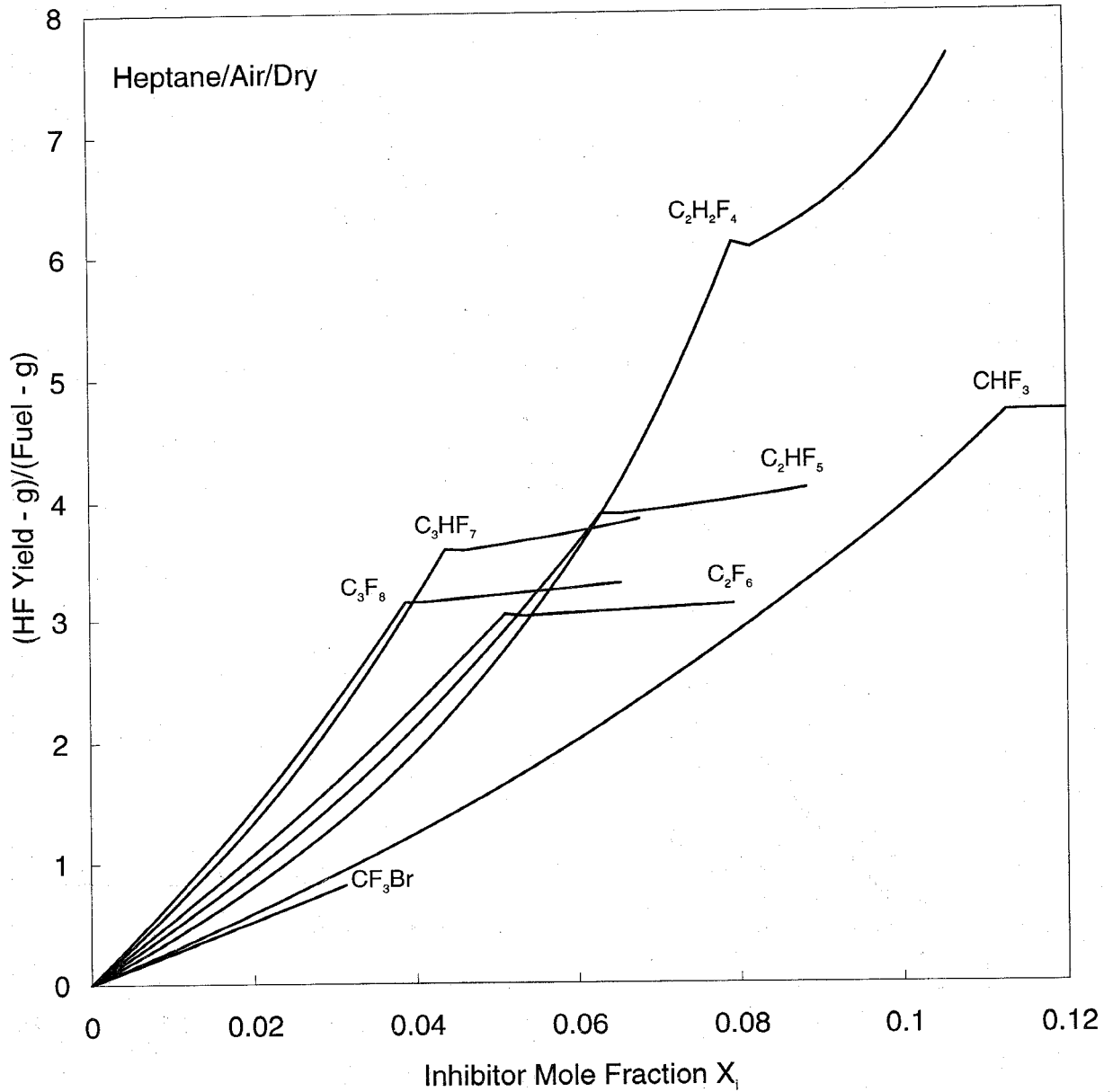


Figure 56. Stoichiometric model predictions of the HF formed in heptane-air flames under steady-state with CHF_3 , C_2HF_5 , $C_2H_2F_4$, C_3HF_7 , C_2F_6 , C_3F_8 , and CF_3Br .

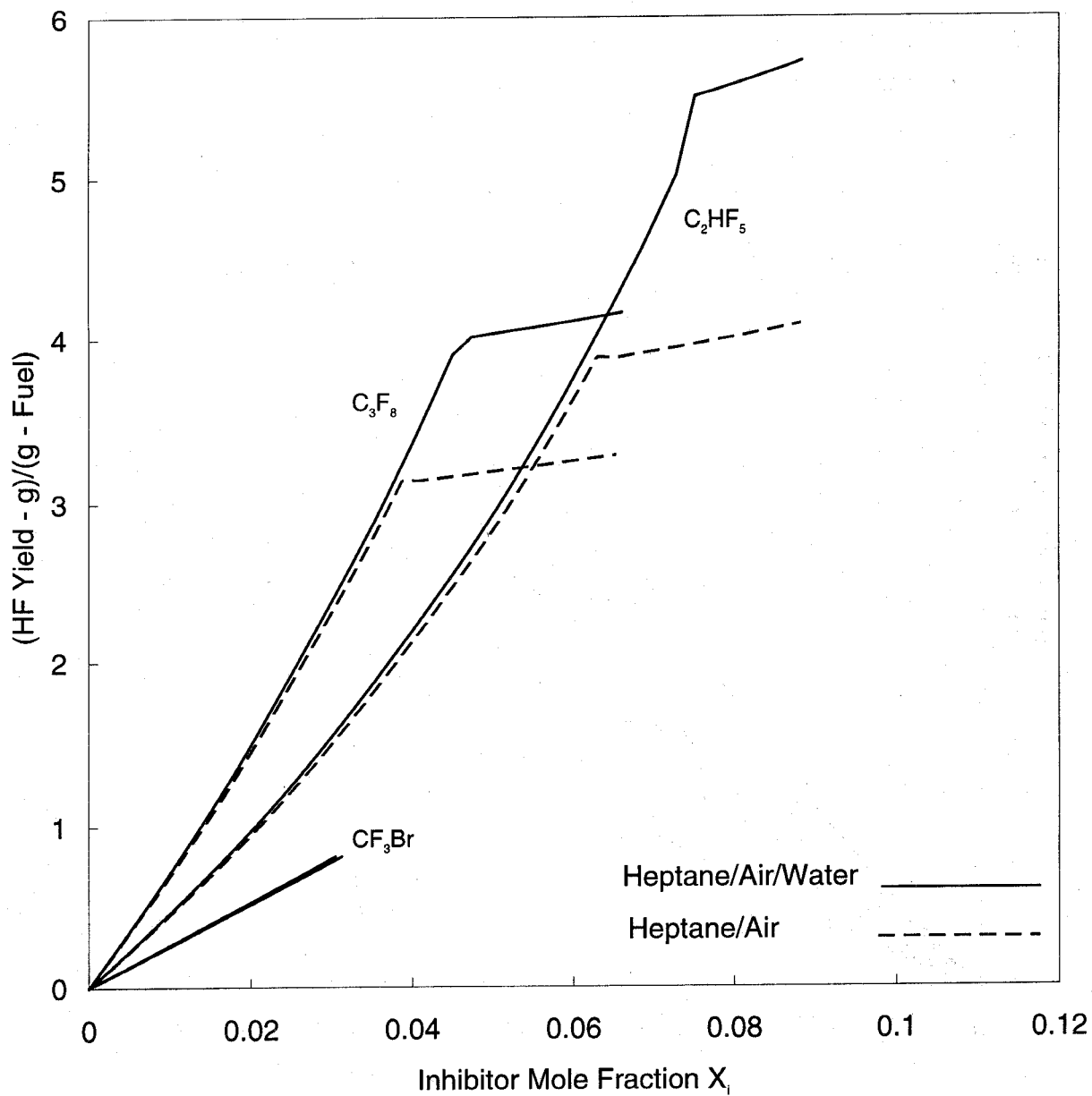


Figure 57. Stoichiometric model predictions of HF formed in heptane-air flames at steady-state with C_2HF_5 , C_3F_8 , and CF_3Br . Dotted lines: dry air; solid lines: wet air.

hydrogen flux. At high inhibitor loading, however, there becomes more fluorine than hydrogen in the flame, and any additional hydrogen from water vapor can increase the production rate of HF.

Figure 58 illustrates the effect of fuel type on the steady-state HF production in flames inhibited by C_2HF_5 by showing curves for JP8, heptane (C_7H_{16}), propane (C_3H_8), and methane (CH_4). The different fuels have a different carbon to hydrogen ratio, which affects the HF production rate, since the fuel is the major source of hydrogen in the flame, and hydrogen is necessary for the efficient production of HF (the kinetic rates get much slower in hydrogen-starved flames as described above). The amount of HF formed is lowest for JP8, followed by heptane, propane and methane. Note that the amount of HF formed in transient flames is represented by the area under the curves in Figure 59, so that the differences in HF formation between the fuel types can be quite large.

As discussed above in the description of the model for HF formation, transiently suppressed fires produce HF according to the area under the steady-state generation curve as in Figure 56. For a given inhibitor, fuel type, water vapor concentration, and extinction condition, the area under the curve will be a constant.

Two additional factors can affect the total quantity of HF formed: 1) the fuel consumption rate, and 2) the time for the fire to be extinguished. The first of these is obvious since the HF production rate is normalized by the fuel consumption rate. Fuel consumption is the driving force for transport of inhibitor and air to the reaction zone, so that increased fuel consumption increases HF production proportionally. The effect of the inhibitor injection rate (or alternatively, the fire out time, since they are strongly related) is to change the fuel consumption. That is, if the flame is extinguished slowly, more HF is produced because during the longer time, more fuel is consumed.

Figure 59 indicates the total HF produced during extinguishment of a heptane air flame by CF_3Br , CHF_3 , C_3F_8 , C_3HF_7 , C_2HF_5 , and $C_2H_2F_4$ in dry air. As the figure shows, the quantity of HF produced is linearly proportional to the extinction time.

Finally, the effect of extinguishment at lower inhibitor concentrations is described. In the above figures, the extinction condition of the fire was assumed to be equal to the cup burner extinction value for the agent and fuel. If the flame is more easily extinguished, less acid gas will be produced during extinction. This is because if a flame extinguishes more easily, the curves in Figures 56 will be integrated up to a lower concentration, and the area under the curve (which represents the total HF produced) will be proportionally less. This is illustrated in Figure 60 which shows the quantity of HF produced by heptane-air flames with dry air extinguished by CHF_3 , CF_3Br , C_2HF_5 , C_3HF_7 , and C_3F_8 as a function of the flame's extinction concentration for a constant fire out time (10 s). As the figure illustrates, flames which extinguish at lower concentrations of inhibitor produce less HF, in an approximately linear fashion.

It should be emphasized that the analyses demonstrated above examine the effects of several parameters on the HF source, the fire, under the assumption of thermodynamic equilibrium. As shown previously in Figures 34 - 38 for propane flames, there can be significantly less HF formed than predicted by chemical equilibrium, although for heptane, the agreement is excellent. Consequently, the predictions described here are upper limit estimates probably with about 30 % of actual results.

10.10.2 Conclusions. The following conclusions can be drawn based on the diffusion flame experiments, modeling, and parametric analysis:

1. The stoichiometric model, based on relatively simple but fundamental assumptions, is a useful tool for understanding HF formation in suppressed fires. The predictions of the model provide good estimates of the upper limit for formation of HF, and are valid for both steady-state and transient modes of inhibition.

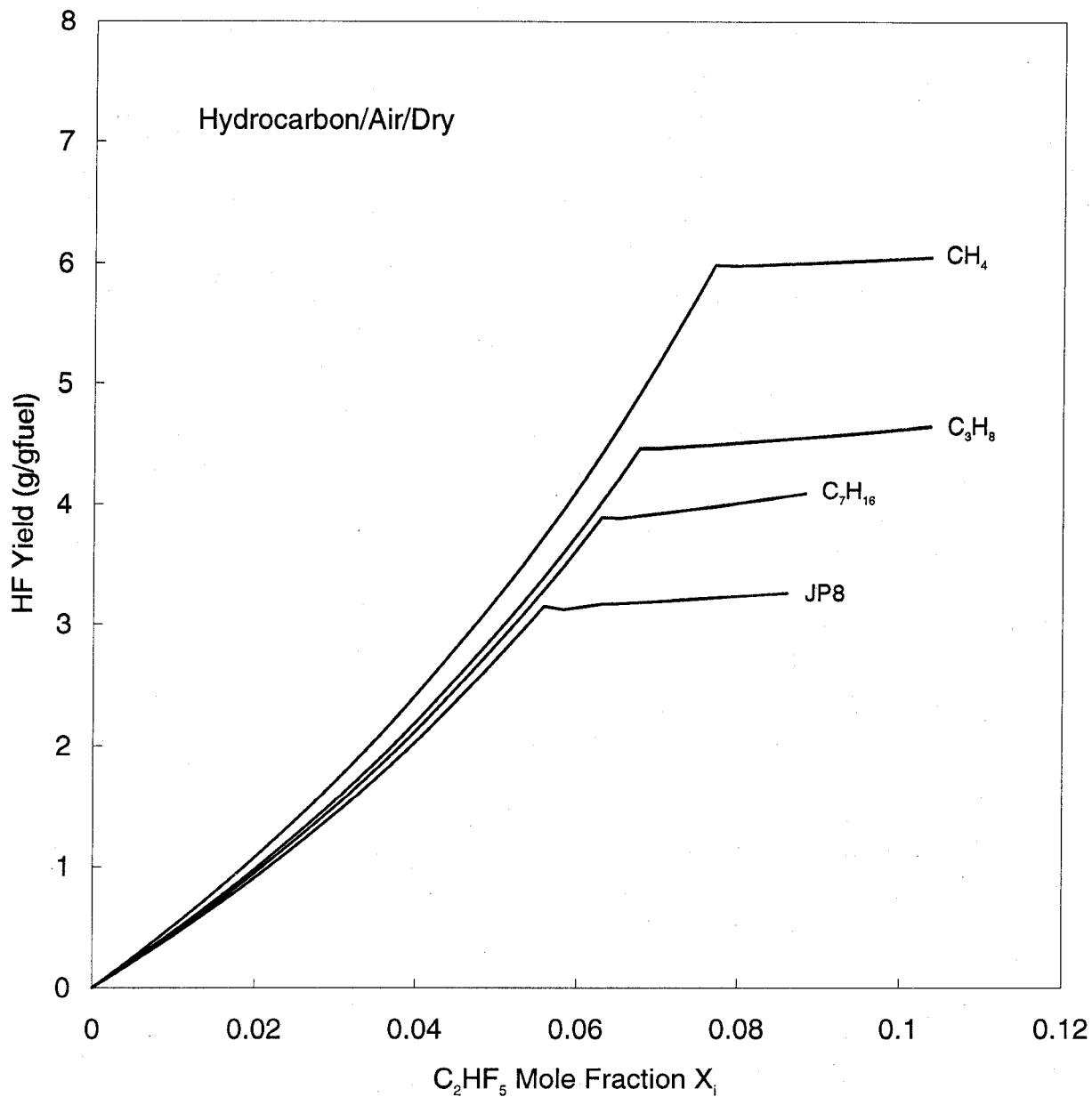


Figure 58. Stoichiometric model predictions of HF formed in heptane-air flames at steady-state with C₂HF₅ added to air stream with various fuels (CH₄, C₃H₈, C₇H₁₆, and JP8).

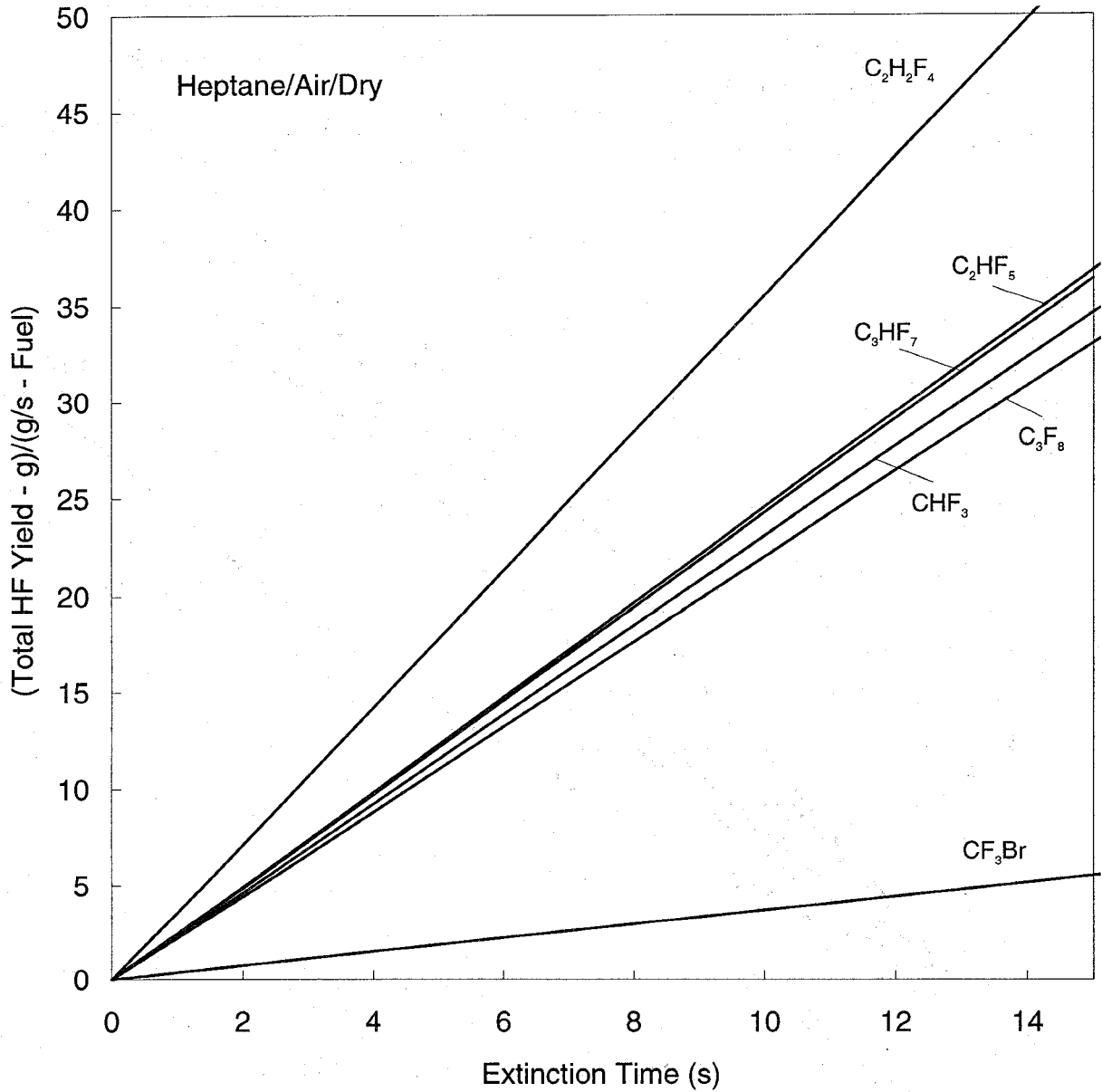


Figure 59. Total HF predicted during extinguishment of heptane-air flames for CHF_3 , C_2HF_5 , C_3HF_7 , C_3F_8 , CF_3Br versus extinction time.

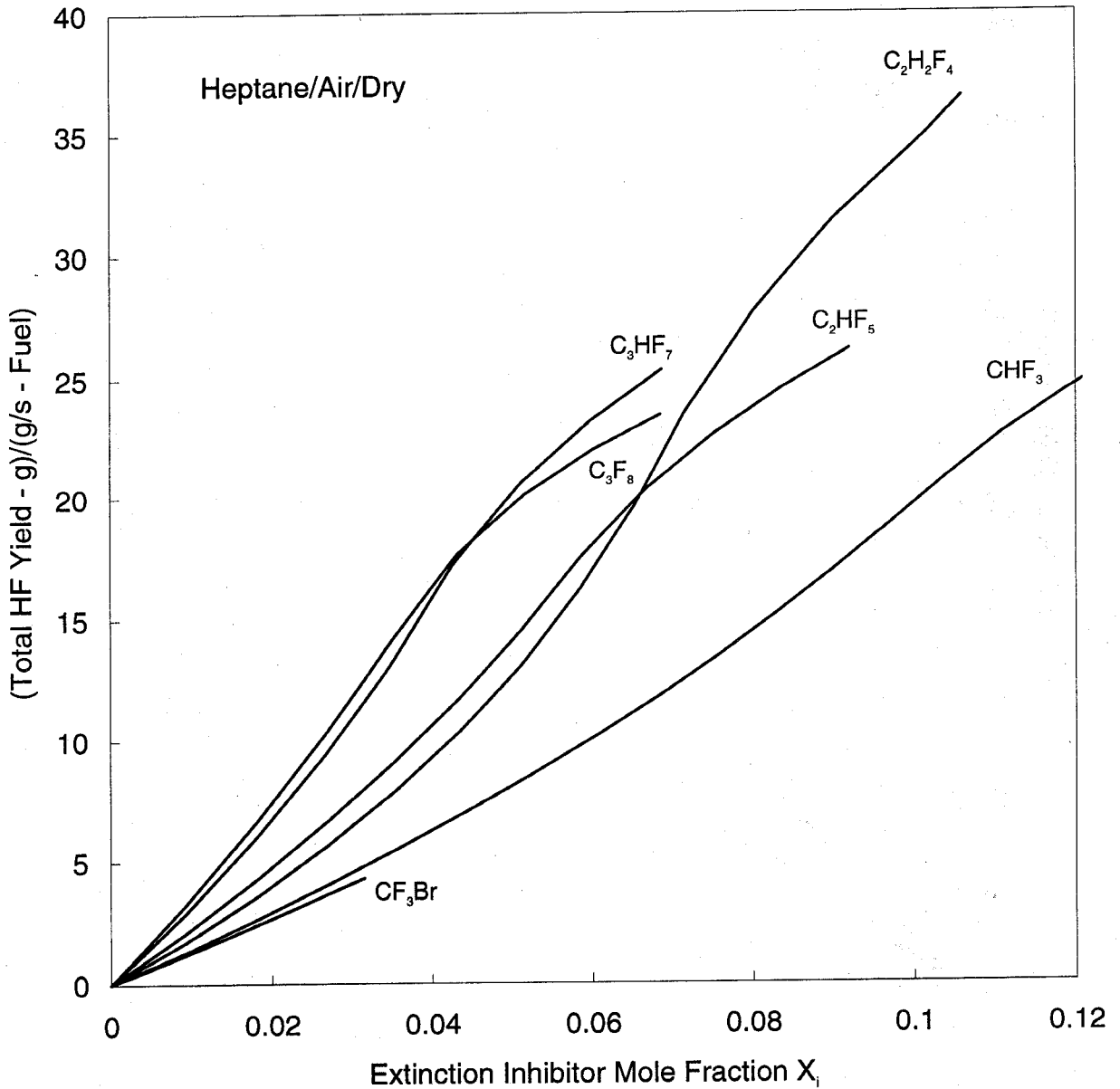


Figure 60. Total HF predicted during extinguishment of heptane-air flames for CHF_3 , C_2HF_5 , $C_2H_2F_4$, C_3HF_7 , C_3F_8 , CF_3Br versus extinction concentration.

2. The predictive model indicates that HF formation increases approximately linearly with fire size and extinguishing time and decreases approximately linearly with extinction concentration of the inhibitor.
3. The formation of HF is affected somewhat by the hydrogen to carbon ratio of the fuel, hydrogen to fluorine ratio in the agent, and the water vapor content of the air.
4. While predictions of HF produced in suppressed flames and intermediate scale fires are within about 25 % of the experimental results (which have large scatter), the estimated quantities of HF formation based on chemical equilibrium can overestimate the steady-state HF production by up to a factor of two for some agents.
5. Based on the analyses above, it should be possible to predict the HF formation by any arbitrary fluorocarbon which has a chemical structure similar (but not identical) to those agents analyzed above.

10.11 Predicting HF in Dry-Bay and Engine Nacelle Fires

Dry-bay and engine nacelle fires are expected to be distinctly different from each other, and as a result, the estimation of HF formation in each will require application of different methods. In the engine nacelle fire threat, the most likely scenario is expected to be a broken fuel or hydraulic line spraying into the nacelle region, with an attached, stabilized spray diffusion flame. Conversely, the dry-bay fire threat will most likely occur from an incendiary device rupturing the fuel tank, creating a large rapidly advancing turbulent flame progressing into the basically premixed dry-bay region. Because the model for HF formation developed above is based on first principles, it is possible to apply it to the cases of engine nacelle and dry-bay fires. For each fire type, the important parameters controlling HF formation will be discussed, and specific methods for estimating the amount of HF produced during suppression will be presented.

10.11.1 Engine Nacelle Fires. A likely scenario for an engine nacelle fire is that of a spray diffusion flame of a liquid fuel. The time for fire suppression in this case is assumed to be seconds. In many respects, the flame will resemble a laboratory diffusion flame of a hydrocarbon fuel. Typically, the burning rate of a diffusion flame is controlled by the rate of transport of oxidizer to the reaction zone. In a similar way, the production of HF is also controlled by the rate of transport of inhibitor to the reaction zone. Although equilibrium calculations described in Section 10.4 above indicate that complete decomposition of the inhibitors to HF, COF_2 , and CO_2 is favored, it is necessary to estimate the flux of the inhibitor to the reaction zone to determine the amount of reactants available. In addition, kinetic limitations to HF formation must be considered since complete and rapid destruction of the inhibitors is not assured at the high inhibitor concentrations typical of the extinction concentrations for diffusion flames, and in addition, slower rates of destruction reduce the transport rate to the reaction zone.

In the model for HF production described in Section 10.6 above, the inhibitor is assumed to be consumed in the reaction zone as a reactive species. The agent can be thought of as an additional fuel species, having its own oxygen demand, yet coming from the air side of the flame. It must be transported to the hot reaction zone which serves as a sink for the inhibitor. Thus fuel, oxygen and inhibitor are consumed in the reaction zone in stoichiometric proportions, with the stoichiometry

determined from a balanced chemical reaction to the most stable products. Total HF production is often limited by the availability of atomic hydrogen both for formation of HF itself and as an important intermediate which permits rapid decomposition of the inhibitor.

The predictive model for HF formation described in Section 10.6 indicates that HF formation in diffusion flames will increase approximately linearly with fire size, extinguishing time, and the concentration at which the flame extinguishes. In addition, HF formation will be affected somewhat by the hydrogen to carbon ratio of the fuel, hydrogen to fluorine ratio in the agent, and the water vapor content of the air.

Fire size influences the HF production rate for two main reasons. First, the fuel serves as the source of hydrogen, which is necessary for HF formation and for production of H-atoms which promote the rapid reaction of both the fuel and agent. Second, the fuel reaction produces the high temperatures necessary for inhibitor thermal decomposition and for production of H, O, and OH radicals which are the main promoters of inhibitor decomposition.

For similar reasons, the longer it takes for the inhibitor to build to the concentration which extinguishes the flame, the more HF that will be produced, since the fire is the driving force for inhibitor decomposition and HF formation. Thus, the HF production is linearly proportional to the fire-out time. The concentration at which the inhibitor extinguishes the flame is also directly related to the amount of HF produced during extinction. Since the HF production is linearly related to the concentration of inhibitor in the air stream, high extinction concentrations cause correspondingly higher HF production rates. As described above in Section 10.10, fuels or agents with higher hydrogen contents, or water vapor in the air stream typically cause higher production rates of HF. This is true because, to a large extent, trapping of the hydrogen atoms available from any source is how the agents reduce the reaction rate (and extinguish the flame) and also produce HF. For the present fluorinated agents, the amount of HF is often controlled more by the supply of hydrogen than by the amount of fluorine.

Application of the model for HF formation follows that outlined in Section 10.6. The necessary inputs are:

- the fuel type,
- fuel consumption rate m_f ,
- agent type,
- fire-out time t_{out} ,
- concentration of agent at which the fire is extinguished C_{ext} .

While the values for these parameters may not be immediately available, they can be estimated from the characteristics of the aircraft. For example, the fire fuel may be aircraft jet fuel (JP8), and the flow rate could be estimated from the fuel line size and pressure. The most difficult parameters to specify then are the fire-out time and the extinction concentration. The fire-out time can be left as a variable; an estimate for the extinction concentration is the cup-burner extinction value. It should be noted that actual extinction concentrations can be higher or lower.

With the above information, prediction of the HF becomes possible with the present model.

$$HF (g) = G (g/g \text{ fuel}) \cdot m_f (g/s) \cdot t_{out} (s) \cdot C_{ext} / C_{ext,cup}$$

where the HF generation parameter G is a function of the fuel and inhibitor type. Values for G for heptane and JP8 for CF_3H , C_2HF_5 , C_3HF_7 , C_3F_8 , and CF_3Br are given in Table 3.

Table 3. The generation parameter G for heptane and JP8

Inhibitor	Heptane		JP8	
	Dry	Wet	Dry	Wet
CHF ₃	2.3	2.3	2.2	2.2
C ₂ HF ₅	2.5	2.8	1.7	1.7
C ₃ HF ₇	2.4	2.8	1.6	1.7
C ₃ F ₈	2.2	2.5	1.5	1.6
CF ₃ Br	0.4	0.4	0.1	0.1

10.11.2 Dry-Bay Fires. The dry-bay fire threat is harder to specify, but is envisioned to be a very rapidly expanding fireball driven by an incendiary device. These fires can be described as a rich, premixed turbulent flame, rapidly accelerating. As such, the conditions for HF formation are those of a premixed flame as described above in Sections 10.5 and 10.6.1. In these cases, the mass flux of both fuel and agent into the reaction zone are well specified.

As described in the section above describing the equilibrium calculations, the most abundant products of agent decomposition are CO, CO₂, HF, and COF₂. The model adopted in the present work assumes that the fluorinated agents decompose to the most thermodynamically favorable products and that finite rate kinetics are not important for HF formation. The validity of these assumptions are based on the extensive numerical modeling of premixed flames as described above. Complete conversion of the inhibitor to HF in premixed flames has been demonstrated above for conditions where the inhibitor is present at concentrations such that the atomic hydrogen to fluorine ratio is less than unity. As described in Section 10.5 above, complete conversion to HF may also be expected for higher temperature and pressure flames since the mechanism for agent decomposition becomes more dependent upon thermal decomposition under these conditions. In addition, there will be residual water vapor present in the dry-bay from the combustion which occurred prior to agent injection; this water vapor will hydrolyse COF₂ (which is the favored product in the absence of sufficient hydrogen) to produce HF.

The time for extinction of dry-bay fires is expected to be much shorter (tens of milliseconds) as compared to engine nacelle fires. Consequently, it is necessary to discuss the influence of these short times on the HF formation. Premixed flames have propagation rates on the order of 1 m/s and flame thicknesses of about a millimeter. This corresponds to a characteristic time on the order of 1 ms. However, the reaction zone in a premixed flame is typically about a tenth of the flame thickness, so that the characteristic chemical time is less than a millisecond. Since the chemical time is much shorter than the extinction time, the effects of the transient extinction do not influence the chemical considerations; results which describe steady-state flame are also applicable to transient suppression.

Essentially, all of the agent which is encountered by the expanding flame is expected to be converted to HF. To estimate the amount of HF formed, it is only necessary to specify:

- the volume of the space, V
- the agent type and number of fluorines/molecule, n_F
- the design mole fraction of agent in the space, X_i
- the fraction of the space over which the flame interacts with the inhibitor/air mixture prior to extinguishment, χ .

$$\text{HF (g)} = 19 \cdot V \cdot X_i \cdot n_F \cdot \chi / (22.4 \cdot T/273 \cdot 101/P)$$

where P is the pressure (kPa) and T is the temperature (K).

Note that in these fire threats, the time is so short and the process so rapid that the volume of the space becomes more important than the time of the process or the fuel consumption rate. If the time is long, then the HF formation should be treated as in the engine nacelle case described above.

10.12 Summary

Comprehensive chemical equilibrium calculations for hydrocarbon-air flames with halogenated inhibitors have been performed. These calculations, followed by detailed flame structure calculations for premixed flames have provided a theoretical basis for development of a simple model for HF formation.

Extensive tests for HF production have been performed in laboratory flames. In these carefully designed and executed experiments, the HF formation rates in steady-state premixed and diffusion flames have been determined. The experiments encompass both gaseous and liquid fuels, including methane, propane, and heptane. Transient experiments for HF formation have been performed for propane-air diffusion flames. These data provide an experimental basis for comparing the agents and for testing the stoichiometric model which was developed. In addition the model was tested against intermediate-scale tests of HF production conducted at the Naval Research Laboratory.

Dry-bay fires most likely resemble a rapidly accelerating turbulent premixed flame. For these flames, numerical calculations of the flame structure indicate that there will be complete conversion of the fluorine in the agent in the protected space to HF. Premixed experiments at elevated pressures and the accompanying modeling also indicate complete conversion of the inhibitor to HF.

Engine nacelle fires are expected to resemble turbulent diffusion flames. For these flames, the stoichiometric model which has been developed is able to predict HF formation in transiently suppressed flames within about 30 % of the experimental results for all the data against which it has been tested.

The formation rate of HF in diffusion flames is strongly influenced by the mass flux of inhibitor into the flame sheet. For diffusion flames with the inhibitor added to the air stream, there appear to be kinetic limitations to the rate of HF formation for most but not all of the agents tested which increase as the inhibitor concentration in the air stream increases. Many of the agents (for example $\text{C}_2\text{H}_2\text{F}_4$, C_2HClF_4 , $\text{C}_3\text{H}_2\text{F}_6$, $\text{CH}_2\text{F}_2/\text{C}_2\text{HF}_5$, CF_3Br and CHClF_2) produced HF at rates within about 25 % of that given by equilibrium thermodynamics in the diffusion flames tested. Most of the perfluorinated agents tested (C_2F_6 , C_3F_8 , and C_4F_{10}) and the agents C_4F_8 , C_2HF_5 and C_3HF_7 produced 0 to 35 % less than the equilibrium values except when the estimated fluorine to hydrogen flux into the flame goes above unity when they show no further increase with increasing inhibitor concentration in the air stream.

The stoichiometric model, based on relatively simple but fundamental assumptions, is a useful tool for understanding HF formation in suppressed fires. The predictions of the model provide good estimates of the upper limit for formation of HF, and are valid for both steady-state and transient modes of inhibition.

The following conclusions can be drawn concerning HF formation in suppressed fires - for diffusion flames:

1. HF formation increases linearly with fire size (*i.e.*, fuel consumption rate) for any given fuel and suppressant.

2. Assuming a constant agent injection rate, the HF formation increases approximately linearly with the time it takes for the fire to extinguish, for any given fuel and suppressant
3. For a given agent and fuel, the HF produced decreases approximately linearly with the concentration at which the flame is extinguished. That is, flames that are extinguished at lower inhibitor concentrations produce correspondingly less HF.
4. The hydrogen to carbon ratio of the fuel can influence the amount of HF produced by up to a factor of two for a given agent, with the higher hydrogen fuels making more HF.
5. The agents C_2HF_5 , C_3HF_7 , and C_3F_8 will make about four times as much HF as will CF_3Br for heptane flames for the same fire-out time. If the fire goes out faster (which will probably occur with CF_3Br since a lower concentration is required to extinguish the flame and that can probably be attained faster), the amount of HF will be proportionally less.
6. Large differences in the amount of HF produced by the agents C_2HF_5 , C_3HF_7 , and C_3F_8 are not expected.
7. The hydrogen to fluorine content of the agent influences the HF formation, with higher hydrogen content agents making more HF.
8. Water vapor in the air will increase the HF formation slightly.

and for premixed flames:

1. Complete conversion of the fluorine in the inhibitor to HF is expected.
2. The amount of HF produced depends upon: a) the volume of air consumed by the fire before extinction; b) the concentration of agent in that volume.

The predictions of the stoichiometric model are summarized in Figure 61. This figure presents the mass of HF formed (g) per gram of fuel consumed, and shows the cup burner extinction value for heptane. The effect of the fuel type is shown, as well as the effects of the agent type and presence of water vapor in the air. The prediction assumes a 10 second extinction time and cup burner extinction concentrations. For shorter extinction times or lower extinction concentrations, the amount of HF is reduced proportionally.

While predictions of HF produced in suppressed flames and intermediate scale fires are within about 25 % of the experimental results (which have large scatter), the estimated quantities of HF formation based on chemical equilibrium can overestimate the steady-state HF production by up to a factor of two for some agents. An examination of the chemical kinetics of suppressed diffusion flames can lead to an understanding of the relevant phenomena, and may indicate approaches for reduction of the HF production by halon alternatives.

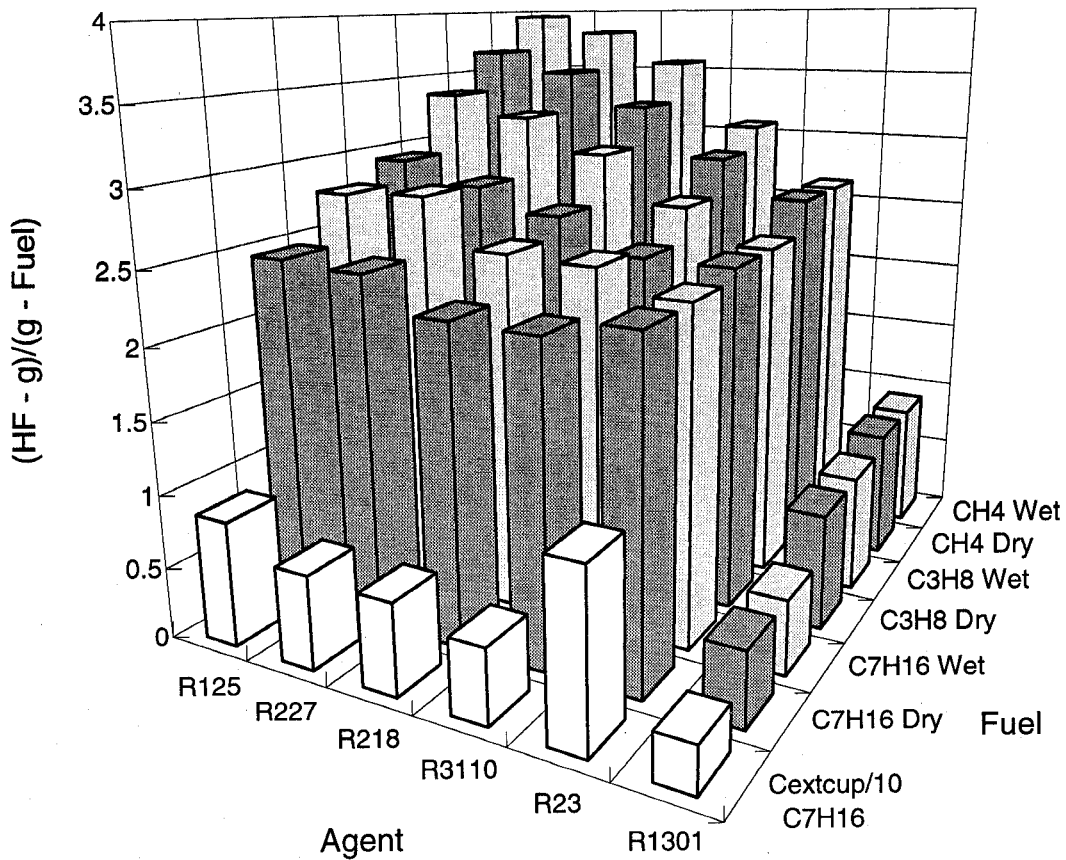


Figure 61. Predicted HF production (g) per gram of fuel consumed during the suppression. Effects of fuel and inhibitor type and wet and dry air are shown. The first row shows the cup burner extinction concentration (divided by 10) for heptane.

10.13 Acknowledgments

This research was supported by the U.S. Naval Air Systems Command; U.S. Army Aviation and Troop Command; Federal Aviation Administration Technical Center; and the U.S. Air Force. The author especially appreciates the support and technical direction of Mr. J. Michael Bennett at the Wright Patterson AFB Flight Dynamics Laboratory, Survivability Enhancement Branch. The authors are grateful to Drs. D. Burgess, W. Tsang, P. Westmoreland, and M. Zachariah for helpful conversations and for making their mechanism and publications available prior to publication; to Drs. J. Vandooren and P. Van Tiggelen for helpful suggestions concerning the experimental techniques; and to Dr. J. Hodges for help with the image processing; and to Dr. K. Smyth for helpful conversations throughout the project. It is a pleasure to acknowledge the collaboration with L. Truett in making the measurements, and the assistance of Mr. Arnold Liu and Miss Cynthia Yu in writing the data acquisition and image processing software, performing the numerical calculations, and reducing the data. The authors are grateful to M. King, R. Harris, Y.E. Hsin, C. Womeldorf, and A. Liu for careful performance of the experiments. Helpful conversations with Dr. R. Sheinson at the Naval Research Laboratory concerning the intermediate-scale experiments are gratefully acknowledged.

10.14 References

- Andrews, G.E. and Bradley, D. *Combust. Flame* 18, 133-153 (1972).
- Bajpai, S.N. J. *Fire and Flammability*, 1974, 5, 255.
- Belles, F.E. and O'Neal, C. Jr., *Sixth Symposium (Int'l) on Combustion*, The Combustion Institute, Pittsburgh, PA, 1957, 806.
- Biordi, J.C., Lazzara, C.P., and Papp, J.F. *XIVth Symposium (Int'l) on Combustion*, The Combustion Institute, Pittsburgh, PA, 1973, 367.
- Biordi, J.C.; Lazzara, C.P.; Papp, J.F. *XIVth Symposium (Int'l) on Combustion*, The Combustion Institute, Pittsburgh, PA, 1973, 367-381.
- Biordi, J.C., Lazzara, C.P., and Papp, J.F. *XVth Symposium (Int'l) on Combustion*, The Combustion Institute, Pittsburgh, PA, 1974, 917.
- Biordi, J.C., Lazzara, C.P., and Papp, J.F. 1976, *J. Phys. Chem.* 80, 1042-1048.
- Biordi, J.C., Lazzara, C.P., and Papp, J.F. 1977, *J. Phys. Chem.* 81, 1139-1145.
- Biordi, J.C., Lazzara, C.P., and Papp, J.F. 1978, *J. Phys. Chem.* 82, 125.
- Booth, K.; Melina, B.J.; Hirst, R. 1973, *Imperial Chemical Industries Limited*, Mond Division, Cheshire UK, 31 August.
- Burdon, M.C.; Burgoyne, J.A.; Weinberg, F.J. *Vth Symposium (Int'l) on Combustion*, Reinhold Publishing Corp., New York, NY, 1955, 647-651.
- Burgess, D., Jr., Tsang, W., Westmoreland, P.R., Zachariah, M.R. *Third International Conference on Chemical Kinetics*, July 12-16, 1992, Gaithersburg, MD, 1993, p. 119.
- Burgess, D.R.F.; Jr., Zachariah, M.R.; Tsang, W.; and Westmoreland, P.R. *Thermochemical and Chemical Kinetic Data for Fluorinated Hydrocarbons in Flames*, National Institute of Standards and Technology, Gaithersburg MD, 1994, NIST Technical Note, submitted.
- Burgess, D.R.F., Jr., Zachariah, M.R., Tsang, W., and Westmoreland, P.R. *Thermochemical and Chemical Kinetic Data for Fluorinated Hydrocarbons in Flames*, National Institute of Standards and Technology, Gaithersburg MD, 1994, NIST Technical Note, submitted.

Burgess, D.R.F., Jr., Zachariah, M.R., Tsang, W., and Westmoreland, P.R. Thermochemical and Chemical Kinetic Data for Fluorinated Hydrocarbons, to appear as a special issue of *Progress in Energy and Combustion Science*, 1995.

Burgoyne, J.H. and Williams-Lier, G., *Proceedings of the Royal Society*, A193, 525, (1948).
Burgoyne *et al.*, 1948; Coleman, 1951; Belles *et al.*, 1957.

Burke, S.P.; Schumann, T.E.W. 1928, *Ind. Eng. Chem.* a4 20, 998.

Coleman, E.H., *Fuel*, 30, 114, (1951).

Di Nenno, P.J.; Forssell, E.W.; Peatross, M.J.; Wong, J.T.; Maynard, M. *Halon Alternatives Technical Working Conference*, New Mexico Engineering Research Institute, Albuquerque, NM, May 11-13, 1992.

Ferreira, M.J.; Hanauska, C.P.; Pike, M.T. *Halon Alternatives Technical Working Conference*, New Mexico Engineering Research Institute, Albuquerque, NM, May 11-13, 1992.

Ferreira, M.J.; Hanauska, C.P.; Pike, M.T. *Halon Alternatives Technical Working Conference*, New Mexico Engineering Research Institute, Albuquerque, NM, May 11-13, 1992.

Filipczak, R.A. *Halon Alternatives Technical Working Conference*, New Mexico Engineering Research Institute, Albuquerque, NM, May 11-13, 1993, 149-159.

Filipczak, R.A. *Halon Options Technical Working Conference*, New Mexico Engineering Research Institute, Albuquerque, NM, May 3-5, 1994, 165-176.

Frenklach, M., Wang, H., Bowman, C.T., Hanson, R.K., Smith, G.P., Golden, D. Gardiner, W. Lissianski, V., Poster 3-26, *Twenty-fifth Symposium (Int'l) on Combustion*, The Combustion Institute, Pittsburgh, PA, 1994.

Gann, R.G., Ed., *Halogenated Fire Suppressants*; ACS Symposium Series No. 16, The American Chemical Society, Washington, DC, 1975.

Garner, F.H., Long, R., Graham, A.J., and Badakhshan, A., *Sixth Symposium (Int'l) on Combustion*, The Combustion Institute, Pittsburgh, PA, 1957, 802.

Grosshandler, W.L.; Gann, R.G.; Pitts, W.M.; Eds. *Evaluation of Alternative In-Flight Fire Suppressants for Full-Scale Testing in Simulated Aircraft Engine Nacelles and Dry Bays*, National Institute of Standards and Technology, Gaithersburg, MD, 1994; NIST SP 861.

Hastie, J.W., *High Temperature Vapors: Science and Technology*, New York, NY, 1975, Academic Press, 332.

Hochgreb, S., Hsin, Y.E., and Linteris, G.T., *Laminar Flame Speeds of CF3H-Propane-Air Mixtures at Elevated Pressures*, NIST Annual Conference on Fire Research, Oct. 17-20, 1994, Gaithersburg, MD.

VanDerWege, B., Bush, M.T., Hochgreb, S., and Linteris, G.T., "Inhibition of CH₄ Laminar Flame Speeds by CF₃H and C₂F₆ in a Combustion Bomb," to be submitted to *Combustion Science and Technology*, July, 1995.

Kee, R.J., Miller, J.A. and Jefferson, T.H. *CHEMKIN: a General-Purpose, Transportable, Fortran Chemical Kinetics Code Package*, Sandia National Laboratories Report, 1980, SAND80-8003.

Kee, R.J., Warnatz, J., Miller, J.A. *A Fortran Computer Code Package for the Evaluation of Gas-Phase Viscosities, Conductivities, and Diffusion Coefficients*, Sandia National Laboratories Report, 1983, SAND83-8209.

Kee, R.J., Grcar, J.F., Smooke, M.D. and Miller, J.A. *A Fortran Program for Modeling Steady Laminar One-dimensional Premixed Flames*, Sandia National Laboratories Report, 1991, SAND85-8240.

Kee, R.J., Warnatz, J., Miller, J.A. *A Fortran Computer Code Package for the Evaluation of Gas-Phase Viscosities, Conductivities, and Diffusion Coefficients*, Sandia National Laboratories Report, 1983, SAND83-8209.

Lask, G., Wagner, H.G., *Thirteenth Symposium (Int'l) on Combustion*, Williams and Wilkins Co., Baltimore, 1962, 432.

Linnett, J.W. *Fourth Symposium (Int'l) on Combustion*, Williams & Wilkins, Baltimore, 1953, p. 20.

Linteris, G.T.; King, M.D.; Liu, A.; Womeldorf, C.; Hsin, Y.E. *Halon Options Technical Working Conference*, New Mexico Engineering Research Institute, Albuquerque, NM, May 3-5, 1994, 177-190.

Linteris, G.T.; Gmurczyk, G.W. Parametric Study of Hydrogen Fluoride Formation in Suppressed Fires, *Halon Options Technical Working Conference*, Albuquerque, NM, 1995.

Linteris, G.T., and Truett, L.F., Inhibition of Premixed Methane-Air Flames by Fluoromethanes, accepted for publication in *Combustion and Flame*, June, 1995a.

Linteris, G.T. and Truett, L., Inhibition of Premixed Methane-Air Flames by Halon Alternatives, *Proc. of International Conf. on Fire Research and Engineering*; Sept. 10-15, 1995b; Orlando, FL.

Linteris, G.T., Effect of inhibitor concentration on the inhibition mechanism of fluoromethanes in premixed methane-air flames, to appear in "Halon Replacements: Technology and Science," *American Chemical Society Symposium Series* (A.W. Miziolek, and W. Tsang, Eds.), Washington, DC, 1995a.

Linteris, G.T., Acid gas production in inhibited propane-air diffusion flames, to appear in *Halon Replacements: Technology and Science, American Chemical Society Symposium Series* (A.W. Miziolek, and W. Tsang, Eds.), Washington, DC, 1995b.

Linteris, G.T., Numerically predicted flame structure and burning rates of premixed CO-Ar-O₂-H₂ flames inhibited by CF₃H, submitted to *Combustion and Flame*, Feb. 1995b.

Mache, H. and Hebra, A. *Sitzungsber. Osterreich. Akad. Wiss., Abt. IIa*, 150, 157 (1941).

Metghalchi, M. and Keck, J. C., *Combust. Flame* 38, 143 (1980).

Moore, T.A.; Dierdorf, D.S.; Hanauska, C. *Halon Options Technical Working Conference*, New Mexico Engineering Research Institute, Albuquerque, NM, May 3-5, 191.

Nyden, M.R., Linteris, G.T., Burgess, D.R.F., Jr., Westmoreland, P.R., Tsang, W., and Zachariah, M.R., in *Evaluation of Alternative In-Flight and Dry Bays*, (W.L. Grosshandler, R.G. Gann, and W.M. Pitts, Eds.), National Institute of Standards and Technology, Gaithersburg MD, 1994, NIST SP 861, p. 467.

Pitts, W.M.; Nyden, M.R.; Gann, R.G.; Mallard, W.G.; Tsang, W. *Construction of an Exploratory List of Chemicals to Initiate the Search for Halon Alternatives*; National Institute of Standards and Technology, Gaithersburg MD, 1990; NIST SP 1279.

Rosser, W. A., Wise, H., and Miller, J., *Seventh Symposium (Int'l) on Combustion*, Butterworths Scientific Publications, Butterworths, London, 1959, 175.

Safieh, H.Y.; Vandooren, J.; Van Tiggelen, P.J. *XIXth Symposium (International) on Combustion*, The Combustion Institute, 1982, Pittsburgh, PA, 117-127.

Sheinson, R.S.; Musick, J.K.; Carhart, H.W. 1981, *Journal of Fire and Flammability*, 12, 229.

Sheinson, R.S.; Alexander, J.I. Fall Meeting, *Eastern States Section Meeting/The Combustion Institute*, 1982, Pittsburgh, PA, Paper 62.

Sheinson, R.S., Penner-Hahn, J.E., and Indritz, D. 1989, *Fire Safety Journal* 15, 437.

Sheinson, R.S.; Eaton, H.G.; Black, B.; Brown, R.; Burchell, H.; Smith, W.D. *Halon Options Technical Working Conference*, New Mexico Engineering Research Institute, Albuquerque, NM, May 3-5, 1994, 43-53.

Simmons, R.F. and Wolfhard, H.G., *Transactions of the Faraday Society*, 52, 53 (1956).

Simmons *et al.*, 1956; Garner *et al.*, 1957; Rosser *et al.* 1959; Lask and Wagner, 1962.

Smith, W.D.; Sheinson, R.S.; Eaton, H.G.; Brown, R.; Salmon, G.; Burchell, H.; St. Aubin, H.J. *Sixth International Fire Conference*, Interflam '93, Interscience Communications Limited, 1993, 757-764.

Thorpe, R.K., Gmurczyk, G.W.: *Technical Support Services and Assistance to the Halon Compatibility Project.* Science Applications International Corporation, Report for the National Institute of Standards and Technology, Contract No. 52SBNB4C8144, 1995.

Yamashika, S. 1973, *Report of Fire Research Institute of Japan*, 36, 7.

Yamashika, S.; Hosokai, R.; Morikawa, T. 1974, *Report of Fire Research Inst. of Japan*, 38, 1.

Vagelopoulos, C.M., Egolfopoulos, F.N., and Law, C.K., *Twenty-fifth Symposium (Int'l) on Combustion*, The Combustion Institute, Pittsburgh, 1994, p. 1341.

VanDerWege, B., Bush, M.T., Hochgreb, S., and Linteris, G.T., *Inhibition of CH₄ Laminar Flame Speeds by CF₃H and C₂F₆ in a Combustion Bomb*, to be submitted to *Combustion Science and Technology*, July, 1995.

Vandooren, J. F.; da Cruz, N.; P. Van Tiggelen *XXIInd Symposium (International) on Combustion*, The Combustion Institute, Pittsburgh, PA, 1988, 1587-1595.

Van Wonerghem, J. and Van Tiggelen, A. *Bull. Soc. Chim. Belg.* 63, 235-260 (1954). Van Wonerghem and Van Tiggelen, 1954.

Westbrook, C.K. *Combust. Sci. and Tech.* 1983, 34, 201.

Westmoreland, P.R., Burgess, D.F.R. Jr., Tsang, W., and Zachariah, M.R. *XXVth Symposium (Int'l) on Combustion*, The Combustion Institute, Pittsburgh, PA, 1994.

Wilson, W.E., Jr. *Xth Symposium (International) on Combustion*, The Combustion Institute, Pittsburgh, PA, 1965, 47-54.

World Meteorological Organization, 1989, *Scientific Assessment of Stratospheric Ozone: 1989*, Report No. 20, *Alternative Fluorocarbon Environmental Acceptability Study (AFEAS)*.

Zallen, D.M., 1992, *Halon Replacement Study*, SBIR Report No. ZIA-92-001 to Aeronautical Systems Division, Wright-Patterson AFB, Zallen International Associates.

Appendix A. The Computer Program Predicting Formation of HF

```

c The Computer Program:
c Composition of Combustion/Inhibition Products
c For the Reaction of Hydrocarbon/Air/Water/Halocarbon
c with Species Diffusion and Convection Transport - 4/12/95
c*****
c
c Greg W. Gmurczyk
c SAIC c/o NIST
c Building and Fire Research Laboratory
c Gaithersburg, MD 20899
c phone: (301) 975-6888
c e-mail: gmurczyk@tiber.nist.gov
c*****
c
c List of Variables:
c
c al - alfa (fuel moles)
c be - beta (halocarbon moles)
c becr - beta critical
c ga - gamma (oxygen moles)
c ni - nie (nitrogen moles)
c et - eta (hf moles)
c ph - phi (hcl moles)
c ep - epsylon (cof2 moles)
c dz - dzeta (cocl2 moles)
c de - delta (co2 moles)
c la - lambda (product h2o moles)
c mu - miu (substrate h2o moles)
c q*i - inlet species volume flow (slpm)
c q* - outlet species volume flow (slpm)
c d*i - inlet species densities (kg/m3)
c d* - outlet species densities (kg/m3)
c m*i - inlet species mass flow (g/s)
c m* - outlet species mass flow (g/s)
c X*i - inlet species mole fractions (l/l)
c X* - outlet species mole fractions (l/l)
c Y*i - inlet species mass fractions (kg/kg)
c Y* - outlet species mass fractions (kg/kg)
c w* - species molecular mass (kg/kmole)
c *r - species consumed/generated in flame (slpm)
c *u - species unreacted in flame (slpm)
c roi - ro (inhibitor/oxygen(fuel) diff.coeff.rat.)
c row - ro (water/oxygen(fuel) diff.coeff.rat.)
c ron - ro (nitrogen/oxygen(fuel) diff.coeff.rat.)
c ros - ro (star)

```

```

c   ri - r (inhibitor/oxygen(fuel) flow rat.)
c   rw - r (water/oxygen(fuel) flow rat.)
c   rn - r (nitrogen/oxygen(fuel) flow rat.)
c   a,b,c,d,e,f - a,b & c,d,e,f (fuel & inhibitor composition)
c   vm = 24.415 (l/mole)
c   si = 0.0 (standard case)
c   hl = 0.0 (low h2: la=0.0), 1.0 (high h2: ep=0.0, dz=0.0)
c*****
c
  program coeff
  implicit double precision (a-h,j-z)
c
  common /atom/ a,b,c,d,e,f
  common /coef/ al,be,becr,ga,de,ep,dz,ph,et,la,mu
  common /w/ wo2,wn2,wair,wc,wh,wf,wcl,wco2,wh2o,
&      whf,whcl,wcof2,wcocl2,wfu,win,wmi,wm
  common /rat/ ri,rw,roi,row,ros,hl,si
  common /dif/ do2n2,dfun2,dinn2,dh2on2
  common /therm/ vm,lm3,p,t,ru,cm
  common /qi/ qini,qh2oi,qfui,qo2i,qn2i,qairi,qti,dq
  common /di/ dini,dfui,do2i,dn2i,dco2i,dh2oi,dhfi,dhcli,dcof2i,
&      dcocli,denmi,dmi
  common /mi/ mini,mfui,mo2i,mn2i,mco2i,mh2oi,mhfi,mhcli,mcof2i,
&      mcocli,mti
  common /Xi/ Xini,Xh2oi,Xfui,Xo2i,Xn2i
  common /Yi/ Yini,Yh2oi,Yfui,Yo2i,Yn2i
  common /qr/ qinr,qfur,qo2r,qn2r,qco2r,qh2or,qhfr,qhclr,qcof2r,
&      qcoclr,qr
  common /dr/ dinr,dfur,do2r,dn2r,dco2r,dh2or,dhfr,dhclr,dcof2r,
&      dcoclr,denmr,dmr
  common /mr/ minr,mfur,mo2r,mn2r,mco2r,mh2or,mhfr,mhclr,mcof2r,
&      mcoclr,mtr
  common /Xr/ Xinr,Xfur,Xo2r,Xn2r,Xco2r,Xh2or,Xhfr,Xhclr,Xcof2r,
&      Xcoclr
  common /Yr/ Yinr,Yfur,Yo2r,Yn2r,Yco2r,Yh2or,Yhfr,Yhclr,Ycof2r,
&      Ycoclr
  common /q/ qin,qfu,qo2,qn2,qco2,qh2o,qhf,qhcl,qcof2,
&      qcocl2,qt
  common /d/ din,dfu,do2,dn2,dco2,dh2o,dhf,dhcl,dcof2,
&      dcocl2,denm,dm
  common /m/ min,mfu,mo2,mn2,mco2,mh2o,mhf,mhcl,mcof2,
&      mcocl2,mt,mhffu
  common /n/ nin,nfu,no2,nn2,nco2,nh2o,nhf,nhcl,ncof2,
&      ncocl2,nt,nti,dn
  common /X/ Xin,Xfu,Xo2,Xn2,Xco2,Xh2o,Xhf,Xhcl,Xcof2,Xcocl2
  common /Y/ Yin,Yfu,Yo2,Yn2,Yco2,Yh2o,Yhf,Yhcl,Ycof2,Ycocl2
c
  open(unit=1, file='i', form='formatted', status='old')

```

```

open(unit=2, file='o', form='formatted', status='unknown')
*
*****
*   input data
*   fuel and inhibitor composition
*   inlet species volume flows, flame configuration
*   inlet pressure and temperature
*****
*
  read(1,*) a,b,c,d,e,f
  read(1,*) qinit,qh2oi,qfui,qairi,si
c
  qini=0.0d0
5000 qini=qini+0.02d0*qinit
*
*****inlet pressure and temperature*****
*
  ru=8313.0d0
  p=1.0d5
  t=298.0d0
  dmi=p/(ru*t)
*
*****conversion factors*****
*
  vm=24.415d0
  lm3=1.0d-3
  if(si) 1250,15,17
15 al=1.0d0
  go to 19
17 ga=1.0d0
*
*****species molecular weights*****
*
19 wo2=32.0d0
  wn2=28.0d0
  wair=29.0d0
  wc=12.0d0
  wh=1.0d0
  wf=19.0d0
  wcl=35.5d0
  wco2=44.0d0
  wh2o=18.0d0
  whf=20.0d0
  whcl=36.5d0
  wcof2=66.0d0
  wcocl2=99.0d0
c
  wfu=a*wc+b*wh

```

```

win=c*wc+d*wh+e*wf+f*wcl
*
*****species diffusion coefficient corrections*****
*
do2n2=dsqrt((wo2+wn2)/(wo2*wn2))
dfun2=dsqrt((wfu+wn2)/(wfu*wn2))
if(win) 1250,1,2
1 dinn2=0.0d0
go to 3
2 dinn2=dsqrt((win+wn2)/(win*wn2))
3 dh2on2=dsqrt((wh2o+wn2)/(wh2o*wn2))
*
*****inlet species mole fractions*****
*
qti=qini+qh2oi+qfui+qairi
qo2i=0.21d0*qairi
qn2i=0.79d0*qairi
Xini=qini/qti
Xh2oi=qh2oi/qti
Xfui=qfui/qti
Xairi=qairi/qti
Xo2i=qo2i/qti
Xn2i=qn2i/qti
*
*****inlet species mole flows*****
*
nti=qti/vm
nini=qini/vm
nh2oi=qh2oi/vm
nfui=qfui/vm
nairi=qairi/vm
no2i=qo2i/vm
nn2i=qn2i/vm
*
*****inlet species densities*****
*
wmi=Xini*win+Xh2oi*wh2o+Xfui*wfu+Xo2i*wo2+Xn2i*wn2
denmi=dmi*wmi
dini=dmi*win
dfui=dmi*wfu
dh2oi=dmi*wh2o
do2i=dmi*wo2
dn2i=dmi*wn2
dairi=dmi*wair
*
*****inlet species mass flows*****
*
mti=qti*denmi*lm3*1.0d3/60.0d0

```

```

mini=qini*dini*lm3*1.0d3/60.0d0
mfui=qfui*dfui*lm3*1.0d3/60.0d0
mh2oi=qh2oi*dh2oi*lm3*1.0d3/60.0d0
mo2i=qo2i*do2i*lm3*1.0d3/60.0d0
mn2i=qn2i*dn2i*lm3*1.0d3/60.0d0
mairi=qairi*dairi*lm3*1.0d3/60.0d0

```

```

*
*****inlet species mass fractions*****
*

```

```

Yini=Xini*win/wmi
Yfui=Xfui*wfu/wmi
Yh2oi=Xh2oi*wh2o/wmi
Yo2i=Xo2i*wo2/wmi
Yn2i=Xn2i*wn2/wmi
Yairi=Xairi*wair/wmi

```

```

*
*****
*

```

main computations

```

*****
*

```

```

* a) no inhibitor in the system

```

```

*****
*

```

```

if(si) 1250,4,5

```

```

*
*****
*

```

```

1. standard case: with/without water, fuel inside, o2/n2 outside

```

```

*****
*

```

```

4 rw=qh2oi/qo2i
row=dh2on2/do2n2
if(qini) 1250,6,9
6 call noins
go to 1300

```

```

*

```

```

5 rw=qh2oi/dfui
row=dh2on2/dfun2
if(qini) 1250,7,9
7 call noini
go to 1350

```

```

*

```

```

*****
*

```

```

* b) inhibitor in the system

```

```

*****
*

```

```

9 if(si) 1250,50,650

```

```

*

```

```

*****

```

```

*   2. standard case: inhibitor outside, fuel inside, o2/n2 outside
*****
*
50 ri=qini/qo2i
   rw=qh2oi/qo2i
   roi=dinn2/do2n2
   row=dh2on2/do2n2
c
   call betas
   if(be.le.becr) then
     hl=1.0d0
   else
     hl=0.0d0
   endif
c
   if(mu) 1250,100,400
*
*****3.1 no h2o in substrates: mu=0.0*****
*
100 if(hl) 1250,200,300
*
**   3.1.1 low level of hydrogen: la=0.0
*
200 call coefls
   go to 1300
*
**   3.1.2 high level of hydrogen: ep=0.0, dz=0.0
*
300 call coefhs
   go to 1300
*
*****3.2 h2o in substrates*****
*
400 if(hl) 1250,500,600
*
**   3.2.1 low level of hydrogen: la=0.0
*
500 call coefls
   go to 1300
*
**   3.2.2 high level of hydrogen: ep=0.0, dz=0.0
*
600 call coefhs
   go to 1300
*
650 ri=qini/xfui
   rw=qh2oi/xfui
   roi=dinn2/dfun2

```

```

row=dh2on2/dfun2
c
call betai
if(be.le.becr) then
  hl=1.0d0
else
  hl=0.0d0
endif
c
if(mu) 1250,700,1000
*
*****4.1 no h2o in substrates: mu=0.0*****
*
700 if(hl) 1250,800,900
*
** 4.1.1 low level of hydrogen: la=0.0
*
800 call coefli
go to 1350
*
** 4.1.2 high level of hydrogen: ep=0.0, dz=0.0
*
900 call coefhi
go to 1350
*
*****4.2 h2o in substrates*****
*
1000 if(hl) 1250,1100,1200
*
** 4.2.1 low level of hydrogen: la=0.0
*
1100 call coefli
go to 1350
*
** 4.2.2 high level of hydrogen: ep=0.0, dz=0.0
*
1200 call coefhi
go to 1350
c
1250 write(*,*) ' '
write(2,*) ' '
write(*,*) ' 1250 negative value '
write(2,*) ' 1250 negative value '
go to 1600
*
*****
* flows of species consumed/generated in flame
* flows of species unreacted

```

* outlet volume and mass flows, mole and mass fractions

*

```

1300 qfur=qfui
    qinr=qfur*be/al
    qo2r=qfur*ga/al
    qn2r=qfur*3.762d0*ga/al
    qco2r=qfur*de/al
    qh2or=qfur*(1a-mu)/al
    qhfr=qfur*et/al
    qhclr=qfur*ph/al
    qcof2r=qfur*ep/al
    qcocl2r=qfur*dz/al

```

c

```

qfuu=0.0d0
qinu=qini-qinr
qo2u=qo2i-qo2r
qn2u=qn2i-qn2r
qh2ou=qh2oi-qh2or
qco2u=0.0d0
qhfu=0.0d0
qhclu=0.0d0
qcof2u=0.0d0
qcoclu=0.0d0

```

c

```

qin=qinu
qfu=0.0d0
qo2=qo2i-qo2r
qn2=qn2i
qh2o=qh2oi+qh2or
qco2=qco2r
qhf=qhfr
qhcl=qhclr
qcof2=qcof2r
qcocl2=qcocl2r

```

c

call molef

c

call massf

c

call molefl

c

go to 1550

c

```

1350 qo2r=qo2i
    qinr=qo2r*be/ga
    qfur=qo2r*al/ga
    qn2r=qn2i

```

```

qco2r=qo2r*de/ga
qh2or=qo2r*(1a-mu)/ga
qhfr=qo2r*et/ga
qhclr=qo2r*ph/ga
qcof2r=qo2r*ep/ga
qcoclr=qo2r*dz/ga

```

c

```

qinu=qini-qinr
qfuu=qfui-qfur
qo2u=0.0d0
qn2u=0.0d0
qh2ou=qh2oi-qh2or
qco2u=0.0d0
qhfu=0.0d0
qhclu=0.0d0
qcof2u=0.0d0
qcoclu=0.0d0

```

c

```

qin=qinu
qfu=qfuu
qo2=0.0d0
qn2=qn2i
qh2o=qh2oi+qh2or
qco2=qco2r
qhf=qhfr
qhcl=qhclr
qcof2=qcof2r
qcocl2=qcoclr

```

c

```
call molef
```

c

```
call massf
```

c

```
call moleff
```

*

```
*****
```

```
* output data
```

```
*****
```

*

```

1550 write(*,*) ' fu o2 in h2os co2 h2op hf hcl
& cof2 cocl2 (coeff)'
write(*,1500) al,ga,be,mu,de,la,et,ph,ep,dz
write(2,*) ' fu o2 in h2os co2 h2op hf hc
&l cof2 cocl2 (coeff)'
write(2,1500) al,ga,be,mu,de,la,et,ph,ep,dz
write(*,*) ' qin qfu qo2 qn2 qco2 qh2o qhf qhcl
&qcof2 qcocl2 (slpm)'
write(*,1500) qin,qfu,qo2,qn2,qco2,qh2o,qhf,qhcl,qcof2,qcocl2

```

```

write(2,*) ' qin  qfu  qo2  qn2  qco2  qh2o  qhf  qhcl
& qcof2 qcocl2 (slpm)'
write(2,1500) qin,qfu,qo2,qn2,qco2,qh2o,qhf,qhcl,qcof2,qcocl2
write(*,*) ' min  mfu  mo2  mn2  mco2  mh2o  mhf  mhcl
& mcof2 mcocl2 (g/s)'
write(*,1500) min,mfu,mo2,mn2,mco2,mh2o,mhf,mhcl,mcof2,mcocl2
write(2,*) ' min  mfu  mo2  mn2  mco2  mh2o  mhf  mhcl
write(2,1500) min,mfu,mo2,mn2,mco2,mh2o,mhf,mhcl,mcof2,mcocl2
write(*,*) ' Xin  Xfu  Xo2  Xn2  Xco2  Xh2o  Xhf  Xhcl
& Xcof2 Xcocl2'
write(*,1500) Xin,Xfu,Xo2,Xn2,Xco2,Xh2o,Xhf,Xhcl,Xcof2,Xcocl2
write(2,*) ' Xin  Xfu  Xo2  Xn2  Xco2  Xh2o  Xhf  Xhcl
& Xcof2 Xcocl2'
write(2,1500) Xin,Xfu,Xo2,Xn2,Xco2,Xh2o,Xhf,Xhcl,Xcof2,Xcocl2
write(*,*) ' Yin  Yfu  Yo2  Yn2  Yco2  Yh2o  Yhf  Yhcl
& Ycof2 Ycocl2'
write(*,1500) Yin,Yfu,Yo2,Yn2,Yco2,Yh2o,Yhf,Yhcl,Ycof2,Ycocl2
write(2,*) ' Yin  Yfu  Yo2  Yn2  Yco2  Yh2o  Yhf  Yhcl
& Ycof2 Ycocl2'
write(2,1500) Yin,Yfu,Yo2,Yn2,Yco2,Yh2o,Yhf,Yhcl,Ycof2,Ycocl2
write(*,*) ' nin  nfu  no2  nn2  nco2  nh2o  nhf  nhcl
& ncof2 ncocl2 (mole/min)'
write(*,1500) nin,nfu,no2,nn2,nco2,nh2o,nhf,nhcl,ncof2,ncocl2
write(2,*) ' nin  nfu  no2  nn2  nco2  nh2o  nhf  nhcl
& ncof2 ncocl2(mole/min)'
write(2,1500) nin,nfu,no2,nn2,nco2,nh2o,nhf,nhcl,ncof2,ncocl2
write(*,*) ' nt  deltan  qt  deltaq  mhffu '
write(*,1590) nt,dn,qt,dq,mhffu
write(2,*) ' nt  deltan  qt  deltaq  mhffu '
write(2,1590) nt,dn,qt,dq,mhffu

```

c

```
if(qini.lt.qinit) go to 5000
```

c

```
1400 format(6f7.4)
1500 format(10f12.5)
1590 format(5f8.4)
```

c

```
1600 stop
end
```

*

```
*****
```

*

```
subroutines
```

```
*****
```

*

```
*****
```

```
* a) standard case, no inhibitor - with/without water combustion products
```

```
*****
```

*

```

subroutine noins
implicit double precision (a-h,j-z)
common /atom/ a,b,c,d,e,f
common /coef/ al,be,becr,ga,de,ep,dz,ph,et,la,mu
common /rat/ ri,rw,roi,row,ros,hl,si

```

c

```

ga=al*(a+0.25d0*b)
de=al*a
la1=rw*row*(a+0.25d0*b)
la2=0.5d0*al*b
la=la1+la2
mu=rw*row*al*(a+0.25d0*b)
be=0.0d0
becr=0.0d0
et=0.0d0
ph=0.0d0
ep=0.0d0
dz=0.0d0
return
end

```

*

```

*****

```

```

*   b) no inhibitor - with/without water combustion products

```

```

*****

```

*

```

subroutine noini
implicit double precision (a-h,j-z)
common /atom/ a,b,c,d,e,f
common /coef/ al,be,becr,ga,de,ep,dz,ph,et,la,mu
common /rat/ ri,rw,roi,row,ros,hl,si

```

c

```

al=ga/(a+0.25d0*b)
de=ga/(1.0d0+b/(4.0d0*a))
mu=al*rw*row
be=0.0d0
becr=0.0d0
et=0.0d0
ph=0.0d0
ep=0.0d0
dz=0.0d0
return
end

```

*

```

*****

```

```

*   a) standard case, hydrogen/halocarbon limit - with/without water

```

```

*****

```

*

```

subroutine betas

```

```

implicit double precision (a-h,j-z)
common /atom/ a,b,c,d,e,f
common /coef/ al,be,becr,ga,de,ep,dz,ph,et,la,mu
common /rat/ ri,rw,roi,row,ros,hl,si

```

c

```

be1=al*(4.0d0*a+b)
be2=4.0d0/(roi*ri)
be3=e+f-4.0d0*c-d
be=be1/(be2+be3)
ros=(row*rw)/(roi*ri)
mu=be*ros
ga=be/(ri*roi)
be4=al*b+2.0d0*mu
if(e+f-d) 10,20,10
10 be5=e+f-d
   go to 30
20 be5=e+f-d+0.01d0
30 becr=be4/be5
   return
end

```

*

```

*****

```

```

*   b) hydrogen/halocarbon limit - with/without water

```

```

*****

```

```

subroutine betai
implicit double precision (a-h,j-z)
common /atom/ a,b,c,d,e,f
common /coef/ al,be,becr,ga,de,ep,dz,ph,et,la,mu
common /rat/ ri,rw,roi,row,ros,hl,si

```

c

```

be1=4.0d0*ga
be2=4.0d0*c+d-e-f
be3=4.0d0*(a+b/4.0d0)/(ri*roi)
be=be1/(be2+be3)
ros=(row*rw)/(roi*ri)
mu=be*ros
al=be/(ri*roi)
be4=al*b+2.0d0*mu
if(e+f-d) 10,20,10
10 be5=e+f-d
   go to 30
20 be5=e+f-d+0.01d0
30 becr=be4/be5
   return
end

```

*

```

*****

```

```

*   inhibitor in - with/without water combustion/inhibition products

```

```

*   a) low hydrogen level
*****
*
  subroutine coefls
  implicit double precision (a-h,j-z)
  common /atom/ a,b,c,d,e,f
  common /coef/ al,be,becr,ga,de,ep,dz,ph,et,la,mu
c
  la=0.0d0
  de=2.0d0*ga-al*a-be*c+mu
  if(f.gt.0.0d0) then
    ph1=al*(0.5d0*b-a)
    ph2=0.5d0*be*(d+f+2.0d0*mu-2.0d0*c-e)
    ph=de+ph1+ph2
    dz1=al*(a-0.5d0*b)
    dz2=0.5d0*be*(2.0d0*c+e+f-2.0d0*mu-d)
    dz=0.5d0*(-de+dz1+dz2)
  else
    ph=0.0d0
    dz=0.0d0
  endif
  et1=al*(a+0.5d0*b)
  et2=0.5d0*becr*(2.0d0*c+d+e-2.0d0*mu-f)
  et3=-de+2.0d0*mu+et1+et2
  et=et
  ep=et3-et
  return
  end
*
*****
*   inhibitor in - with/without water combustion/inhibition products
*   b) low hydrogen level
*****
*
  subroutine coefli
  implicit double precision (a-h,j-z)
  common /atom/ a,b,c,d,e,f
  common /coef/ al,be,becr,ga,de,ep,dz,ph,et,la,mu
c
  la=0.0d0
  de=2.0d0*ga-al*a-be*c+mu
  if(f.gt.0.0d0) then
    ph1=al*(0.5d0*b-a)
    ph2=0.5d0*be*(d+f+2.0d0*mu-2.0d0*c-e)
    ph=de+ph1+ph2
    dz1=al*(a-0.5d0*b)
    dz2=0.5d0*be*(2.0d0*c+e+f-2.0d0*mu-d)
    dz=0.5d0*(-de+dz1+dz2)

```

```

else
  ph=0.0d0
  dz=0.0d0
endif
et1=al*(a+0.5d0*b)
et2=0.5d0*becr*(2.0d0*c+d+e-2.0d0*mu-f)
et3=-de+2.0d0*mu+et1+et2
et=et
ep=et3-et
return
end
*
*****
*   inhibitor in - with/without water combustion/inhibition products
*   c) standard case, high hydrogen level
*****
*
  subroutine coefhs
  implicit double precision (a-h,j-z)
  common /atom/ a,b,c,d,e,f
  common /coef/ al,be,becr,ga,de,ep,dz,ph,et,la,mu
c
  ep=0.0d0
  dz=0.0d0
  de=al*a+be*c
  ph=be*f
  et=be*e
  la=2.0d0*ga-2.0d0*de+mu
  return
  end
*
*****
*   inhibitor in - with/without water combustion/inhibition products
*   d) high hydrogen level
*****
*
  subroutine coefhi
  implicit double precision (a-h,j-z)
  common /atom/ a,b,c,d,e,f
  common /coef/ al,be,becr,ga,de,ep,dz,ph,et,la,mu
c
  ep=0.0d0
  dz=0.0d0
  de=al*a+be*c
  ph=be*f
  et=be*e
  la=2.0d0*ga-2.0d0*de+mu
  return

```

end

*

* outlet species mole flows

*

subroutine molefl

implicit double precision (a-h,j-z)

common /qi/ qini,qh2oi,qfui,qo2i,qn2i,qairi,qti,dq

common /q/ qin,qfu,qo2,qn2,qco2,qh2o,qhf,qhcl,qcof2,

& qcocl2,qt

common /X/ Xin,Xfu,Xo2,Xn2,Xco2,Xh2o,Xhf,Xhcl,Xcof2,Xcocl2

common /therm/ vm,lm3,p,t,ru,cm

common /n/ nin,nfu,no2,nn2,nco2,nh2o,nhf,nhcl,ncof2,

& ncocl2,nt,nti,dn

c

qt=qin+qfu+qh2o+qo2+qn2+qco2+qhf+qhcl+qcof2+qcocl2

nt=qt/vm

dn=nt-nti

nin=qin/vm

nfu=qfu/vm

no2=qo2/vm

nn2=qn2/vm

nco2=qco2/vm

nh2o=qh2o/vm

nhf=qhf/vm

nhcl=qhcl/vm

ncof2=qcof2/vm

ncocl2=qcocl2/vm

return

end

*

* outlet species mole fractions

*

subroutine molef

implicit double precision (a-h,j-z)

common /qi/ qini,qh2oi,qfui,qo2i,qn2i,qairi,qti,dq

common /q/ qin,qfu,qo2,qn2,qco2,qh2o,qhf,qhcl,qcof2,

& qcocl2,qt

common /X/ Xin,Xfu,Xo2,Xn2,Xco2,Xh2o,Xhf,Xhcl,Xcof2,Xcocl2

c

qt=qin+qfu+qh2o+qo2+qn2+qco2+qhf+qhcl+qcof2+qcocl2

dq=qt-qti

Xin=qin/qt

Xfu=qfu/qt

Xo2=qo2/qt

```

Xn2=qn2/qt
Xco2=qco2/qt
Xh2o=qh2o/qt
Xhf=qhf/qt
Xhcl=qhcl/qt
Xcof2=qcof2/qt
Xcocl2=qcocl2/qt
return
end

```

```

*

```

```

*****

```

```

*

```

```

* outlet species mass fractions and flows

```

```

*****

```

```

subroutine massf
implicit double precision (a-h,j-z)
common /therm/ vm,lm3,p,t,ru,cm
common /mi/ mini,mfui,mo2i,mn2i,mco2i,mh2oi,mhfi,mhcli,mcof2i,
& mcocli,mti
common /w/ wo2,wn2,wair,wc,wh,wf,wcl,wco2,wh2o,
& whf,whcl,wcof2,wcocl2,wfu,win,wmi,wm
common /X/ Xin,Xfu,Xo2,Xn2,Xco2,Xh2o,Xhf,Xhcl,Xcof2,Xcocl2
common /Y/ Yin,Yfu,Yo2,Yn2,Yco2,Yh2o,Yhf,Yhcl,Ycof2,Ycocl2
common /q/ qin,qfu,qo2,qn2,qco2,qh2o,qhf,qhcl,qcof2,
& qcocl2,qt
common /d/ din,dfu,do2,dn2,dco2,dh2o,dhf,dhcl,dcof2,
& dcocl2,denm,dm
common /m/ min,mfu,mo2,mn2,mco2,mh2o,mhf,mhcl,mcof2,
& mcocli2,mt,mhffu

```

```

c

```

```

wm=Xin*win+Xfu*wfu+Xo2*wo2+Xn2*wn2+Xco2*wco2+Xh2o*wh2o+
& Xhf*whf+Xhcl*whcl+Xcof2*wcof2+Xcocl2*wcocl2
Yin=Xin*win/wm
Yfu=Xfu*wfu/wm
Yo2=Xo2*wo2/wm
Yn2=Xn2*wn2/wm
Yco2=Xco2*wco2/wm
Yh2o=Xh2o*wh2o/wm
Yhf=Xhf*whf/wm
Yhcl=Xhcl*whcl/wm
Ycof2=Xcof2*wcof2/wm
Ycocl2=Xcocl2*wcocl2/wm

```

```

c

```

```

qt=qin+qfu+qh2o+qo2+qn2+qco2+qhf+qhcl+qcof2+qcocl2
mt=mti
dm=mt/(qt*wm)
min=qin*win*dm
mfu=qfu*wfu*dm

```

```
mo2=qo2*wo2*dm
mn2=qn2*wn2*dm
mco2=qco2*wco2*dm
mh2o=qh2o*wh2o*dm
mhf=qhf*whf*dm
mhcl=qhcl*whcl*dm
mcof2=qcof2*wcof2*dm
mcocl2=qcocl2*wcocl2*dm
```

c

```
if(mfui.le.0.0d0) then
  mhffu=0.0d0
else
  mhffu=mhf/mfui
endif
```

c

```
return
end
```